Orientation of Liquid Crystal Molecules at Surfaces

Paul Schuddeboom

1998

Orientation of Liquid Crystal Molecules at Surfaces

Academisch Proefschrift

ter verkrijging van de graad van doctor aan de Universiteit van Amsterdam, op gezag van de Rector Magnificus prof. dr. J.J.M. Franse ten overstaan van een door het college voor promoties ingestelde commissie in het openbaar te verdedigen in de Aula der Universiteit op woensdag 25 november 1998 te 15.00 uur

door

Paul Christiaan Schuddeboom

geboren te Zaandijk

promotor:	Prof. dr. D. Frenkel
	Faculteit der Scheikunde van de Universiteit van Amsterdam en
	FOM-Instituut voor Atoom- en Molecuulfysica te Amsterdam
co-promotor:	dr. B. Jérôme
	Faculteit der Scheikunde van de Universiteit van Amsterdam

Omslag: goede dingen in het leven

The work described in this thesis was performed at the FOM-institutefor Atomic- and Molecular Physics, Kruislaan 407, 1098 SJAmsterdam. The work is part of the research program of the Stichting voor Fundamenteel Onderzoek der Materie [Foundation for Fundamental research on Matter (FOM)] and was made possible by financial support from the Nederlandse Organisatie voor Wetenschappelijk Onderzoek [Netherlands Organisation for the Advancement of Research (NWO)].

Aan mijn ouders,
Sandra, Els, Jeannette

Contents

1 Introduction

1.1 Liquid crystals

Liquid crystals combine the flow properties of liquids with the optical properties of crystals. This ambivalence is not only responsible for their name, but also for their wide use in electro-optical devices. The first observations of this combination of *a priori* antagonistic properties date back to the 1850's. Two biologists R. Virchow and C. F. von Mettenheimer found it in the myelin of nerve core using polarized microscopy. Subsequently, a large number of other animal and plant substances showed the same behavior and were given the name of "living crystals".

The official discovery of liquid crystals is however dated 1888 and attributed to Friedrich Reinitzer and Otto Lehmann. In the course of their study of cholesterol derivates, Lehmann wrote: "It is of high interest for the physicist that crystals exist which are of such considerable softness that one could *almost* call them liquid". Soon thereafter he obviously thought that the word "almost" was too conservative and wrote his famous article entitled: "Über fliessende Krystalle"[1].

It did not take long before it was noticed that liquid crystals had another property of crystals, namely that they could be aligned by contact with another crystal. Starting from 1911, C. Mauguin made several observations of the orientation of liquid crystals by crystalline surfaces [2, 3]. He also noted that liquid crystals did not take a preferred in-plane orientation on glass plates [4]. Somewhat later, P. Chatelain showed that by rubbing the glass plates in a given rubbing direction, this isotropy is broken and the liquid crystal aligns along the rubbing direction [5]. However the systematic development of such surface treatments for the alignment of liquid crystals only started in the 1970's, and the number of known aligning surfaces is huge by now [6]. It is also in that period

that appeared the name "anchoring" given to the phenomenon of orientation of liquid crystals by surfaces.

This sudden interest for alignment surfaces was triggered by the development of one of the major applications of liquid crystals: the nematic liquid crystal display [7]. The first successful example of LCD, the Twisted Nematic display, was patented in 1969 by J. Fergason and its principle described by M. Schadt and W. Helfrich [8]. This principle is based on two earlier discoveries. The first one is due again to C. Mauguin who had observed that by putting a liquid crystal in a cell limited by two surfaces inducing different orientations, the optical axis of the liquid crystal rotated smoothly between these two orientations as one moves from one surface to the other [2–4]. He had also found that if this evolution takes place over a length scale much larger than the optical wavelength, the polarization of a light beam initially parallel to the liquid crystalline axis at the entrance surface of the cell rotates with the liquid crystalline axis as the beam propagates through the cell [9]. This means that if the cell is sandwiched between two polarizers oriented respectively along the optical axis of the liquid crystal at each surface, the cell transmits light and appears clear (Fig. 1.1).

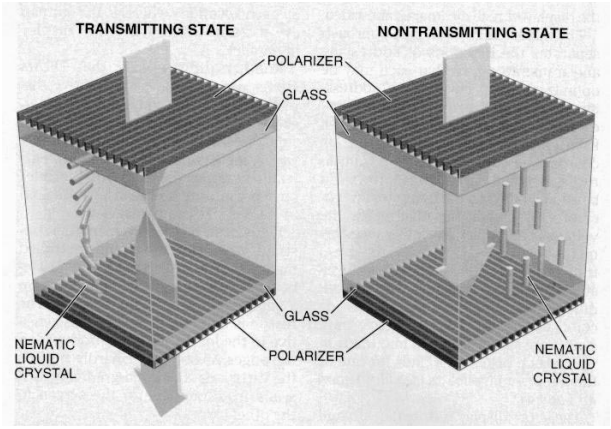

FIGURE 1.1 *Schematic representation of a liquid crystal display cell in the transmitting state (left) and the dark state (right).*

The other important discovery for the development of switchable displays is due to V. Freedericksz in the 1930's. He showed that the orientation of a liquid crystal can be deformed in the bulk of a cell by applying a strong enough electric field [10]. This effect is used to obtain the dark state of a display: an electric field is applied across

the cell by transparent electrodes coated on the surfaces, which destroys the twist of the optical axis in the cell (Fig. 1.1). The polarization of an in-coming beam does not rotate anymore in the cell and light is stopped by the output polarizer; the cell does not transmit light anymore.

In parallel to the development of applications of liquid crystals, a lot of fundamental research has been and is still performed on these materials. The softness of their order and the wide variety of the type of order they exhibit make them ideal model systems to study the ordering or disordering effect of various factors, such as fluctuations, external fields, surfaces, or confinement. In all cases, a full understanding of the observed phenomena requires the understanding of the behavior of the molecules constitutive of the studied materials. The basis of this microscopic understanding was layed down by George Friedel who introduced the idea of orientational order and proposed a classification scheme of the different liquid crystalline phases known at that time (nematic, smectic and cholesteric) based on their structure [11].

In comparison the study of the surface behavior of liquid crystals at a molecular level is very recent. Its development had to wait for the appearance in the 1980's of experimental techniques able to study this molecular behavior (atomic force and scanning tunneling microscopy, second-harmonic and sum-frequency generation, scattering of x-ray synchrotron radiation).

In the remaining of this chapter we describe the structure of liquid crystals and that of their interfaces with a substrate. We end by giving the aim and the outline of the present thesis.

1.2 Structure of liquid crystals

Liquid crystals appear in the so-called mesogens, which are composed of molecules having an anisotropic shape and interacting with each other. In the most disordered condensed phase –the isotropic phase– each molecule uniformly explores positions and orientations throughout the whole available space by diffusion mechanisms (Fig. 1.2). In contrast, in the most ordered crystalline phase, the positions of the molecules are fixed in a lattice as their orientations with respect to this lattice. In between those two situations

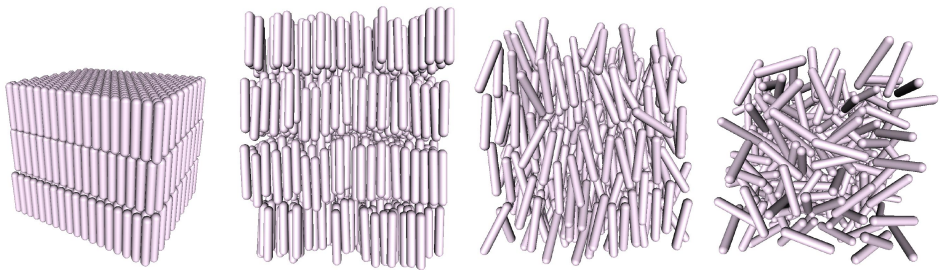

FIGURE 1.2 *Schematic representations of the molecular order in some of the phases observed in liquid crystalline materials. From left to right: a solid crystal, a smectic-A phase, a nematic phase and an isotropic liquid. For simplicity the elongated molecules are represented as rods* [12].

one finds the mesophases or liquid crystalline phases [13–15]. The simplest example of a mesophase is the nematic phase which appears in systems of elongated molecules tending to orient parallel to each other while showing no long-range positional order (Fig. 1.2). The latter gives this phase its liquid character, while the common mean orientation of the molecules results in crystalline properties. In the so-called thermotropic liquid crystals that we consider, the phase sequence isotropic-nematic-crystal is obtained by decreasing temperature.

Some compounds exhibit another liquid crystalline phase intermediate between the nematic and crystalline structure. This phase is called smectic and is characterized by the same orientational order as the nematic phase but with a positional order in one direction. This means that the molecules are organized in layers. The orientation of the molecules with respect to the layers and the degree of positional order within each layer depends on the type of smectic phase considered [16]. The less ordered phase is called smectic A; the molecules are then perpendicular to the layers and have no positional order in the layers (Fig. 1.2).

In this thesis, we mainly deal with nematic phases. The bulk state of such a phase can be described by two parameters. The first one gives the average orientation of the molecules in a volume v_0, which is small compared with the size of the system and large compared with the molecules' size. This orientation is represented by a unit vector $\boldsymbol{n}$ called a director. If the nematic liquid crystal is distorted, the director varies in space

and one has to define the director field $\boldsymbol{n}(\boldsymbol{r})$. The nematogens, that is to say compounds exhibiting a nematic phase, often consist of asymmetric molecules (see e.g. Fig. 1.3).

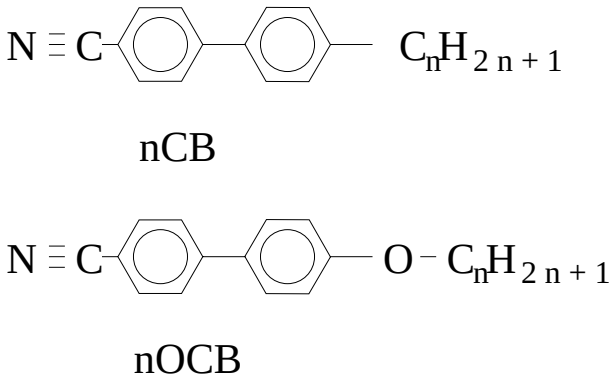

FIGURE 1.3 *Chemical formulas of alkylcyanobiphenyl (nCB) and alkoxycyanobiphenyl (nOCB). These are some of the most widely studied liquid crystals.*

However, as in a small volume of nematic liquid crystal, there are as many molecules pointing in one direction as in the opposite one, and the vectors $\boldsymbol{n}$ and $-\boldsymbol{n}$ cannot be distinguished.

The second parameter, the order parameter Q, characterizes the distribution of orientations of molecules. It is defined as the average over all the molecules of the volume v_0 of $(3\cos^2\theta - 1)/2$, where θ is the angle between a molecule and the director $\boldsymbol{n}$. Q is equal to 1 when all the molecules are aligned parallel to $\boldsymbol{n}$ and to 0 when the distribution of orientations is isotropic. In the bulk nematic phase, the order parameter is of the order of 0.4 at the highest temperatures and 0.6 at the lowest [13]. The distribution of orientations has, apart from the above mentioned order parameter which is simply $\langle P_2(\theta)\rangle$, higher rank order parameters components such as $\langle Y_{3m}\rangle$. These components can be determined from the measured nonlinear susceptibility $\bar{\boldsymbol{\chi}}$ which will be introduced in chapter 2.

1.3 Structure of interfaces

We concentrate on the interface between a nematic liquid crystal and a solid substrate. One can distinguish several regions in this interface [17]. Right at the surface of the

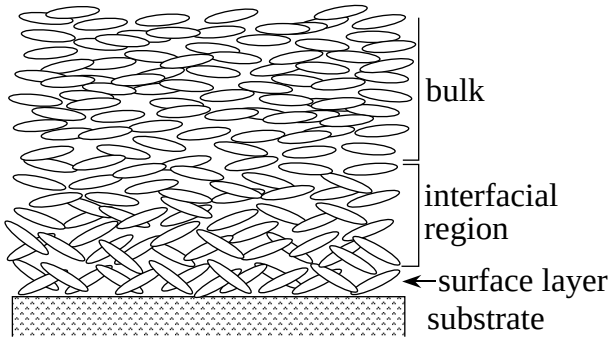

FIGURE 1.4 *Schematic representation of a liquid crystal in contact with a substrate.*

substrate, there is a layer of molecules (the surface layer, see Fig. 1.4) in direct contact with the substrate. The interaction of the molecules with the substrate is in general different from the interaction the molecules have with each other in the bulk. This interaction determines the orientational order of the molecules, and therefore the surface order differs for the bulk order. The surface-induced order is the boundary conditions to which the liquid crystal has to adapt. This adaptation takes place in the interfacial region in which the orientational order evolves from that imposed by the surface to that of the bulk (Fig. 1.4). The thickness of the interfacial region corresponds to the coherence length of the nematic order, approximately 10nm away from any phase transitions [13].

This evolution of the order is associated with some distortion energy. The configuration adopted by the liquid crystal is the one (or one of the configurations) that minimizes this distortion energy. This configuration determines the mean orientation of the molecules outside the interfacial region, i.e. the bulk director. This surface-induced orientation of the director is called the anchoring direction.

If the bulk director is forced to deviate from the imposed anchoring direction (e.g. by the application of an external field or the proximity of another surface), this costs energy, so-called anchoring energy [18, 19]. This energy arises from two effects: as already mentioned, having the order evolve in the interfacial region costs energy. If this evolution is forced to deviate from the one minimizing the distortion energy, this energy increases. The second effect is the possible reorientation of the molecules in the surface layer away from the minimum of their interaction energy with the substrate. This contribution may be called the microscopic anchoring energy.

1.4 Aim and outline of thesis

This thesis deals with the orientational order of liquid crystal molecules at the surface of a substrate and its relation to macroscopic surface properties, such as anchoring directions and anchoring energy. Our study is based on second-harmonic generation measurements of liquid crystal molecules deposited on different substrates. These measurements allow us to specifically probe the orientational order in the surface layer. This technique and it theoretical basis are described in chapter 2.

We present next a study of the anchoring mechanisms leading to a multistable anchoring. This type of anchoring is observed on substrates with a high symmetry by which several anchoring directions with different in-plane orientations are energetically equivalent. This high symmetry of the substrate implies that it induces a type of ordering that does not exist in bulk and therefore disappears in the interfacial region. The symmetry also imposes that the nematic director does not have a preferred in-plane orientation. The question arises then how the bulk director gets oriented by the substrate. To address this question, we have studied the anchoring and surface order on phlogopite mica, which exhibits a three-fold symmetry. The results of the experimental measurements are presented in chapter 3 and a model to account for these results in chapter 4.

We then consider the question: what happens to the orientational order of the surface layer if a strong DC electric field forces the molecules to reorient. The resulting orientational order is determined by the balance between the anchoring energy of the molecules onto the substrate and the energy of the molecular dipoles in the applied electric field. From this orientational distribution, we can thus get information on the microscopic anchoring energy. In chapter 5, we present our measurements on a simple model substrate, namely fused quartz plates. Since this substrate is isotropic, it allows us to examine in detail the orienting effect of a DC electric field –called poling– on thin liquid crystal films. Such a study is a prerequisite to the analysis of similar measurements performed with anisotropic substrates.

Finally in chapter 6 we examine the reorientation dynamics of liquid crystal molecules in thin films when an electric field is switched on or off. Because of the interaction of

the molecules with the substrate, this dynamics is different from that in bulk. These measurements show how mobile the interfacial molecules are and give some information on their interaction with the substrate.

2 Second-Harmonic Generation

In this chapter, we present the main experimental technique we have used, namely second-harmonic generation. We give the theoretical expressions of the measured signal and the information on the orientational order of the molecules obtained from it. Finally we briefly describe the experimental set-up.

Second-harmonic generation has proven to be a versatile tool to investigate the surface and interfacial properties on the atomic and molecular scale in a wide range of physical systems. These include surfaces of solids [20–22] and liquids [23, 24], molecular adsorbates on solid surfaces [25–28] and solid/solid interfaces [29]. The success of this technique arises from several features. Since it is optical, it is applicable to all interfaces accessible by light, and therefore capable of *in-situ* remote sensing of a surface. It is also non destructive, although heating by the incident laser beam might be a problem for some samples. As the output signal is monochromatic, coherently emitted in a well-defined direction and in well-defined time windows corresponding to the laser pulses used as input, this signal can easily be separated from the background by spectral, spatial and temporal filtering. This implies that very small signals, generated for instance by a submonolayer of molecules, can easily be detected. Last but no least, second-harmonic generation is intrinsicly surface specific. This comes form the fact that second-harmonic generation is forbidden in centrosymmetric media (in the dipole approximation). Thus in the case of an interface between two centrosymmetric media, second-harmonic generation occurs predominantly in the narrow region in which the symmetry of the bulk media is broken.

This surface specificity is enhanced in the case of monolayers of polar molecules taking a polar ordering when deposited on a substrate. There are then well-defined physical entities (namely the molecules) localized at the surface that generate a second-harmonic signal. In this category falls a wide class of liquid crystal molecules (in particular cyanobiphenyl molecules) when deposited on hydrophilic surfaces. Second-harmonic generation has therefore widely contributed to the understanding of anchoring phenomena, and it is the central experimental technique used in the work presented here.

In the following, we present the theory of surface second-harmonic generation at the basis of our measurements and our set-up.

2.1 Theory of surface second-harmonic generation

The theory of second-harmonic generation by adsorbed species at substrate surfaces and its application to the determination of the orientational distribution in liquid crystal monolayers have already been described in detail in different articles [30–32]. We shall only recall here the essential elements for the understanding of our measurements.

2.1.1 Generation of a second-harmonic signal

Let us consider a light beam at frequency ω incident on a substrate surface covered with a film of liquid-crystal molecules such as cyanobiphenyl molecules, whose cyanobiphenyl rigid core exhibits a strong nonlinear polarizability (Fig. 1.3). If the incident beam is sufficiently intense, the system has, in addition to its linear response, a nonlinear response whose first term generates light at frequency 2ω. Because of the boundary condition requiring the wave vector components parallel to the surface to be matched [32], the second-harmonic signal must be coherently generated in the direction of reflection of the incident beam (Fig 2.1). The most important contribution to the reflected second-harmonic signal comes from the induced surface electric dipole polarization $\mathbf{P}_D^{(2)}(2\omega) = \bar{\boldsymbol{\chi}}^D : \mathbf{E}(\omega)\mathbf{E}(\omega)$, where $\mathbf{E}(\omega)$ is the incident field at frequency ω and $\bar{\boldsymbol{\chi}}^D$ is an effective surface nonlinear dipolar susceptibility of the illuminated medium. The bulk contribution to $\bar{\boldsymbol{\chi}}^D$ vanishes in a centrosymmetric system. This is the case for the different substrates we have used (mica and fused quartz), as well as for the liquid crystal aside from the surface layer in contact with the substrate surface. Indeed, away

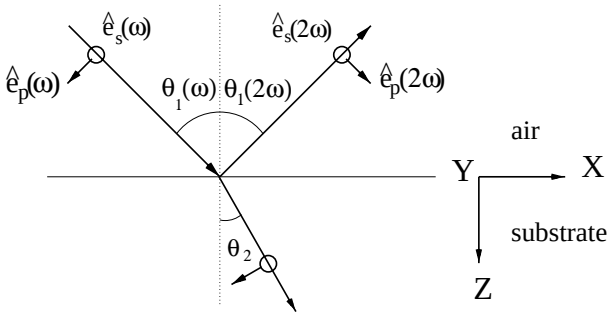

FIGURE 2.1 *Scattering geometry of surface second-harmonic generation in reflection*

from the surface and in the absence of external fields, cyanobiphenyl molecules exhibit a quadrupolar ordering (Fig. 2.2). The electric quadrupole nonlinearities of the substrate

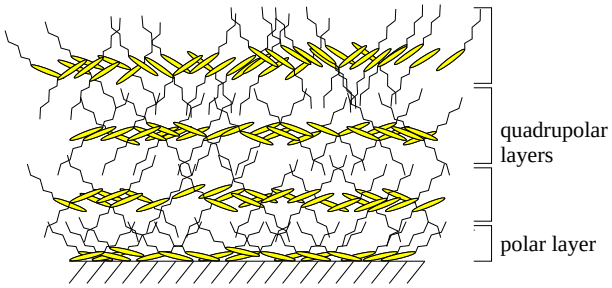

FIGURE 2.2 *Schematic representation of the molecular structure in a film of liquid crystal deposited on a substrate*

and the liquid crystal also contribute to the second-harmonic generation but to a much lesser extent. For the liquid crystal, the induced nonlinear electric quadrupole polarization is $\mathbf{P}_Q^{(2)}(2\omega) = \bar{\boldsymbol{\chi}}^Q : \mathbf{E}(\omega)\nabla\mathbf{E}(\omega)$ where $\bar{\boldsymbol{\chi}}^Q$ is the nonlinear quadrupolar susceptibility of the material [33–35]. Since this term is much smaller than the nonlinear electric dipole polarization of a dipolar layer [36], it is possible to make thin enough liquid-crystal films for which the quadrupolar contribution to the second-harmonic signal can be neglected [37]. Most of our measurements have been performed on such samples, so we consider primarily the case when the quadrupolar contribution is negligible.

The second-harmonic signal generated by the substrate arises from the surface nonlinearity induced by the structural asymmetry and field discontinuity existing at the substrate surface [34]. This substrate contribution is negligible compared to the signal from the liquid crystal molecules in the case of fused quartz. In the case of phlogopite

mica, this is only true for a p polarization of the out-going signal, and we have limited our measurements to this configuration.

Finally, the nonlinear polarizability of volatile molecules such as water molecules that might also be adsorbed at the surface, is too weak to yield a detectable second-harmonic signal. In summary, the second-harmonic signal generated by a multilayer of cyanobiphenyl molecules deposited on the substrates we have used corresponds essentially to the dipolar contribution generated by the liquid-crystal layer adsorbed at the surface, which exhibits a certain degree of polar ordering [36]. The measurement of this signal can thus be used to specifically probe the behavior of this layer. If an external DC field is applied onto the system (as in the experiments reported in chapter 5 and 6), the whole liquid crystal film might then exhibit a polar ordering. The formulas we give in the following for the signal generated by the surface layer apply then to the whole film.

So we consider a liquid crystalline layer sandwiched between medium 1 which is the atmosphere surrounding the sample and medium 2 which is the substrate (Fig. 2.1). The laser beam is incident from medium 1 and the reflected second-harmonic output is detected. The second-harmonic signal is given by [30]:

$$S = \frac{32\pi^3\omega^2 \sec^2\theta_1(2\omega)}{c^3[\epsilon_1(2\omega)]^{1/2}\epsilon_1(\omega)} |\chi_{\text{eff}}|^2 I_\omega^2 T A$$

where I_ω is the intensity of the incident laser beam, T is the laser pulse width, A is the area of the laser spot on the surface, $\epsilon_1(\Omega)$ is the dielectric constant of medium 1 at frequency $\Omega(\Omega = 2\omega$ or $\omega)$, $\theta_1(2\omega)$ is the reflection angle of the second-harmonic signal (Fig. 2.1), and χ_{eff} is the effective nonlinear susceptibility of the layer. The molecules are polarly ordered on the substrate and due to their nonlinear polarizability they form a medium with a nonlinear second-order susceptibility tensor $\bar{\boldsymbol{\chi}}$. The effective susceptibility χ_{eff} is related to $\bar{\boldsymbol{\chi}}$ by:

$$\chi_{\text{eff}} = [\hat{\mathbf{e}}(2\omega)\cdot\bar{\mathbf{L}}(2\omega)]\bar{\boldsymbol{\chi}} : [\hat{\mathbf{e}}(\omega)\cdot\bar{\mathbf{L}}(\omega)][\hat{\mathbf{e}}(\omega)\cdot\bar{\mathbf{L}}(\omega)] \tag{2.1}$$

where $\hat{\mathbf{e}}(\Omega)$ is the unit polarization vector for the incident beam $(\Omega = \omega)$ or the second-harmonic beam $(\Omega = 2\omega)$, and $\bar{\mathbf{L}}(\Omega)$ are the local-field tensors arising from the dielectric discontinuity at the surface.

2.1.2 The dipolar susceptibility of the surface layer

The nonlinear dipolar susceptibility $\bar{\boldsymbol{\chi}}$ of a layer of liquid-crystal molecules can be calculated from the second-order polarizability $\bar{\boldsymbol{\alpha}}^D$ of one molecule. For liquid crystal molecules such as cyanobiphenyls, $\bar{\boldsymbol{\alpha}}^D$ has one dominant element $\alpha^D_{\xi\xi\xi}$ along the long molecular axis $\hat{\boldsymbol{\xi}}$. In this case, $\bar{\boldsymbol{\chi}}$ takes the form:

$$\chi_{ijk} = N_s\langle\alpha^D_{ijk}\rangle = \langle(\hat{\boldsymbol{i}}\cdot\hat{\boldsymbol{\xi}})(\hat{\boldsymbol{j}}\cdot\hat{\boldsymbol{\xi}})(\hat{\boldsymbol{k}}\cdot\hat{\boldsymbol{\xi}})\rangle N_{\mathrm{s}}\alpha^D_{\xi\xi\xi}$$

where N_s is the surface density of liquid-crystal molecules, $\hat{\boldsymbol{i}}$, $\hat{\boldsymbol{j}}$ and $\hat{\boldsymbol{k}}$ are unit vectors of the reference frame (xyz) of the substrate surface (Fig. 2.3) and $\langle\rangle$ denotes the average on all the surface molecules.

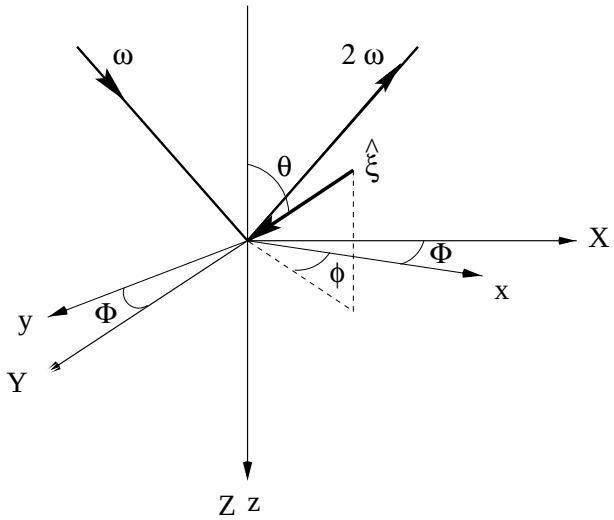

FIGURE 2.3 *Reference frames (xyz) of the substrate surface and (XYZ) of the laboratory. (XZ) is the incident plane of the laser beam and (xz) the mirror plane of the substrate surface. The molecular axis $\hat{\xi}$ is defined with respect to the substrate axes by the spherical coordinated (θ, ϕ).*

The number of independent non-vanishing components of $\bar{\boldsymbol{\chi}}$ depends on the symmetry of this substrate, which imposes the symmetry of the surface layer. In the present work, we have used substrates with three different symmetries. One is the commonly observed mirror symmetry (C_{1v} symmetry). There are then six independent components[1]:

[1]The x axis of the reference frame of the substrate is chosen parallel to (one of) the mirror planes of the substrate.

$$\chi_{zzz} = N_s \left\langle \cos^3\theta \right\rangle \alpha^D_{\xi\xi\xi} \tag{2.2a}$$

$$\chi_{xxx} = -N_s \left\langle \sin^3\theta \cos^3\phi \right\rangle \alpha^D_{\xi\xi\xi} \tag{2.2b}$$

$$\chi_{zyy} = \chi_{yzy} = \chi_{yyz} = N_s \left\langle (\cos\theta - \cos^3\theta)(1 - \cos^2\phi) \right\rangle \alpha^D_{\xi\xi\xi} \tag{2.2c}$$

$$\chi_{zxx} = \chi_{xzx} = \chi_{xxz} = N_s \left\langle (\cos\theta - \cos^3\theta)\cos^2\phi \right\rangle \alpha^D_{\xi\xi\xi} \tag{2.2d}$$

$$\chi_{xzz} = \chi_{zxz} = \chi_{zzx} = -N_s \left\langle (\sin\theta - \sin^3\theta)\cos\phi \right\rangle \alpha^D_{\xi\xi\xi} \tag{2.2e}$$

$$\chi_{xyy} = \chi_{yxy} = \chi_{yyx} = -N_s \left\langle \sin^3\theta(\cos\phi - \cos^3\phi) \right\rangle \alpha^D_{\xi\xi\xi} \tag{2.2f}$$

where (θ, ϕ) are the spherical coordinates defining the molecular axis $\hat{\boldsymbol{\xi}}$ (Fig. 2.3). If the symmetry of the substrate is threefold (C_{3v} symmetry), $\bar{\boldsymbol{\chi}}$ has four independent components[1]:

$$\chi_{zzz} = N_s \langle \cos^3\theta \rangle \alpha^D_{\xi\xi\xi}, \tag{2.3a}$$

$$\chi_{xxx} = -\chi_{xyy} = \frac{1}{4} N_s \langle \sin^3\theta \cos 3\phi \rangle \alpha^D_{\xi\xi\xi}, \tag{2.3b}$$

$$\chi_{xxz} = \chi_{yyz} = \frac{1}{2} N_s \langle (\cos\theta - \cos^3\theta) \rangle \alpha^D_{\xi\xi\xi}, \tag{2.3c}$$

$$\chi_{xxy} = -\chi_{yyy} = \frac{1}{4} N_s \langle \sin^3\theta \sin 3\phi \rangle \alpha^D_{\xi\xi\xi}, \tag{2.3d}$$

Finally if the substrate is isotropic ($C_{\infty v}$ symmetry), the number of independent components reduces to two:

$$\chi_{zzz} = N_s \left\langle \cos^3\theta \right\rangle \alpha^D_{\xi\xi\xi} \tag{2.4a}$$

$$\chi_{zii} = \chi_{izi} = \chi_{iiz} = \frac{1}{2} N_s \left\langle \sin^2\theta \cos\theta \right\rangle \alpha^D_{\xi\xi\xi}, \ i = x, y. \tag{2.4b}$$

In all cases, these components are proportional to moments of the orientational distribution of the surface molecules. They contain the information about the surface orientational distribution which is accessible by second-harmonic generation.

2.1.3 The effective susceptibility χ_{eff}

To obtain the value of the different components of the nonlinear susceptibility $\bar{\boldsymbol{\chi}}$, we need to measure the second-harmonic signal as a function of the in-plane rotation of the sample and of the polarization s (out of the plane of incidence) or p (in the plane of

incidence) of the in-coming and out-going light. Let Φ be the angle between the plane of incidence and the x axis in the plane of the substrate (Fig. 2.3). The full expression of the effective surface susceptibility χ_{eff} can be obtained for the different polarization combinations *sp*, *pp*, *ps* and *ss* using Eq. (2.1) and Eq. (2.2), (2.3) or (2.4) depending on the symmetry of the considered substrate. For a mirror symmetry, one has:

$$\begin{aligned}
\chi_{sp} &= \chi_{xyy}(3\cos^3\Phi - 2\cos\Phi)e_{xyy} + \chi_{xxx}\sin^2\Phi\cos\Phi\ e_{xyy} \\
&\quad + \chi_{zxx}\sin^2\Phi\ e_{zyy} + \chi_{zyy}\cos^2\Phi\ e_{zyy} && \text{(2.5a)} \\
\chi_{pp} &= \chi_{xxx}\cos^3\Phi\ e_{xxx} + 3\chi_{xyy}\sin^2\Phi\cos\Phi\ e_{xxx} + \chi_{xxz}\cos^2\Phi(2e_{xxz} + e_{zxx}) \\
&\quad + \chi_{yyz}\sin^2\Phi(2e_{xxz} + e_{zxx}) + \chi_{xzz}\cos\Phi(2e_{zxz} + e_{xzz}) + \chi_{zzz}e_{zzz} && \text{(2.5b)} \\
\chi_{ps} &= \chi_{xxx}\cos^2\Phi\sin\Phi\ e_{yxx} + \chi_{xyy}(3\sin^3\Phi - 2\sin\Phi)e_{yxx} \\
&\quad + (\chi_{xxz} - \chi_{yyz})\sin 2\Phi\ e_{yxz} + \chi_{xzz}\sin\Phi\ e_{yzz} && \text{(2.5c)} \\
\chi_{ss} &= \chi_{xxx}\sin^3\Phi\ e_{yyy} + 3\chi_{xyy}\cos^2\Phi\sin\Phi\ e_{yyy}. && \text{(2.5d)}
\end{aligned}$$

For a threefold symmetry:

$$\begin{aligned}
\chi_{sp} &= [\chi_{xyy}\cos 3\Phi - \chi_{yyy}\sin 3\Phi]e_{xyy} + \chi_{yyz}\ e_{zyy} && \text{(2.6a)} \\
\chi_{pp} &= [\chi_{yyy}\sin 3\Phi - \chi_{xyy}\cos 3\Phi]e_{xxx} + \chi_{yyz}(e_{zxx} - 2e_{xzx}) \\
&\quad + \chi_{zzz}e_{zzz} && \text{(2.6b)} \\
\chi_{ps} &= [\chi_{xyy}\sin 3\Phi + \chi_{yyy}\cos 3\Phi]e_{yxx} && \text{(2.6c)} \\
\chi_{ss} &= [\chi_{xyy}\sin 3\Phi + \chi_{yyy}\cos 3\Phi]e_{yyy}. && \text{(2.6d)}
\end{aligned}$$

Finally for an isotropic substrate:

$$\begin{aligned}
\chi_{sp} &= \chi_{zxx}e_{zyy} && \text{(2.7a)} \\
\chi_{pp} &= \chi_{zxx}(2e_{xxz} + e_{zxx}) + \chi_{zzz}e_{zzz}. && \text{(2.7b)}
\end{aligned}$$

In these formulas, we define e_{ijk} as:

$$e_{ijk} = e_i(2\omega)L_{ii}(2\omega)e_j(\omega)L_{jj}(\omega)e_k(\omega)L_{kk}(\omega). \qquad \text{(2.8)}$$

The polarization vectors are given by:

$$\hat{\mathbf{e}}_p(\omega) = (-\cos\theta_1(\omega), 0, \sin\theta_1(\omega)) \tag{2.9}$$

$$\hat{\mathbf{e}}_p(2\omega) = (\cos\theta_1(2\omega), 0, \sin\theta_1(2\omega)) \tag{2.10}$$

for the p polarization and:

$$\hat{\mathbf{e}}_s(\Omega) = (0, 1, 0)$$

for the s polarization (Fig. 2.1). For a sufficiently thin film that can be considered as infinitely thin with respect to the wavelength of light, the local field factors $L_{ii}(\Omega)$ are given by [38]:

$$L_{xx}(\Omega) = \frac{2n_1(\Omega)\cos\theta_2(\Omega)}{n_2(\Omega)\cos\theta_1(\Omega) + n_1(\Omega)\cos\theta_2(\Omega)} \tag{2.11a}$$

$$L_{yy}(\Omega) = \frac{2n_1(\Omega)\cos\theta_1(\Omega)}{n_1(\Omega)\cos\theta_1(\Omega) + n_2(\Omega)\cos\theta_2(\Omega)} \tag{2.11b}$$

$$L_{zz}(\Omega) = \frac{2n_1^2(\Omega)n_2(\Omega)\cos\theta_1(\Omega)}{n_f^2(\Omega)[n_2(\Omega)\cos\theta_1(\Omega) + n_1(\Omega)\cos\theta_2(\Omega)]} \tag{2.11c}$$

where $n_i(\Omega)$ $(i = 1, 2)$ and $n_f(\Omega)$ are the refractive indices of media 1 and 2 and of the film at frequency Ω, and $\theta_1(\Omega)$ and $\theta_2(\Omega)$ are the reflection and transmission angles of the different beams (Fig. 2.1). θ_1 is typically 45°. The values of the refractive indices of the different media we have used are given in table 2.1. When we fit the experimental data obtained for the different polarization configurations with the theoretical expressions of χ_{eff} we obtain the values for the different components χ_{ijk} of the nonlinear susceptibility $\bar{\boldsymbol{\chi}}$.

2.1.4 Orientational distributions deduced from $\bar{\boldsymbol{\chi}}$

Once $\bar{\boldsymbol{\chi}}$ is known for a given layer, one possesses *via* Eq. (2.2), (2.3) or (2.4) some information about the orientational distribution of the molecules in the layer. In order to get an "unbiased" estimate of the orientational distribution $f(\theta, \phi)$, i.e. one that does not rely on any *a priori* assumption, we have used the maximum-entropy method [40]. This method gives the widest distribution compatible with the available information on f. This information is the average values of the following functions f_{ijk} obtained from

Medium	$n(\omega)$	$n(2\omega)$
Air	1.00	1.00
Fused quartz	1.46	1.50
Phlogopite mica	1.56	1.56 [38]
Liquid crystal thick film	1.6	1.4+0.2i [39]
Liquid crystal monolayer	1.00	1.00 [38]

TABLE 2.1 *Values of the refractive indices at* $\omega = 2\pi/532nm^{-1}$ *and* $2\omega = 2\pi/266nm^{-1}$ *used in the calculation of the local field factors* L_{ii}.

the measurements of $\bar{\boldsymbol{\chi}}$ and defined by:

$$\chi_{ijk} = N_s \alpha^D_{\xi\xi\xi} \langle f_{ijk}(\theta,\phi)\rangle \tag{2.12}$$

In order not to introduce any bias, we need to maximize the uncertainty on $f(\theta,\phi)$, defined by $H(f) = \int_0^\pi \int_0^{2\pi} f(\theta,\phi)\ln[f(\theta,\phi)]\sin\theta d\theta d\phi$, with the known constraints on $\langle f_{ijk}(\theta,\phi)\rangle$. This is equivalent to maximizing the quantity $H - \sum_{ijk}\lambda_{ijk}f_{ijk}$, where λ_{ijk} are Lagrangian multipliers. This maximization leads to:

$$f(\theta,\phi) = \frac{\exp\left[\Sigma\lambda_{ijk}f_{ijk}(\theta,\phi)\right]}{\iint \exp\left[\Sigma\lambda_{ijk}f_{ijk}(\theta,\phi)\right]\sin(\theta)d\theta d\phi},$$

where λ_{ijk}, are to be calculated from the set of equations:

$$\langle f_{ijk}(\theta,\phi)\rangle = \int\int f_{ijk}(\theta,\phi) f(\theta,\phi)\sin\theta d\theta d\phi$$

The experimental measurements actually give the values of $\chi_{ijk} = N_s\alpha^D_{\xi\xi\xi}\langle f_{ijk}(\theta,\phi)\rangle$. The product $N_s\alpha^D_{\xi\xi\xi}$ is not known since the second-harmonic signal is not measured in absolute units. We can calculate a minimum value for this product by considering the range of values each $\langle f_{ijk}(\theta,\phi)\rangle$ can have. For each value of $N_s\alpha^D_{\xi\xi\xi}$ above this minimum, we can determine the corresponding distribution $f(\theta,\phi)$. As $N_s\alpha^D_{\xi\xi\xi}$ increases, the height of the maxima of $f(\theta,\phi)$ is found to decrease while their positions remain approximately constant. A reasonable value of $N_s\alpha^D_{\xi\xi\xi}$ can be obtained by first assuming a certain shape of $f(\theta,\phi)$ characterized by a number of parameters equal to the number of available components χ_{ijk} minus one [38] and determining these parameters and $N_s\alpha^D_{\xi\xi\xi}$ from the experimental data.

2.1.5 The quadrupolar contribution

If the surface monolayer is covered by a thick film, the quadrupolar contribution of this film to the second-harmonic signal is not negligible any more (see section 2.1.1). This contribution leads to an additional term in some of the components of $\bar{\boldsymbol{\chi}}$ [34, 35]. In the case the film is infinitely thick, these components take the form [38]:

$$\chi^{\text{tot}}_{zxx} = \chi^{\text{surf}}_{zxx} - \frac{\chi^{Q}_{zzxx}}{\epsilon(2\omega)} \tag{2.13a}$$

$$\chi^{\text{tot}}_{zyy} = \chi^{\text{surf}}_{zyy} - \frac{\chi^{Q}_{zzyy}}{\epsilon(2\omega)} \tag{2.13b}$$

$$\chi^{\text{tot}}_{zzz} = \chi^{\text{surf}}_{zzz} - \frac{\chi^{Q}_{zzzz}}{\epsilon(2\omega)\epsilon^2(\omega)} \tag{2.13c}$$

with

$$\chi^{Q}_{ijkl} = \frac{1}{2} N_B \left\langle (\hat{\boldsymbol{i}}\cdot\hat{\boldsymbol{\xi}})(\hat{\boldsymbol{j}}\cdot\hat{\boldsymbol{\xi}})(\hat{\boldsymbol{k}}\cdot\hat{\boldsymbol{\xi}})(\hat{\boldsymbol{l}}\cdot\hat{\boldsymbol{\xi}}) \right\rangle \alpha^{D}_{\xi\xi\xi\xi}\xi_0.$$

N_B is the bulk density of liquid crystal molecules, ξ_0 is the separation between antiparallel chromophores along $\hat{\boldsymbol{\xi}}$, and $\epsilon(\Omega)$ the dielectric constant of the medium at frequency Ω. If the film is thin with respect to the wavelength of light, the effective quadrupolar nonlinear susceptibility tensor which enters in Eq. (2.13) can be approximated by:

$$\chi^{Q}_{ijkl} = N_b N_s \left\langle (\hat{\boldsymbol{i}}\cdot\hat{\boldsymbol{\xi}})(\hat{\boldsymbol{j}}\cdot\hat{\boldsymbol{\xi}})(\hat{\boldsymbol{k}}\cdot\hat{\boldsymbol{\xi}})(\hat{\boldsymbol{l}}\cdot\hat{\boldsymbol{\xi}}) \right\rangle \alpha^{D}_{\xi\xi\xi\xi}\xi_0 k \tag{2.14}$$

where k is the wave number of the incident beam in the liquid crystal $k = \epsilon(\omega)2\pi/\lambda$, and N_b the number of quadrupolar bilayers[2].

2.2 Experimental set-up

Our measurements were performed in reflection from the liquid crystal side. A schematic drawing of our set-up is given in Fig. 2.4. The light source is a frequency-doubled Q-switched mode-locked YAG laser (Coherent, Antares) [41]. The mode-locked pulses have a duration of 80ps and a repetition rate of 76MHz. The Q-switched pulses have a duration of 200ns, which means that they contain approximately 15 mode-locked

[2] In fact, the organization of the liquid crystal molecules in bilayers quickly decays away form the substrate surface since there is no positional order in bulk nematic liquid crystals. It is nevertheless convenient to assume this organization in the whole film.

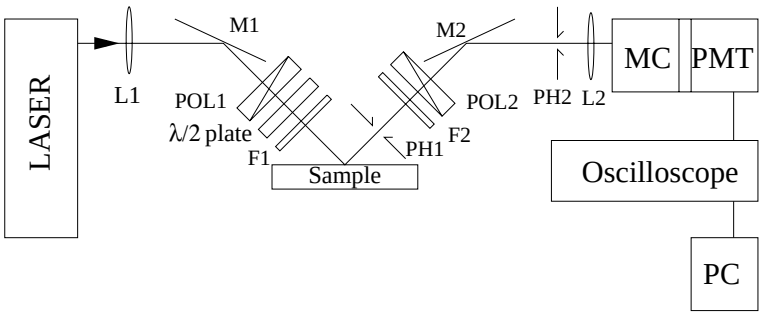

FIGURE 2.4 *Set-up for second-harmonic generation experiments. L1 and L2: lenses, M1 and M2: mirrors, POL1 and POL2: polarizers, PH1 and PH2: diaphragms, MC: monochromator, PMT: photomultiplier tube, F1 is a filter stopping any UV radiation generated by optical elements, F2 is a filter stopping a large part of the green reflected beam.*

pulses and that the effective illumination time is 1.2ns. The repetition rate of the Q-switched pulses can be tuned between 1Hz and 1.2kHz with a constant energy per pulse of 1mJ. The input wavelength is 532nm, and the detected second-harmonic signal at 266nm.

The polarization of the input light is first defined by a Glan-laser polarization prism (POL1) and varied by a halfwave plate. The output polarization is selected by a Rochon polarizer (POL2). The input and output polarizations are calibrated using the fact that the s-in/s-out signal of a cyanobiphenyl monolayer on a clean glass substrate should be zero. The accuracy of the polarizations is approximately 0.5°. The size of the laser beam spot at the sample is controlled by a lens (L1, $f = 40$cm). The position of the lens is chosen so that the waist of the beam (i.e. its smaller diameter) corresponds to the sample. The beam size at the sample in the experiment is about 100μm in diameter. The normal intensity of the beam is tuned by the orientation of the Glan-laser polarizer with respect to the polarization of the laser beam. It is set such that the intensity of the second-harmonic signal is maximal while the laser beam does not damage or significantly heat the sample.

The signal is spatially filtered by a series of diaphragms (PH) and spectrally filtered by a color filter (F2) and a monochromator (MC). It is detected by a photomultiplier tube (PMT) and sent to a digitizing oscilloscope and a personal computer. The oscilloscope

collects one trace per pulse and allows one to determine the number of photons detected in one given laser pulse. This has the advantage that we can measure stronger signals than with a traditional photon counting technique based on a gated integrator. In the latter case, one assigns a number of detected photons 1 or 0 to each pulse. The measurable signal is then limited to 0.2 photons per pulse to avoid the detection of two or more photons during one pulse, which are then counted as one photon. Our counting technique has the disadvantage that the oscilloscope can only accumulate 800 traces per second, which means that the repetition frequency of the laser has to be limited to 800Hz. Also the transfer of trace data between the oscilloscope and the computer is a limiting factor for fast acquisition.

The sample is in a temperature-controlled closed cell, which sits on a tilting stage, itself mounted on a rotational stage. The rotational stage is on a x-y translational stage. With these stages we can align the sample so that the laser beam intersects the axis of the rotational stage at the sample surface, and the normal to the surface is parallel to the rotation axis. An additional translation stage located between the tilt stage and the cell allows us to move the sample with respect to the rotation axis to perform measurements at different positions on a given sample.

The use of a closed cell implies that the incident laser beam and the generated signal go through a quartz window. Since the transmission coefficient through the interfaces of the window depends on the polarization of light, the measured effective nonlinear susceptibilities χ_{eff} need to be corrected by the appropriate coefficients [42]:

$$\chi_{ss} = \frac{\chi_{ss}^{\text{meas}}}{T_s(2\omega)T_s^2(\omega)} \tag{2.15a}$$

$$\chi_{ps} = \frac{\chi_{ps}^{\text{meas}}}{T_s(2\omega)T_p^2(\omega)} \tag{2.15b}$$

$$\chi_{sp} = \frac{\chi_{sp}^{\text{meas}}}{T_p(2\omega)T_s^2(\omega)} \tag{2.15c}$$

$$\chi_{pp} = \frac{\chi_{pp}^{\text{meas}}}{T_p(2\omega)T_p^2(\omega)} \tag{2.15d}$$

with

$$T_s(\Omega) = \frac{4n_q(\Omega)\cos\theta_q(\Omega)\cos\theta_1(\Omega)}{[\cos\theta_1(\Omega)+n_q(\Omega)\cos\theta_q(\Omega)]^2} \tag{2.16a}$$

$$T_p(\Omega) = \frac{4n_q(\Omega)\cos\theta_q(\Omega)\cos\theta_1(\Omega)}{[\cos\theta_q(\Omega)+n_q(\Omega)\cos\theta_1(\Omega)]^2} \tag{2.16b}$$

$n_q(\Omega)$ is the refractive index of fused quartz at frequency Ω (see table 2.1) and $\theta_q(\Omega)$ is the refraction angle of the light in the quartz defined by $\sin\theta_1(\Omega) = n_q(\Omega)\sin\theta_q(\Omega)$.

3 Anchoring on Phlogopite Mica: Experiments

Substrates with a high in-plane symmetry (three-fold or higher) induce multistable anchorings in nematic liquid crystals: the preferred nematic axis in the bulk can take several equivalent orientations with different in-plane directions. To elucidate the mechanisms leading to this degeneracy, we have investigated the relation between the orientational order of cyanobiphenyl molecules at the surface of phlogopite mica plates (exhibiting a three-fold symmetry) and the observed bulk orientations induced by these surfaces. In particular, in-plane bulk reorientations were observed when the system was put in the presence of water vapor. These appear to be driven by changes in the tilt distribution of the surface molecules.

3.1 Introduction

Numerous new substrates are being developed to achieve tailored alignment patterns of nematic liquid crystals (see for instance [43–46]), however, the mechanisms by which a surface can impose this orientation in a liquid-crystalline phase are not very well understood [17]. Some progress has been made in recent years in the understanding of the anchoring on smooth surfaces such as rubbed polymer films [28, 47–49] and mica [37, 50, 51]. On these substrates, the anchoring direction imposed on the bulk director is fully determined by the nematic component of the orientational order in the surface layer [48–50]; this surface nematic order is characterized by defining a surface director as the average orientation of the surface molecules, and a surface order parameter indicating the degree of alignment of these molecules along the surface director. The evolution of the orientational order in the interfacial region is well described using the standard second-order Landau-de Gennes theory of the nematic phase: the anchoring directions

deduced from measured surface orientational distributions agree quantitatively with the experimental observations. The anchoring direction has the same in-plane orientation as the surface director and its tilt with respect to the surface is determined by both the tilt of the surface director and the surface order parameter.

A common characteristic of the substrates studied so far is that their surface has a mirror symmetry. Such a low symmetry allows the director in the surface layer to be either tilted or parallel to the surface. The in-plane component of the surface director introduces an in-plane anisotropy in the orientational order, with respect to which the bulk can orient.

The case of substrates with a threefold symmetry or higher[1] is different. On the one hand, they induce so-called multistable anchorings in which the bulk liquid crystal has the choice between several thermodynamically equivalent anchoring directions [17]. On the other hand, such a symmetry imposes the surface director to be perpendicular to the surface. This means that in terms of nematic ordering, the surface layer is isotropic in the plane of the surface. According to the anchoring mechanism proposed so far for low-symmetry surfaces, the bulk anchoring direction resulting from such an isotropic surface layer should have no preferred in-plane orientation (degenerate anchoring) or be perpendicular to the surface (homeotropic anchoring). However, most known examples of smooth substrates with high symmetry induce anchoring directions parallel to the substrate surface with definite in-plane orientations [52–57]. In the present work, we investigate the mechanism that induces these preferred in-plane orientations on high-symmetry surfaces.

We have studied the anchoring behavior of two cyanobiphenyl liquid crystals (5OCB and 7CB) on phlogopite mica crystals, whose surface exhibits a threefold symmetry and induces tristable planar anchorings [57]. These systems exhibit first-order anchoring transitions (i.e. discontinuous changes in anchoring directions) when water vapor is added

[1]The case of a twofold symmetry is intermediate and can be classified as low or high symmetry depending on the orientation of the surface director. If the surface director is parallel to the surface (which is allowed by symmetry), the situation is similar to that of the surfaces with a mirror symmetry and the induced anchoring is monostable. If the surface director is perpendicular to the surface, the situation is similar to that of surfaces with a threefold symmetry or higher and multistability may be induced.

to the atmosphere surrounding the system [57]. These transitions have been attributed to the adsorption of water molecules at the interface between the liquid crystal and the mica surface, hence their name of "adsorption-induced" anchoring transitions [58]. These transitions allow us to study different anchoring conditions in a given system and so to test the validity of the proposed anchoring mechanisms.

To investigate the anchoring behavior in these systems, we have used different experimental techniques (described in section 3.2). The anchoring directions induced by the substrate on the bulk liquid crystals have been observed using polarizing microscopy and the orientational distribution of the liquid crystal layer at the substrate surface has been determined with optical second-harmonic generation. These measurements give the variation of the bulk anchoring directions and of the surface orientational distribution across an anchoring transition occurring in the presence of water vapor. Our results indicate that the bulk in-plane reorientation observed at the transition is due to changes in the tilt distribution of the surface molecules (section 3.3).

3.2 Experimental techniques

3.2.1 Determination of bulk anchoring directions

The anchoring directions have been determined by depositing a nematic droplet and letting it spread on the mica surface. This investigation method is based on the selection of anchoring directions by the spreading conditions of a liquid crystal on a substrate. It has indeed been shown [56, 59] that when a substrate induces different possible anchoring directions, the orientation which is effectively taken by the liquid crystal depends on the direction of the spreading flow and on the contact angle between the free surface and the substrate.

During the spreading of a droplet, all the points of the nematic-substrate interface are wet under different conditions. The inside of the spread droplet is then divided into several domains where different anchoring directions have been selected. Moreover, the spreading is radial and the contact angle evolves from π when the droplet touches the substrate to zero when the droplet is completely spread. Therefore, all the wetting

conditions are explored by such a spreading process and all the anchoring directions induced by the substrate are found in the droplet.

From the observation under a polarizing microscope of the texture of a nematic droplet spread on a substrate, one can deduce the following information [56, 59]:

(1) The number of anchoring directions induced by the substrate is half the number of domains with different orientations existing in the spread droplet.

(2) The azimuthal orientation of the projection of the anchoring directions in the substrate plane is determined by the observation of the extinction of the different domains between crossed polarizers.

(3) The tilt of the anchoring directions is indicated by the shape of the walls separating the domains with different orientations. In particular, planar anchorings with anchoring directions parallel to the substrate lead to radial walls. This is, however, true only for nematic liquid crystals (such as the ones used in the present study) having homeotropic anchoring conditions at the nematic-air interface, i.e. when the molecules are perpendicular to this interface.

3.2.2 Determination of surface orientational order

The orientational distribution of the surface molecules has been determined by optical second-harmonic generation (see chapter 2). The measurements consist in following the dependence of the second-harmonic signal as a function of the rotation of the sample in its plane for different combinations of the input and output polarizations. By fitting this data, we can determine the four non-zero independent components of the nonlinear susceptibility tensor $\bar{\boldsymbol{\chi}}$ of the surface layer (section 2.1.2):

$$\chi_{zzz} = \langle\cos^3\theta\rangle N_s \alpha^D_{\xi\xi\xi}, \tag{3.1a}$$

$$\chi_{xxx} = -\chi_{xyy} = \frac{1}{4}\langle\sin^3\theta\cos 3\phi\rangle N_s \alpha^D_{\xi\xi\xi}, \tag{3.1b}$$

$$\chi_{xxz} = \chi_{yyz} = \frac{1}{2}\langle(\cos\theta - \cos^3\theta)\rangle N_s \alpha^D_{\xi\xi\xi}, \tag{3.1c}$$

$$\chi_{xxy} = -\chi_{yyy} = \frac{1}{4}\langle\sin^3\theta\sin 3\phi\rangle N_s \alpha^D_{\xi\xi\xi}, \tag{3.1d}$$

where (θ, ϕ) are the spherical coordinates defining the molecular axis $\hat{\boldsymbol{\xi}}$ (Fig. 2.3). To estimate the orientational distribution itself, we use the maximum-entropy method, which gives the widest distribution compatible with the measured moments χ_{ijk} (section 2.1.4).

For the samples used in the present study, the second-harmonic signal in the s-in-p-out and p-in-p-out polarization configurations is much stronger than the signal in the p-in-s-out and s-in-s-out configurations for which the second-harmonic signal produced by the mica substrate is not negligible with respect to that of a cyanobiphenyl layer. Since $\bar{\boldsymbol{\chi}}$ can be fully determined from the measurements the effective susceptibilities of χ_{sp} and χ_{pp}, corresponding to the s-in-p-out and p-in-p-out configuration (section 2.1.3), we have only used these two effective susceptibilities to calculate $\bar{\boldsymbol{\chi}}$.

3.2.3 Samples

To prepare our samples we have used freshly cleaved phlogopite mica as substrate. A detailed description of the structure of mica can be found elsewhere [39]. Here we give the important features which are necessary to understand the experiments described in this article. Phlogopite mica is made of a stack of sheets and cleaves easily between these sheets, which makes it possible to obtain an atomically smooth surface free of steps. The surface of these sheets exhibits a threefold symmetry with three equivalent mirror planes σ (symmetry group C_{3v}). The orientation of these planes can be determined from the cracks formed in a mica plate after perforating it with a needle and which coincide with the mirror planes σ [60].

As liquid crystals, we have used two different substituted cyanobiphenyls, 7CB and 5OCB (Fig. 3.1). The first one exhibits a nematic phase between 29.7°C and 42.8°C and the second one between 48.2°C and 67.6°C [61], with the possibility of super-cooling the nematic phase of the latter down to room temperature.

For second-harmonic generation measurements, liquid-crystal molecules were deposited onto a mica plate in the presence of a dry atmosphere by evaporating them from a hot source located 1mm above the mica plate and letting them condense onto the plate kept at room temperature. The deposition was monitored by measuring the second-harmonic signal generated by the film. The signal first increases with time and

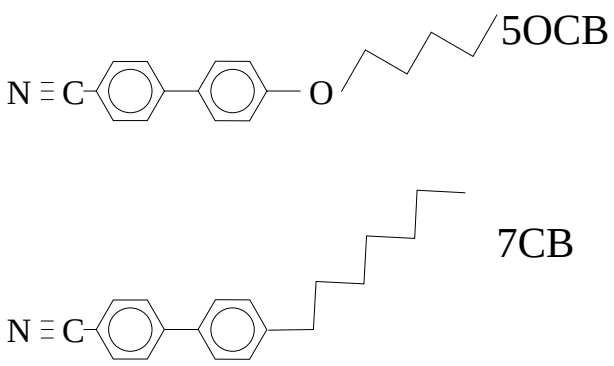

FIGURE 3.1 *The chemical structure of the liquid crystals 5OCB and 7CB used in the present work*

then abruptly saturates indicating that a full monolayer has been formed [37]. The resulting second-harmonic signal is essentially independent of the amount of liquid crystal deposited above this monolayer. This shows that this monolayer is little affected by the presence or absence of a bulk on top of it, as was already observed in other systems [38].

To study the effect of water vapor on the anchoring, the samples were placed in a chamber with a controlled atmosphere. The atmosphere composition was fixed by a slow lamellar flow of a mixture of dry nitrogen and nitrogen saturated with water vapor [58]. The composition of the atmosphere in the chamber can be characterized by the reduced partial vapor pressure $\tilde{p} = p/p_s$ of water, which is the ratio of the partial pressure p over the saturation vapor pressure p_s of water vapor. Fixing $\tilde{p}$ corresponds to fixing the chemical potential of water in the system.

3.3 Experimental results

3.3.1 Bulk anchoring directions

Both 5OCB and 7CB give spread droplets exhibiting radial walls between domains of different orientations (Fig. 3.2). This means that the bulk orientation for both 5OCB and 7CB is parallel to the surface [56, 59]. The droplets contain six domains; the bulk liquid crystal has the choice between three possible anchoring directions separated by an angle of 120°, as expected from the threefold symmetry of the phlogopite mica surface.

As the water vapor pressure increases, anchoring transitions are observed which are characterized by a bulk reorientation in the plane parallel to the substrate. 5OCB

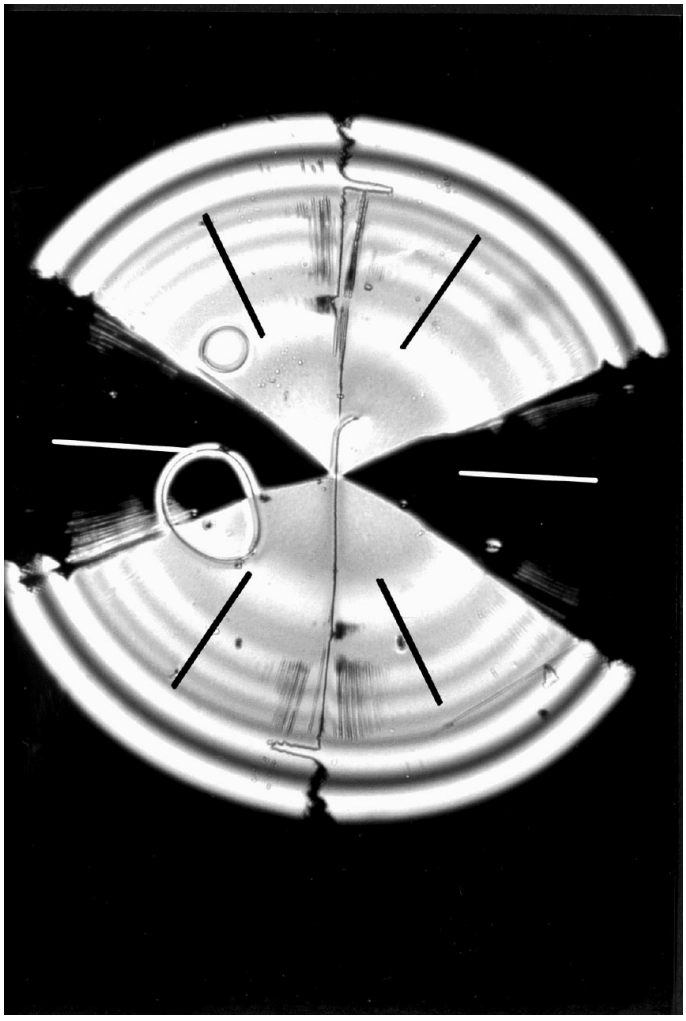

FIGURE 3.2 *Droplet of cyanobiphenyl liquid crystal deposited on phlogopite mica observed with a microscope between crossed polarizers. The bars indicate the bulk orientation in the different domains.*

and 7CB differ in the in-plane orientation of the anchoring directions (Fig. 3.3). In an atmosphere of dry nitrogen, 5OCB orients perpendicular to one of the mirror planes σ of the mica surface. When water vapor is added, this system exhibits a first-order anchoring transition at a given reduced partial vapor pressure $\tilde{p}_1$ of water. At this transition, the orientation of the nematic phase jumps abruptly to a direction parallel to σ. In contrast 7CB orients parallel to σ in a dry atmosphere while it orients perpendicular to σ after the anchoring transition.

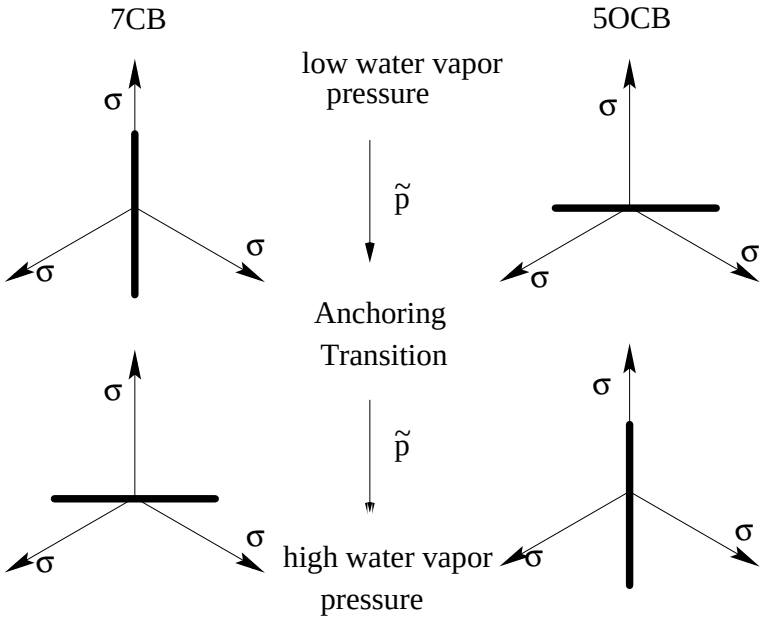

FIGURE 3.3 *Anchoring of 7CB and 5OCB on phlogopite mica under the influence of water vapor. The arrows indicate the orientations of the three mirror planes σ. The thick bar indicates one of the anchoring direction; the others can be deduced from it by applying the three-fold symmetry.*

3.3.2 Surface orientational order

Figures 3.4 and 3.5 show the polar plots of the square root of the second-harmonic signal generated respectively by a layer of 5OCB and 7CB on phlogopite mica, as a function of the in-plane rotation angle Φ of the sample (Fig. 2.3) for different partial water vapor pressures. In all cases, the shape of the plots shows a threefold symmetry indicating that the surface liquid crystalline layer follows the symmetry of the substrate. The maxima of the signal correspond to the same in-plane rotation Φ for both 5OCB and 7CB, but the in-plane anisotropy is stronger for 7CB.

The general trend in both sets of plots is that, as the partial pressure of water vapor is increased, the anisotropy decreases. Moreover the maxima in the plots corresponding to the *s*-in-*p*-out polarization configuration increase for 5OCB and decrease for 7CB. All these changes are reversible provided the system has not been exposed to water vapor for more than approximately a day. Figures 3.6 and 3.7 show the resulting orientational distribution functions of the surface liquid-crystal molecules. For both liquid crystals and for all pressures, the distribution exhibits four peaks from which one is pointing

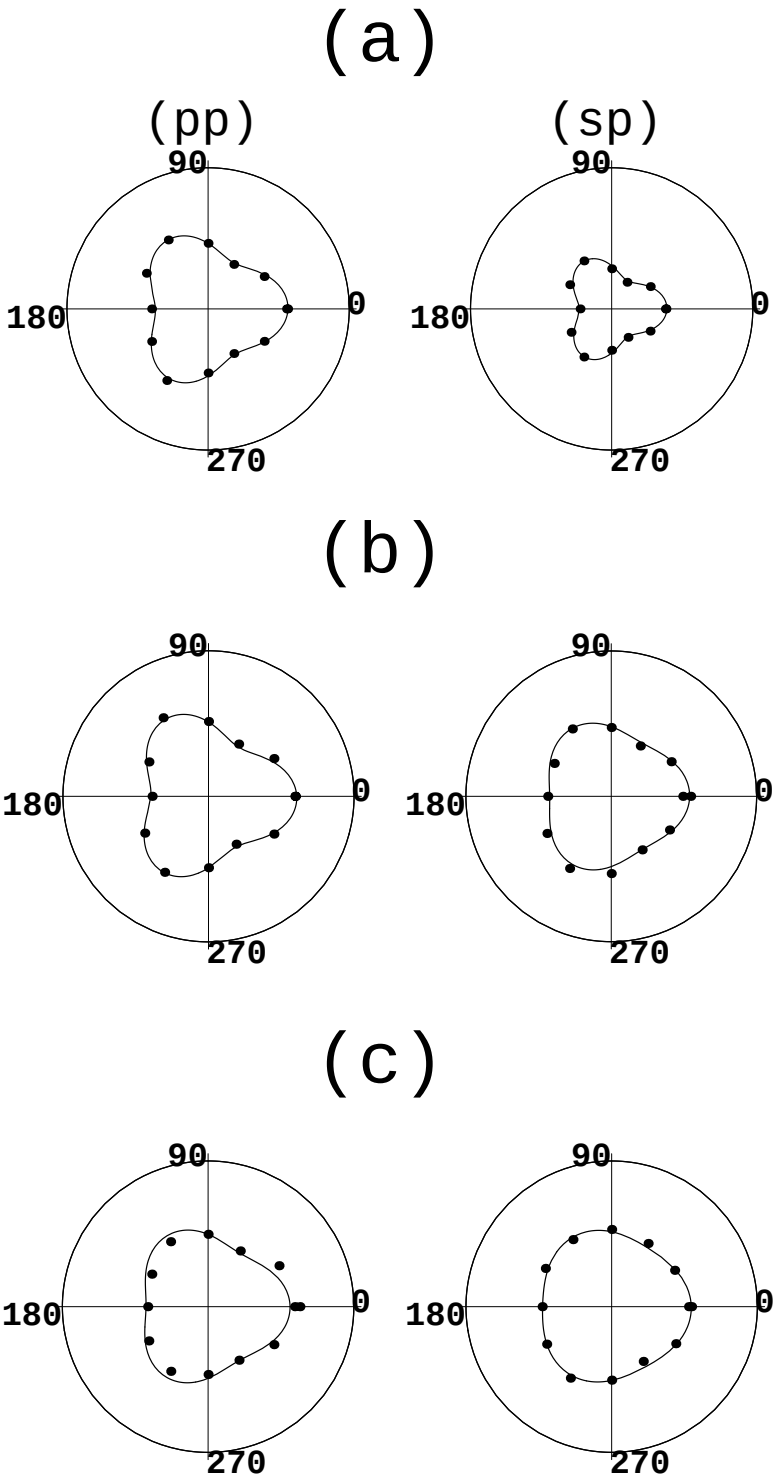

FIGURE 3.4 *Polar plots of the square root of the second-harmonic signal versus the angle* Φ *between the incidence plane of the laser beam and one of the mirror planes* σ *of the mica surface for a 5OCB film deposited on phlogopite mica in an atmosphere containing water vapor with (a)* $\tilde{p} = 0$*, (b)* $\tilde{p} = 0.4$*,(c)* $\tilde{p} = 0.75$*. The data points correspond to an average of the signal over 1200 Q-switch laser pulses. The solid lines are fits to the data points using Eq. 2.6.*

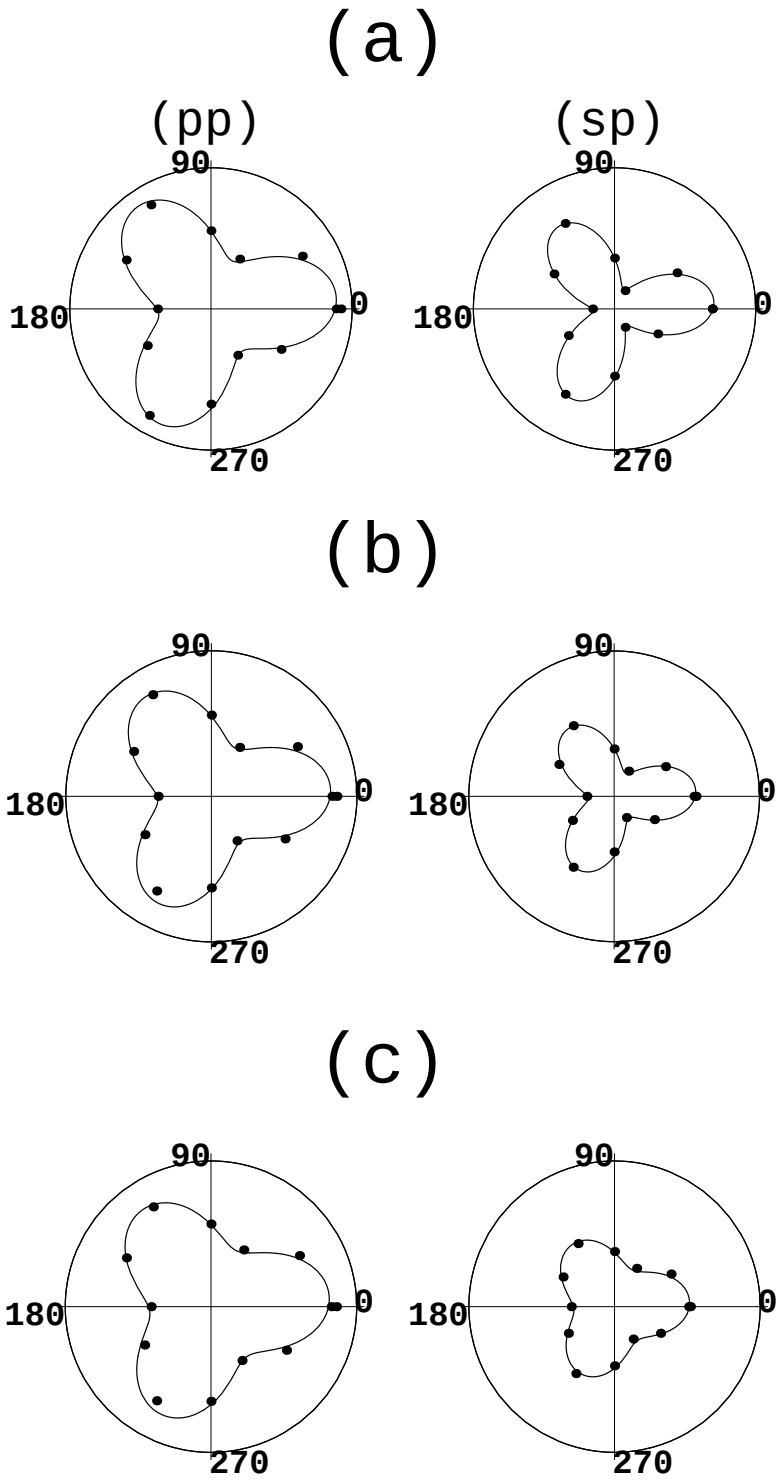

FIGURE 3.5 *The same as figure 3.4 for 7CB with (a)* $\tilde{p} = 0$*, (b)* $\tilde{p} = 0.4$ *(c)* $\tilde{p} = 0.75$.

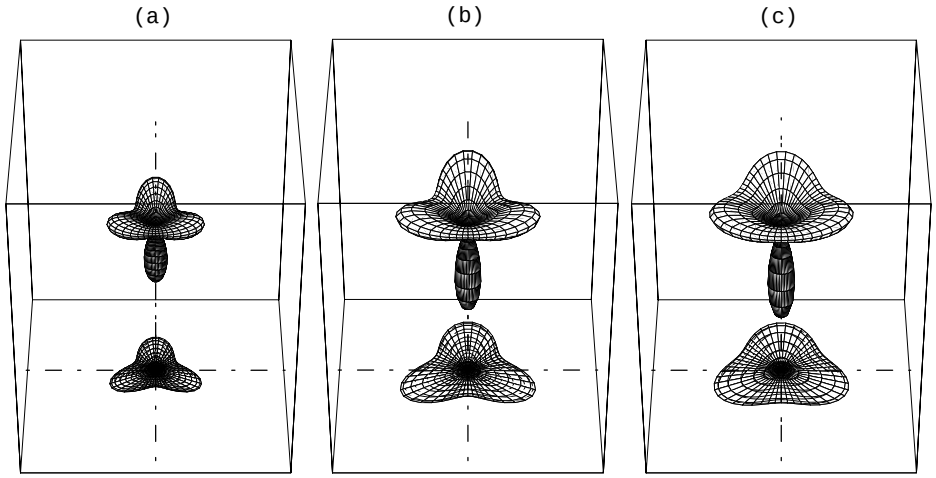

FIGURE 3.6 *The evolution of orientational distribution $f(\theta, \phi)$ in a layer of 5OCB liquid crystal molecules on a substrate of phlogopite mica, for different partial water vapor pressures (a) $\tilde{p} = 0$, (b) $\tilde{p} = 0.4$ and (c) $\tilde{p} = 0.75$. The distribution function is displayed in a box and has a projection on the lower plane.*

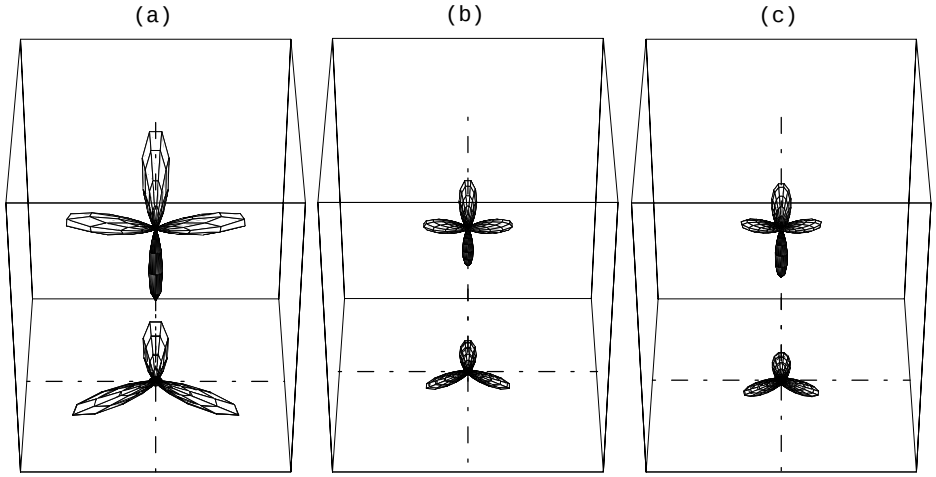

FIGURE 3.7 *The same as figure 3.6 for 7CB and different partial water vapor pressures (a) $\tilde{p} = 0$, (b) $\tilde{p} = 0.4$ and (c) $\tilde{p} = 0.75$.*

downward, corresponding to molecules pointing with their cyano-group away from the surface. The other three peaks lie on a cone around the $z-$axis with an opening angle of approximately $58°$, and in the mirror planes σ of the substrate.

In agreement with the decrease of in-plane anisotropy in the second-harmonic signal (Fig. 3.4 and 3.5), one observes in these distributions that the width of the peaks increases when the water vapor pressure increases. However, the in-plane orientation of the peaks is independent of the liquid crystal and of the composition of the atmosphere. This is in contrast with the strong variations of the bulk anchoring directions on these parameters.

To quantify the detailed evolution of the surface orientational order with water vapor pressure, we have calculated the evolution of the different order parameters characterizing the surface orientational order. The number of independent order parameters can be reduced to three, two parameters for the threefold component of the ordering:

$$Q_{111} = \left\langle \frac{\cos 3\phi \sin^3 \theta}{4} \right\rangle$$
$$Q_{333} = \left\langle \frac{3\cos\theta}{20} + \frac{\cos 3\theta}{4} \right\rangle$$

and one parameter characterizing the nematic-like uniaxial ordering:

$$Q_{33} = \left\langle \frac{3\cos^2\theta - 1}{2} \right\rangle .$$

Q_{111} is associated to the anisotropic in-plane ordering and Q_{333} is a measure of the up-down asymmetry along the surface normal. Q_{33} is the usual scalar order parameter of the nematic order indicating how well the molecules are aligned along the surface normal. In both liquid crystalline compounds, the value of Q_{111} increases with increasing vapor pressure, while the values of Q_{333} and Q_{33} decrease in 5OCB and increase in 7CB, with in both cases a change of sign for Q_{33} (Fig. 3.8).

3.4 Discussion and conclusions

From the above experimental results, we can draw several conclusions on the anchoring behavior of cyanobiphenyl molecules on phlogopite mica.

Concerning the bulk anchoring directions, we have observed that 5OCB and 7CB orient differently on phlogopite mica. In a dry atmosphere, 5OCB orients perpendicular to the mirror planes of the mica surface, whereas 7CB orients parallel to these planes. If water vapor is added in the atmosphere surrounding the liquid crystal, both liquid

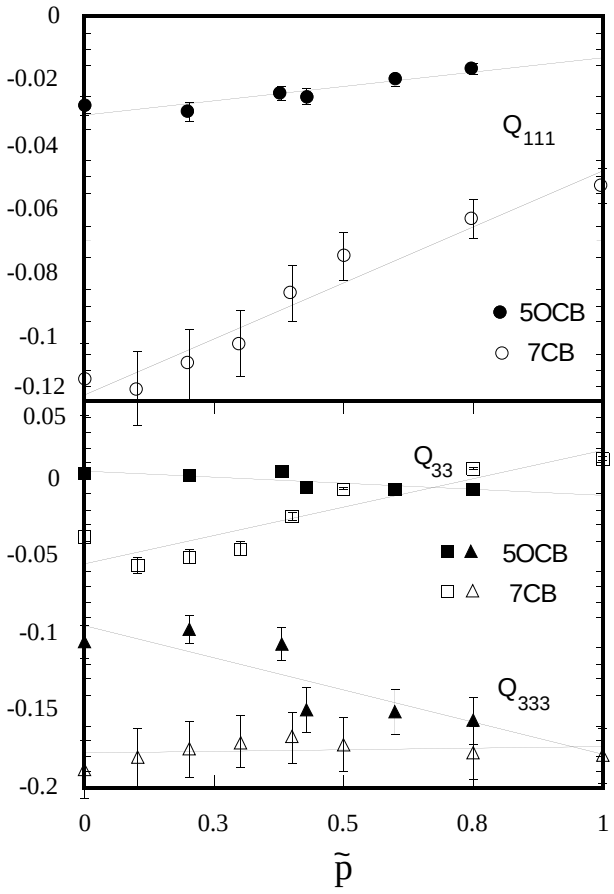

FIGURE 3.8 *The surface order parameters versus the reduced water vapor pressure $\tilde{p}$ for 5OCB and 7CB: (a) Q_{111}, (b) Q_{333} and (c) Q_{33}.*

crystals exhibit an anchoring transition where the bulk reorients in the plane parallel to the substrate. After this transition, 5OCB orients parallel to the surface mirror planes while 7CB orients perpendicular to these planes.

In contrast, the preferred alignment of the molecules in the surface layer in direct contact with the substrate is essentially independent of the liquid crystal and the presence of water vapor. The orientational distributions in the surface layer always exhibits four peaks. One peak is oriented perpendicular to the substrate, the other three peaks are oriented in the surface mirror planes on a cone of opening approximately 58° with respect to the surface normal.

These orientational distributions all have the same symmetry as the substrate surface, namely a three-fold symmetry. This is shown by the measured second-harmonic signal

(Fig. 3.4 and 3.5). However these measurements cannot exclude the presence of a small asymmetry between the peaks of the orientational distribution, which would be hidden by statistical errors in the second-harmonic generation measurements. This possibility can be excluded by considering the fact that both liquid crystals used in our study orient in the bulk perpendicular to the surface preferred molecular orientations under the appropriate water vapor pressure. If there was any asymmetry making one of the peaks in the surface orientational distribution larger than the others, the bulk would necessarily orient along this direction and the bulk anchoring directions would always be parallel to the preferred orientations of the surface molecules.

We find that the difference in the in-plane orientation of the bulk anchoring directions which is observed between 5OCB and 7CB, before and after the anchoring transitions, is not due to a difference in the preferred in-plane orientation of the surface molecules. This is in contrast with to what was found on muscovite mica [37, 51]. By considering the evolution of the order parameter Q_{111} in the surface layer (which is related to the in-plane width of the peaks of the orientational distribution), it seems unlikely that the bulk orientation is affected by the in-plane distribution of the surface molecules: Q_{111} increases with increasing water vapor pressure in both 7CB and 5OCB, while the bulk anchoring directions vary in the opposite ways in these two compounds. Such an opposite behavior of 5OCB and 7CB is found in the evolution of the two order parameters Q_{333} and Q_{33} characterizing the tilt distribution of the surface molecules. This strongly suggests that the in-plane orientation of the bulk director is determined by the tilt distribution of the surface molecules. In particular, the in-plane rotation of the bulk orientation occurring at the anchoring transition induced by addition of water vapor appears to be driven by changes in the surface tilt distribution.

In the next chapter, we present a model based on an extension of the Landau- de Gennes theory that confirms this conjecture. Such an in-plane reorientation of anchoring directions driven by a change in surface tilt angle has also be found in theoretical calculations based on a microscopic model of liquid crystals [62]. J. Chakrabarti and B. Mulder have calculated the preferred bulk orientation of a slab of liquid crystal in contact with a substrate having a threefold symmetry. They use a generalized Lebwohl-Lasher lattice model [63, 64] in which the potential of the interaction of two molecules

making an angle γ is a linear combination of $P_2(\cos\gamma)$, $P_4(\cos\gamma)$ and $P_6(\cos\gamma)$, where P_n is the Legendre polynomial of order n. They impose the molecules at the surface to take one of three equivalent orientations deduced from each other by a three-fold axis.

They find that for correctly chosen values of the interaction parameters, the in-plane orientation of the bulk director rotates by 90° for a critical value Q_{33}^c of Q_{33}.

4 Anchoring on Phlogopite Mica: Theory

In this chapter we develop a theoretical model accounting for our experimental observations of the anchoring behavior of cyanobiphenyl liquid crystals on phlogopite mica presented in chapter 3. Starting from these observations, we derive a possible anchoring mechanism by which the bulk liquid crystal adopts the observed definite anchoring directions in the plane parallel to the surface. We then formalize this mechanism by extending the Landau-de Gennes theory to take into account the specific ordering induced by the substrate close to its surface.

4.1 Principles of our model

On the one hand, the second-harmonic generation experiments have shown that the orientational ordering in the surface layer of molecules in contact with the mica surface exhibits the same symmetry as the substrate, namely a threefold symmetry. On the other hand, the orientational ordering of the bulk nematic liquid crystal is uniaxial. There are therefore two components of the molecular orientational order which play a role at the interface: the nematic ordering and the surface-induced threefold ordering. The threefold ordering disappears as one moves away from the surface layer into the bulk. The degree of nematic order is low in the surface layer, as shown by the low values of the surface order parameter Q_{33} (Fig. 3.8); this nematic order grows as one moves into the bulk.

The director in the bulk of the liquid crystal has three preferred orientations parallel to the substrate surface, either parallel or perpendicular to the mirror planes of this surface (depending on the system considered). However in the surface layer the in-plane symmetry of the orientational order imposes the director to be perpendicular to

the substrate surface. This means that the boundary conditions of the nematic order are isotropic in the plane. Therefore the nematic order cannot orient its director in a particular in-plane direction by itself, as it grows in the interfacial region. It needs to get its orientation from the only source of anisotropy in the boundary conditions, which is the component of the order with a threefold symmetry. This implies that the nematic and the threefold component of the orientational order have to be coupled. Considering the correlation that we find experimentally between the tilt distribution of the molecules in the surface layer and the in-plane orientation of the bulk director, this coupling between nematic and threefold orientational order must be such that changes in the surface tilt distribution can induce an in-plane reorientation of the bulk director.

In the following sections, we model this anchoring mechanism and the evolution of the orientational order from the surface layer towards the bulk using a Landau type of description. We introduce two different order parameters describing the two different types of ordering involved in the anchoring process. These order parameters characterize the degree of ordering as well as the overall orientation of the corresponding orientational distributions. They are therefore tensors, of the second rank for the nematic order (Eq. 4.1) and of the third rank for the threefold order (Eq. 4.10).

The evolution of the orientational order in the interfacial region is determined by the set of trajectories of the order parameters for which the free energy is minimal. We use an expansion of the free energy of the system in these order parameters of the following form: $F_{\text{tot}} = F_2 + F_3 + F_C$. F_2 is the contribution associated to the nematic ordering, given by the Landau-de Gennes theory [65] (see Eq. 4.5). F_3 is the contribution associated with the threefold ordering. We write it as a development in the third-rank order parameter tensor in the spirit of the Landau-de Gennes free energy (Eq. 4.13). The effect of the threefold ordering on the nematic order is taken into account by introducing the coupling term F_C written as a contraction of the two considered order parameter tensors (Eq. 4.20). The influence of the coupling term F_C on the evolution of the nematic and threefold order is considered to be small. In our calculations we therefore treat the evolution of these different types of order independently (in section 4.2 and 4.3 for the nematic and threefold order respectively) and the coupling term as a perturbation (section 4.4).

4.2 Evolution of the nematic ordering

To describe the nematic order in the framework of the Landau-de Gennes theory, we define the $z-$dependent order parameter tensor [65]:

$$Q_{ij}(z) = \left\langle \frac{1}{2}(3\xi_i\xi_j - \delta_{ij}) \right\rangle = \frac{1}{2}\int 3\xi_i\xi_j f(\theta,\phi,z)d\Omega - \delta_{ij}, \tag{4.1}$$

where $\hat{\boldsymbol{\xi}}$ is the molecular orientation $(-\cos\phi\sin\theta, \sin\phi\sin\theta, \cos\theta)$, $f(\theta,\phi,z)$ is the distribution of these molecular orientations at distance z from the surface, and $d\Omega = \sin\theta d\theta d\phi$ is an elementary solid angle. We choose for convenience the frame of reference $(\hat{\mathbf{x}}\hat{\mathbf{y}}\hat{\mathbf{z}})$ in such a way that the director stays in the $\hat{\mathbf{x}}\hat{\mathbf{z}}$ plane. In that case Q_{ij} can be written as:

$$\begin{bmatrix} -Q_{22}-Q_{33} & 0 & Q_{13} \\ 0 & Q_{22} & 0 \\ Q_{13} & 0 & Q_{33} \end{bmatrix} \tag{4.2}$$

In the bulk this order parameter has the following form:

$$\begin{bmatrix} \frac{Q_b(1-3\cos 2\Theta)}{4} & 0 & \frac{3Q_b\sin 2\Theta}{4} \\ 0 & -\frac{Q_b}{2} & 0 \\ \frac{3Q_b\sin 2\Theta}{4} & 0 & \frac{Q_b(1+3\cos 2\Theta)}{4} \end{bmatrix} \tag{4.3}$$

where Θ is the angle between the bulk director and the $z-$axis perpendicular to the substrate surface, and Q_b is the bulk scalar order parameter (approximately 0.6). At the surface Q_{ij} takes the form:

$$\begin{bmatrix} -\frac{Q_{33}|_{z=0}}{2} & 0 & 0 \\ 0 & -\frac{Q_{33}|_{z=0}}{2} & 0 \\ 0 & 0 & Q_{33}|_{z=0} \end{bmatrix}. \tag{4.4}$$

In this case, the director is perpendicular to the surface.

The Landau-de Gennes free energy density associated with the nematic ordering can be written as [65]:

$$F_2(z) = \sum_{i,j=1}^{3}\left[\frac{A_q}{2}(Q_{ij}-Q_{b,ij})^2 + \frac{l_1}{2}\left(\frac{\partial Q_{ij}}{\partial z}\right)^2 + \frac{l_2}{2}\left(\frac{\partial Q_{i3}}{\partial z}\right)^2\right]. \tag{4.5}$$

This free energy density is minimal when $Q_{ij} = Q_{b,ij}$ and $\partial Q_{ij}/\partial z = 0$, i.e. for a uniformly ordered bulk. It is non-zero only in the interfacial region; its integration over the semi-infinite space occupied by the liquid crystal ($z < 0$) yields the interfacial energy.

We insert equations (4.2) and (4.3) in the free energy expansion (4.5) and perform for convenience the substitution $g(z) = 2Q_{22}(z) + Q_{33}(z)$. We also introduce new constants which are related to the characteristic decay lengths of the components Q_{ij}:

$$\xi_1 = \sqrt{\frac{l_1}{A_q}}, \tag{4.6a}$$

$$\xi_2 = \sqrt{\frac{3l_1 + 2l_2}{3A_q}} \tag{4.6b}$$

$$\xi_3 = \sqrt{\frac{2l_1 + l_2}{2A_q}}. \tag{4.6c}$$

For numerical calculations we use the same values for the constants l_1, l_2 and A_q as in [50]: $l_1/l_2 = 2/5$ and $A_q/l_2 = .01\text{nm}^{-2}$. $F_2(z)$ can now be written as:

$$\begin{aligned}\frac{F_2(z)}{A_q} = {} & \frac{3}{4}Q_b^2 - \frac{3}{2}Q_{13}(z)Q_b \sin 2\Theta + Q_{13}(z)^2 + Q'_{13}(z)^2\xi_3^2 \\ & - \frac{3Q_b}{8}(1 + 3\cos 2\Theta)Q_{33}(z) + \frac{3Q_{33}(z)^2}{4} + \frac{3Q'_{33}(z)^2}{4}\xi_2^2 \\ & + \frac{3}{8}Q_b(1 - \cos 2\Theta)g(z) + \frac{g(z)^2}{4} + \frac{g'(z)^2}{4}\xi_1^2.\end{aligned} \tag{4.7}$$

By solving the corresponding Euler-Lagrange equations with as boundary conditions equations (4.3) and (4.4) for respectively the bulk ($z = -\infty$) and the surface layer ($z = 0$), we find:

$$Q_{13}(z) = -\frac{3Q_b}{4}(\exp[z/\xi_3] - 1)\sin 2\Theta, \tag{4.8a}$$

$$Q_{33}(z) = \exp[z/\xi_2]Q_{33}|_{z=0} + \frac{Q_b}{4}(1 - \exp[z/\xi_2])(1 + 3\cos 2\Theta), \tag{4.8b}$$

$$g(z) = \frac{3Q_b}{2}(\exp[z/\xi_1] - 1)\sin^2\Theta. \tag{4.8c}$$

From this z-dependence of Q_{ij}, we can calculate the interfacial energy $\mathcal{F}_2$ whose minima correspond to the anchoring directions:

$$\begin{aligned}\mathcal{F}_2 = \int_{-\infty}^{0} \frac{F_2}{A_q} dz \;\; = \;\; & \left\{ \frac{27Q_b^2}{128}\xi_1 + \frac{33Q_b^2}{128}\xi_2 - \frac{3Q_bQ_{33}|_{z=0}}{8}\xi_2 + \frac{3(Q_{33}|_{z=0})^2}{4}\xi_2 \right. \\ & + \frac{9Q_b^2}{32}\xi_3 + \left(-\frac{9Q_b^2}{32}\xi_1 + \frac{9Q_b^2}{32}\xi_2 - \frac{9Q_bQ_{33}|_{z=0}}{8}\xi_2 \right) \cos 2\Theta \\ & \left. + \left(\frac{9Q_b^2}{128}\xi_1 + \frac{27Q_b^2}{128}\xi_2 - \frac{9Q_b^2}{32}\xi_3 \right) \cos 4\Theta) \right\} \end{aligned} \tag{4.9}$$

A contour plot of $\mathcal{F}_2$ *versus* the surface scalar order parameter $Q_{33}|_{z=0}$ and the bulk tilt Θ shows that the preferred orientations of the director are parallel ($\Theta = \pi/2$) or perpendicular ($\Theta = 0$) to the surface depending on $Q_{33}|_{z=0}$ (Fig. 4.1). The bulk director is parallel to the surface when the stability condition $\frac{\partial^2 F(\Theta, Q_{33}|_{z=0})}{\partial \Theta^2}|_{\Theta=\pi/2} > 0$ is satisfied, which means that $Q_{33}|_{z=0} < Q_b(\frac{2\xi_3 - \xi_2 - \xi_1}{2\xi_2}) \approx 0.0676$. Such a first-order anchoring transition in which the bulk tilt angle varies from $\frac{\pi}{2}$ to 0 as the surface order parameter $Q_{33}|_{z=0}$ increases from negative to positive has also been found in theoretical calculations an simulations performed with a Lebwohl-Lasher lattice model [66].

We have found experimentally that $Q_{33}|_{z=0}$ is always smaller than 0.02 (see Fig. 3.8); this means that the planar anchoring is stable, which corresponds to the experimental observation. In the following we consider only the case $\Theta = \pi/2$.

4.3 Evolution of the threefold ordering

We proceed with the evolution of the threefold ordering as with the nematic ordering. For this, we need an order parameter describing this type of ordering and terms in the free energy which determine the evolution of the components of this order parameter as a function of z. As order parameter we take a traceless symmetric third-rank tensor defined as:

$$Q_{ijk}(z) = \int [\xi_i\xi_j\xi_k - 1/5(\xi_i\delta_{jk} + \xi_j\delta_{ik} + \xi_k\delta_{ij})] f(\theta, \phi, z) d\Omega. \tag{4.10}$$

$Q_{ijk}|_{z=0}$ has to satisfy the threefold symmetry of the surface layer. Moreover there is no spontaneous symmetry breaking away form the surface and thus the tensor $Q_{ijk}(z)$

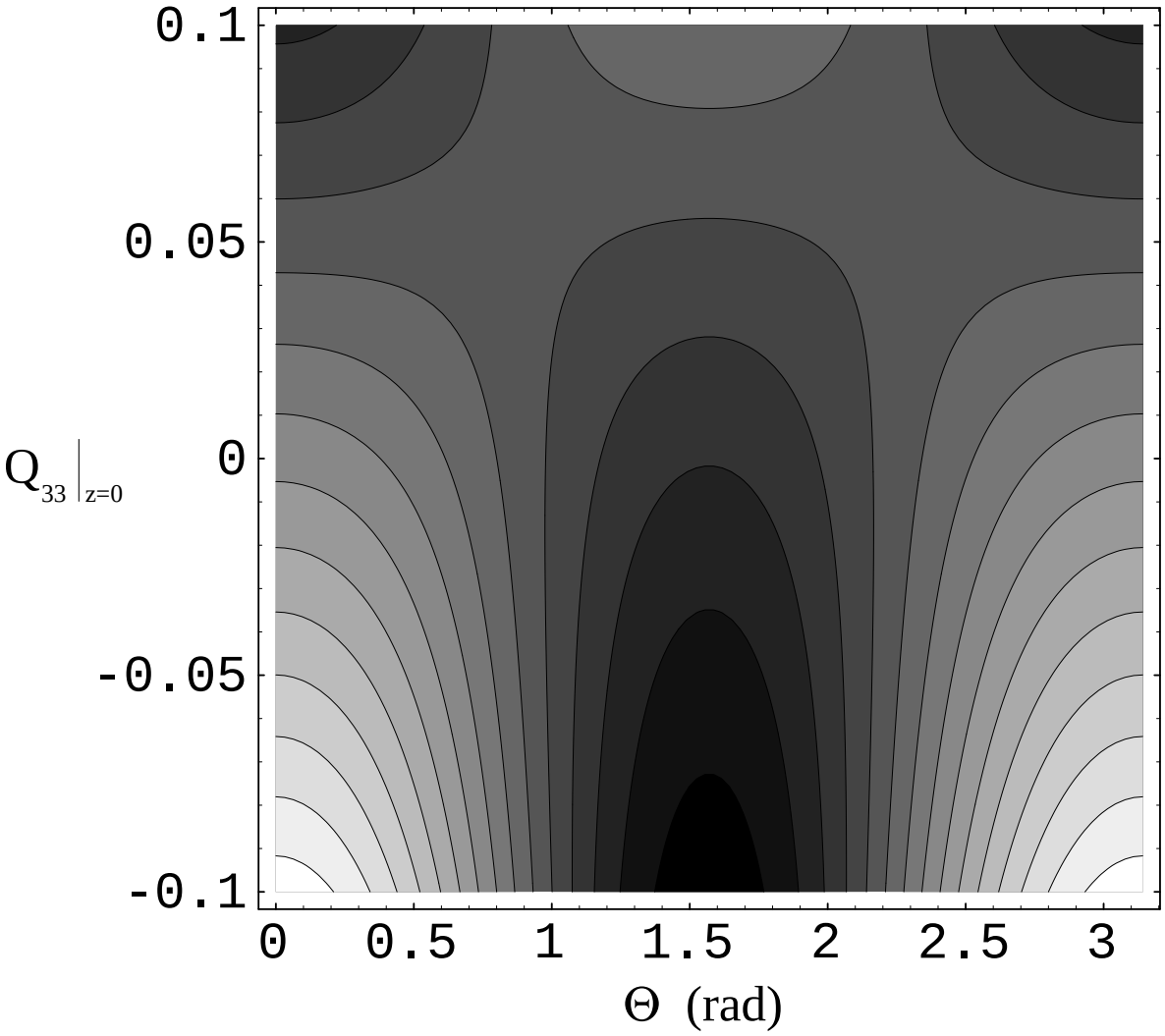

FIGURE 4.1 *Contour plot of the contribution $\mathcal{F}_2$ to the interfacial energy as a function of the surface scalar order parameter $Q_{33}|_{z=0}$ and the angle Θ of the bulk director with respect to the $z-$axis. The darker regions correspond to a higher free energy than the whiter regions.*

conserves the threefold symmetry it has in the surface layer for any z[1]. This threefold symmetry reduces the number of independent non-vanishing components of Q_{ijk} to three:

[1] We have also calculated the evolution of the tensor Q_{ijk} in the general case without imposing *a priori* a threefold symmetry at any z. As expected if we impose on this general solution the boundary conditions at $z = 0$ with the threefold symmetry of the surface layer, the tensor Q_{ijk} conserves this threefold symmetry for any z.

$$Q_{122}(z) = -Q_{111}(z) = -\left\langle \frac{\cos 3\phi \sin^3\theta}{4} \right\rangle \tag{4.11a}$$

$$Q_{222}(z) = -Q_{112}(z) = -\left\langle \frac{\sin 3\phi \sin^3\theta}{4} \right\rangle \tag{4.11b}$$

$$Q_{223}(z) = Q_{113}(z) = -Q_{333}(z)/2 = -\left\langle \frac{3\cos\theta}{40} + \frac{\cos 3\theta}{8} \right\rangle \tag{4.11c}$$

$Q_{122}(z)$ and $Q_{222}(z)$ describe the anisotropy in the plane and depend on the angle Ψ between the $\hat{\boldsymbol{x}}\hat{\boldsymbol{z}}$ plane containing the director and one of the mirror planes σ of the substrate surface. These components can be written as:

$$Q_{122}(z) = \cos 3\Psi h(z) \tag{4.12a}$$

$$Q_{222}(z) = -\sin 3\Psi h(z). \tag{4.12b}$$

We construct an expansion of the free energy density as a function of Q_{ijk} in a way similar to the Landau-de Gennes expansion in the second-rank nematic order parameter[2]:

$$F_3(z) = \sum_{i,j,k=1}^{3} \left[\frac{A_1}{2}(Q_{ijk})^2 + \frac{\lambda_1}{2}\left(\frac{\partial Q_{ijk}}{\partial z}\right)^2 + \frac{\lambda_2}{2}\left(\frac{\partial Q_{ij3}}{\partial z}\right)^2 \right]. \tag{4.13}$$

This free energy density is minimal for an uniformly absent threefold ordering ($Q_{ijk} = \partial Q_{ijk}/\partial z = 0$).

We introduce the decay lengths of this ordering:

$$\xi_4 = \sqrt{\lambda_1/A_1} \tag{4.14}$$

$$\xi_5 = \sqrt{(5\lambda_1 + 3\lambda_2)/5A_1} \tag{4.15}$$

Because the evolution of this type of ordering has not been studied before, we have no guess values for these characteristic lengths. These lengths however are expected to be much shorter than the decay lengths of the nematic order, since this surface-induced ordering does not normally occur in nematic liquid crystals.

[2]In principle other gradient terms should be added to our expression of F_3. However, each of these terms is associated with an unknown coefficient. Since we focus on the effect of the coupling between nematic and threefold order, we keep the number of gradient terms (and therefore unknown parameters) limited.

Using equations (4.11) and (4.12) and the decay lengths ξ_4 and ξ_5 (4.14 and 4.15), we can write the free energy as:

$$\frac{F_3(z)}{A_1} = 2\left[h(z)^2 + \xi_4^2 h'(z)^2\right] + 5\left[Q_{223}(z)^2 + \xi_5^2 Q'_{223}(z)^2\right] \tag{4.16}$$

Minimizing this free energy and imposing the boundary conditions on Q_{ijk} at the substrate surface gives the solutions:

$$h(z) = Q_A^{(3)} \exp[z/\xi_4], \tag{4.17a}$$

$$Q_{223}(z) = -\frac{Q_{333}|_{z=0}}{2} \exp[z/\xi_5]. \tag{4.17b}$$

where we define $Q_A^{(3)} = \sqrt{Q_{122}|_{z=0}^2 + Q_{222}|_{z=0}^2}$.

4.4 Coupling between threefold and nematic order

So far, we have considered the threefold and nematic orderings to evolve independently of each other. In this section, we add an interaction of the nematic ordering with the threefold ordering, by introducing a coupling term in the free energy. Such a coupling term is a rotationally invariant contraction of the order parameter tensors associated with different types of ordering. One can construct many coupling terms with tensors of the second and third rank. The question arises which term gives a Ψ-dependence of the free energy expansion. The lowest order terms not involving any gradients and showing a Ψ-dependence are:

$$\sum_{i,j,k,l,m,n=1}^{3} Q_{ijk} Q_{lmn} Q_{ij} Q_{kl} Q_{mn}, \tag{4.18a}$$

$$\sum_{i,j,k,l,m,n=1}^{3} Q_{ijk} Q_{lmn} Q_{il} Q_{jm} Q_{kn} \tag{4.18b}$$

where summation over repeated indices is assumed. Both terms have, apart from a constant term, a Ψ-dependence of the interfacial energy of the form:

$$\int_{-\infty}^{0} -\frac{1}{2} h(z)^2 g(z)^3 dz \cos 6\Psi = C_1 \cos 6\Psi. \tag{4.19}$$

$g(z)$ and $h(z)$ have been defined in Eq. 4.8c and 4.17a respectively. The extrema of this Ψ-dependent term lie at $\Psi = 0$ and $\Psi = \pi/6$, with a period of $\pi/3$. Whether one of the extrema is a minimum (corresponding to an anchoring direction) or a maximum is

determined by the sign of the coefficient C_1. For a negative (resp. positive) C_1 this coupling term leads to anchoring directions parallel (resp. perpendicular) to the mirror planes of the substrate.

The experimentally observed anchoring transitions correspond to a change of the location of the minima of the coupling term with the orientational order in the surface layer. With the present term, this can only be obtained if the coefficient C_1 changes sign as a function of the surface order. This coefficient C_1, however, is quadratic in $h(z)$ and cubic in $g(z)$. Since the latter is independent of the surface order, C_1 cannot change sign as a function of the surface order: this coupling term cannot give rise to any anchoring transition. The terms given by Eq. 4.18 are obviously not relevant for the anchoring behavior we observe and can thus be neglected.

We consider therefore higher order coupling terms:

$$\sum_{i,j,k,l,m,n,p=1}^{3} Q_{ijk}Q_{lmn}Q_{ij}Q_{kl}Q_{mp}Q_{np}, \tag{4.20a}$$

$$\sum_{i,j,k,l,m,n,p=1}^{3} Q_{ijk}Q_{lmn}Q_{il}Q_{jm}Q_{kp}Q_{np}. \tag{4.20b}$$

Performing the summations (4.20) and not considering the Ψ-independent terms yields for both expressions:

$$\int_{-\infty}^{0} \frac{1}{2} Q_{33}(z) h(z)^2 g(z)^3 dz \cos 6\Psi = C_2 \cos 6\Psi, \tag{4.21}$$

The amplitude of $\cos 6\Psi$ in (4.21) is determined, apart from the factor $h(z)^2 g(z)^3$, by the component $Q_{33}(z)$ of the nematic order parameter tensor. This factor $Q_{33}(z)$ can change the sign of C_2 if $Q_{33}|_{z=0}$ varies and therefore can give rise to the anchoring transitions observed experimentally.

Performing the integration in (4.21) yields:

$$\begin{aligned} C_2 \;=\; & \frac{27}{16} Q_b^3 (Q_A^{(3)})^2 \left\{ \frac{Q_b \xi_4}{4} + \frac{3 Q_b \xi_1 \xi_4}{4(\xi_1 \xi 4)} - \frac{3 Q_b \xi_1 \xi_4}{2(\xi_1 \xi 4)} \right. \\ & - \frac{(Q_b + 2Q_{33}|_{z=0})\xi_2 \xi_4}{2(2\xi_2 + \xi_4)} - \frac{3(Q_b + 2Q_{33}|_{z=0})\xi_1 \xi_2 \xi_4}{2(2\xi_1 \xi_2 + \xi_1 \xi_4 + \xi_2 \xi_4)} \\ & \left. - \frac{3(Q_b + 2Q_{33}|_{z=0})\xi_1 \xi_2 \xi_4}{2(2\xi_1 \xi_2 + \xi_1 \xi_4 + 2\xi_2 \xi_4)} + \frac{(Q_b + 2Q_{33}|_{z=0})\xi_1 \xi_2 \xi_4}{2(2\xi_1 \xi_2 + \xi_1 \xi_4 + 3\xi_2 \xi_4)} \right\} \end{aligned} \tag{4.22}$$

Since ξ_4 is expected to be much smaller than ξ_1 and ξ_2, we perform a Taylor expansion of (4.22) in ξ_4/ξ_i (i=1,2). After factorization, one gets:

$$C_2 = \frac{27}{16} Q_b^3 (Q_A^{(3)})^2 \frac{3\xi_4^4}{8\xi_1^3} \left[Q_b \frac{\xi_4}{\xi_2} + Q_{33}|_{z=0} (-1 + 3\frac{\xi_4}{\xi_1} + 2\frac{\xi_4}{\xi_2}) + \mathcal{O}[\xi_4^2] \right]. \tag{4.23}$$

The first factor in (4.23) cannot change the sign of C_2, however the second factor does change sign for a certain value Q_{33}^c of $Q_{33}|_{z=0}$ with:

$$Q_{33}^c = Q_b \xi_1 \xi_4 / (\xi_1 \xi_2 - 3\xi_2 \xi_4 - 2\xi_1 \xi_4) \approx Q_b \xi_4 / \xi_2 \tag{4.24}$$

The above coupling term gives thus rise to a reorientation of the bulk director in the plane of the substrate driven by an evolution of the nematic order parameter $Q_{33}|_{z=0}$ around Q_{33}^c. Values of $Q_{33}|_{z=0}$ below Q_{33}^c result in a director parallel to the surface mirror planes. Above this critical value Q_{33}^c the director orients perpendicular to the mirror planes.

Using our experimental results, we can now estimate the range of ξ_4. Since we find experimentally that $Q_{33}|_{z=0}$ is always smaller than 0.02 (fig.3.8), Q_{33}^c must also be smaller than this limit, which means $0 \leq \xi_4 \leq Q_{33}^c \xi_2 / Q_b \approx 0.4$nm (taking $\xi_2 \approx 10$nm and $Q_b = 0.6$). ξ_4 is indeed much smaller than ξ_2; it corresponds to one layer of molecules oriented parallel to the surface. As was anticipated in section 4.3, the surface-induced threefold order decays over a much smaller length scale than the nematic ordering.

4.4.1 Evolution of the orientational distribution in the interfacial region

In the former sections, we have determined the evolution of the order parameters of the nematic and threefold ordering in the interfacial region. The components of these order parameters are simply related to the coefficients of the expansion of the orientational distribution into spherical harmonics:

$$f(\theta, \phi, z) = \sum_{l=0}^{\infty} \sum_{m=-l}^{l} \langle Y_l^m(z) \rangle Y_l^m(\theta, \phi). \tag{4.25}$$

From our calculations, we know the spatial evolution of the following coefficients corresponding to $l = 2, 3$ (the other coefficients $\langle Y_l^m(z)\rangle|_{l=2,3}$ are zero):

$$\langle Y_2^0(z)\rangle = \sqrt{\frac{5}{4\pi}} Q_{33}(z) \tag{4.26a}$$

$$\langle Y_2^{-1}(z)\rangle = -\langle Y_2^1(z)\rangle = \frac{1}{6}\sqrt{\frac{30}{\pi}} Q_{13}(z) \tag{4.26b}$$

$$\langle Y_2^{-2}(z)\rangle = \langle Y_2^2(z)\rangle = -\frac{1}{6}\sqrt{\frac{30}{\pi}}\Big(Q_{22}(z) + \frac{Q_{33}(z)}{2}\Big) \tag{4.26c}$$

$$\langle Y_3^0(z)\rangle = \frac{35}{4\sqrt{7\pi}} Q_{333}(z) \tag{4.26d}$$

$$\langle Y_3^{-3}(z)\rangle = -\frac{1}{2}\sqrt{\frac{35}{\pi}}\Big(Q_{122}(z) + iQ_{222}(z)\Big) \tag{4.26e}$$

$$\langle Y_3^3(z)\rangle = \frac{1}{2}\sqrt{\frac{35}{\pi}}\Big(Q_{122}(z) - iQ_{222}(z)\Big) \tag{4.26f}$$

Since we do not know the other coefficients $\langle Y_l^m(z)\rangle$, we can only calculate that part of the expansion of $f(\theta, \phi, z)$ corresponding to $l = 2, 3$, which we will denote $\tilde{f}$. $\tilde{f}$ contains however the two most important components of the ordering for the anchoring behavior we want to describe. Since $\tilde{f}$ is not the complete distribution function, it can take negative values. To facilitate a spherical representation of $\tilde{f}$, we add for every z a positive constant to $\tilde{f}(\theta, \phi, z)$ in such a way that the minimum of $\tilde{f}(\theta, \phi, z)$ is zero.

As an example of how $\tilde{f}$ evolves with z in the case of bulk anchoring directions parallel and perpendicular to the preferred orientations of the surface molecules, Fig. 4.2 shows the evolution of $\tilde{f}$ in 7CB for partial vapor pressures of $\tilde{p} = 0.2$ and $\tilde{p} = 0.75$. For $z = 0$ Fig. 4.2 shows a distribution which resembles the distribution $f(\theta, \phi)$ determined with the maximum entropy method from the second-harmonic generation measurements Fig. 3.7 with the difference that the present plot shows only the part of the distribution corresponding to $\langle Y_l^m(z)\rangle$ components with $l = 2, 3$.

4.4.2 Conclusions

Our theoretical description of the behavior of nematic liquid crystals on a surface with a threefold symmetry leads to the following predictions. The conventional Landau-de Gennes model of the nematic order predicts that planar anchoring of the bulk nematic phase occurs if the scalar nematic order parameter $Q_{33}|_{z=0}$ at the surface is smaller

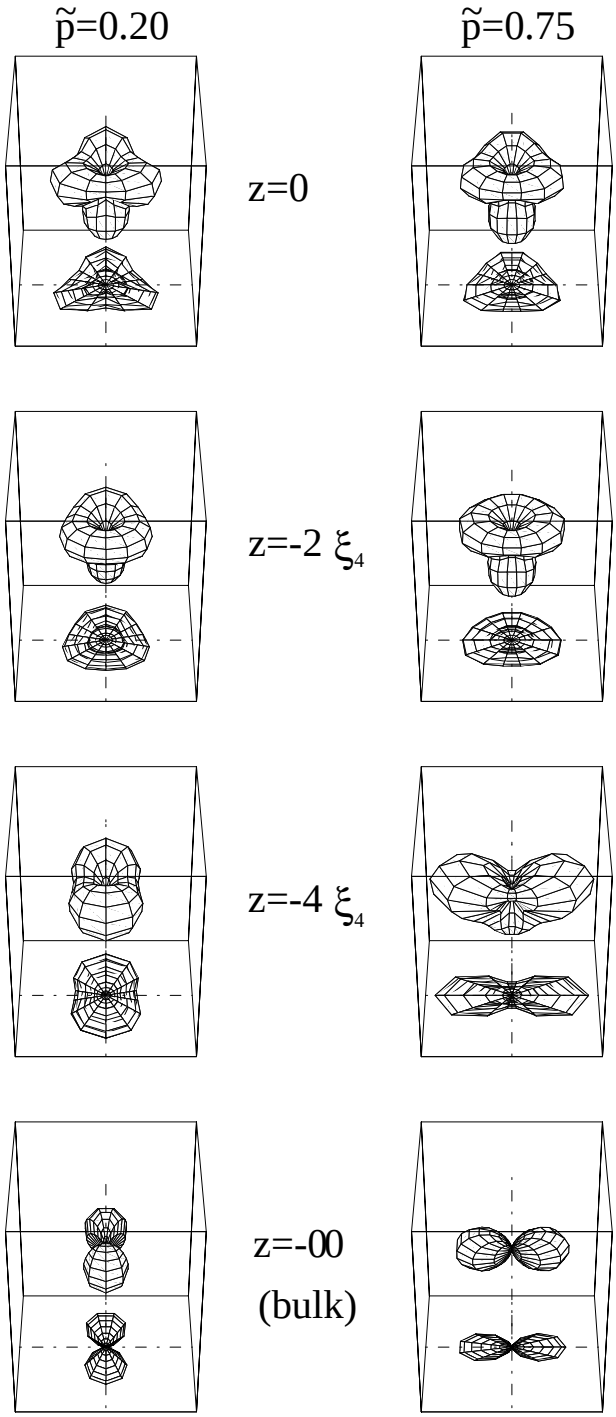

FIGURE 4.2 *Evolution of the function* $\tilde{f}$ *versus the distance* z *with respect of the surface* $(z = 0, -2\xi_4, -4\xi_4, -\infty)$ *for a bulk anchoring direction (a) parallel, and (b) perpendicular to a mirror plane* σ*.* ξ_4 *has been set equal to* $0.016\xi_2$*.*

than 0.07. For values of $Q_{33}|_{z=0}$ larger than this limit, homeotropic anchoring of the bulk phase is predicted. This is in agreement with our experimental observations as the experimentally measured surface order parameter $Q_{33}|_{z=0}$ did not exceed this value of 0.07 and only planar anchorings were observed. However this conventional model does not predict any preferred in-plane orientation for the bulk nematic liquid crystal. When the surface-induced threefold ordering is taken into account and coupled to the nematic ordering, our calculations show that the bulk director has the choice between three energetically equivalent in-plane orientations: the anchoring is tristable as observed experimentally.

The bulk orientation can be either parallel or perpendicular to the surface mirror planes. Which case occurs is determined by the value of $Q_{33}|_{z=0}$. If $Q_{33}|_{z=0}$ decreases from a value larger than a certain threshold Q_{33}^c to a value smaller than Q_{33}^c, a first-order anchoring transition is induced at which the bulk director changes from an orientation perpendicular to an orientation parallel to the mirror planes of the mica surface: this is what we have observed experimentally in 5OCB. In the case $Q_{33}|_{z=0}$ increases from below Q_{33}^c to above Q_{33}^c, the reverse anchoring transition is induced, which is what we have observed in 7CB. The value Q_{33}^c is related to the decay length ξ_4 of the threefold ordering. From the experimentally determined value of Q_{33}^c ($Q_{33}^c \leq 0.02$) we can estimate an upper limit for this decay length: $0 \leq \xi_4 \leq 0.4$nm.

The agreement of our theoretical results with our experimental results shows the validity of the anchoring mechanism we had postulated in section 4.1. We can generalize it and propose an anchoring mechanism by which a substrate with a threefold symmetry or higher can induce several definite in-plane anchoring directions on a bulk liquid crystal. This mechanism involves two components of the orientational order: the uniaxial nematic order existing in the bulk of the liquid crystal, and the surface-induced order with the symmetry of the substrate surface found in the surface layer of liquid crystal molecules. This surface-induced order extends over a certain distance from the surface which is significantly shorter than the coherence length of the nematic ordering. Because of the surface symmetry, the boundary conditions on the nematic order at the surface are isotropic in the plane. The nematic order gets oriented in the surface plane by a coupling to the surface-induced order that exists over the narrow interfacial region where both

the nematic and surface-induced orders are present. This anchoring mechanism can be formalized by extending the Landau-de Gennes theory to take into account the surface-induced component of the orientational order and its coupling to the nematic order.

In the framework of a microscopic model based on intermolecular interactions, the surface-induced order can be imposed by adding a potential of interaction between the surface molecules and the substrate. The range of the interaction potential is then equivalent to the decay length ξ_4 of the threefold ordering in the Landau-de Gennes type of calculation.

5 Poling of Thin Films

In this chapter we describe the effect of a DC electric field applied on thin films of liquid crystals. We first predict the expected polar ordering induced by the field and the corresponding second-harmonic signal generated by a poled film. Comparing these predictions with experimental measurements show that the electric field can induce a polar ordering if the molecules form polar clusters, which have a higher dipole moment than the individual molecules. Our measurements also allow us to draw some conclusions on the anchoring of liquid crystal molecules on fused quartz.

5.1 Introduction

Most electro-optical applications of liquid crystals are based on the switching of the orientation of the liquid crystal between different states under the effect of an electric field (see e.g. liquid crystal displays, Fig. 1.1). The macroscopic observation of this switching phenomenon proves that the average alignment of the bulk molecules changes orientation under the effect of an electric field. On the other hand, the director has a preferred orientation close to the surfaces (the anchoring direction) arising from the orientation of the molecules in the surface layer by their interaction with the surface [17, 19]. This means that the reorientation of the bulk of the liquid crystal is in competition with the orienting effect of the surfaces. This raises several questions:

1. *Do the molecules in contact with the substrate also reorient if the bulk reorients and how much energy does it cost?* The questions have indirectly been addressed by measurements of the anchoring energy associated with reorientations of the director in the bulk [18, 19, 67]. This macroscopic anchoring energy is however

a property of the whole interfacial region between the surface and the bulk (see section 1.3). We need rather to measure the microscopic anchoring energy of the molecules in the surface layer.

2. *Are the molecules adsorbed onto the substrate and what is the energy associated with this adsorption?* There have been several experimental observations showing that once a liquid crystal has taken a given orientation on a substrate, this orientation becomes favored with respect to the others. For instance, an azimuthal anchoring strength can be measured on isotropic substrates after that the bulk is aligned by an external field [68, 69]. This alignment is also retained if the sample is heated well in the isotropic phase and cooled down in the absence of external field [70, 71]. However, if a second external field is applied for a long time (hours) in a different direction than the original orienting field, the surface director slowly rotates (glides) towards the second field[72]. The anchoring strength measured on an undulated substrate was also found[73] to be one order of magnitude larger than expected from the topographic anchoring mechanism proposed by Berreman [74]. These observations suggest that the molecules in the surface layer get adsorbed onto the substrate in the orientation they adopt. The anisotropic part of this adsorption energy provides an additional contribution to the microscopic anchoring energy.
3. *What is the reorientation dynamics of the surface molecules?* How fast do they reorient when a distortion is applied and how fast do they relax towards their equilibrium order when the distortion is removed? This dynamics is expected to be strongly influenced by the adsorption we have just mentioned. There have been very few direct measurements of the mobility of the surface molecules [75], although measurements of the dynamic properties close to interfaces and in strongly confined systems indicate that the surface dynamics is slower than the bulk dynamics (see e.g. [76, 77]).

Addressing these questions at the molecular level requires studying the behavior of molecules in very thin layers when they are forced to reorient away from their equilibrium order. One way to induce such a reorientation is to apply a high DC electric field. This process is used in particular for the poling of side-chain polymer liquid crystals to make

nonlinear optical materials [78, 79]. Electric fields ranging between 1kVmm^{-1} and a few 100kVmm^{-1} are able to induce a polar ordering of the liquid crystalline side-groups (in particular cyanobiphenyl groups) of these polymers. As a result the poled materials generate a second-harmonic signal.

The above formulated questions can be addressed by studying the following model system: a thin liquid crystal film consisting of polar molecules deposited onto the considered substrate in between two electrodes providing an electric field parallel to the substrate. The applied field tends to align the dipoles carried by the molecules along its own orientation, inducing a polar anisotropy in the plane of the substrate. The resulting orientational distribution of the molecules arises from a balance between the anchoring energy of the molecules onto the substrate and the energy of the molecular dipoles in the applied electric field. This orientational distribution gives therefore information on the anchoring energy of the molecules onto the substrate. The time evolution of this distribution when switching the field on and off gives information on the reorientation dynamics of the surface molecules. Since second-harmonic generation is specifically sensitive to polar ordering, it is an ideal tool to measure the degree of electric-field-induced polar ordering of the molecules and its time dependence.

A prerequisite to the analysis of this type of experimental data is the understanding of the effect of the electric field on the orientational order of the liquid crystal molecules and the resulting second-harmonic signal generated by the poled liquid crystal film. We have studied this effect of poling on thin liquid crystal films by taking fused quartz as substrate. This substrate is isotropic in its plane (symmetry $C_{\infty v}$), so that it does not induce a preferred azimuthal orientation of the liquid crystal molecules.

In the following two sections, we derive the expected electric-field-induced order in a thin liquid crystal film (section 5.2) and the corresponding second-harmonic signal (section 5.3). After describing the experimental conditions (section 5.4), we compare the experimental results with the expected behavior (section 5.5). This leads us to the conclusion that the polar units reorienting under the application of a field are not single molecules but clusters of molecules with a polar ordering. Finally we discuss our results both in terms of poling and anchoring properties of fused quartz plates (section 5.6).

5.2 Effect of electric field on molecular orientation

5.2.1 Structure of films

To examine the effect of an electric field on the orientational distribution of liquid crystal molecules in a thin film, we use the following considerations. A film of polar molecules deposited on a substrate can be divided into two parts:

1. *The surface layer*: this is the polar layer of molecules in contact with the substrate. In the absence of electric field, it is known that these molecules preferentially point with their polar head towards the substrate (Fig. 5.1) and make an angle

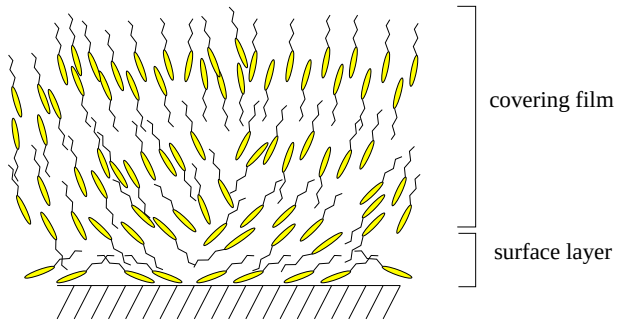

FIGURE 5.1 *Schematic representation of the structure of a liquid crystal film deposited on a substrate in the absence of external field.*

of approximately 70° with respect to the substrate normal [80]. On fused quartz however, they have no preferred azimuthal orientation. If an electric field is applied in the plane of the substrate, it induces an in-plane anisotropy by orienting the molecular dipoles along its own direction. Since in the molecules we have used (cyanobiphenyl) the dipole moment is parallel to the molecular axis, we consider only this case. To calculate the resulting orientational distribution of the surface molecules, we assume that the applied electric field does not modify the tilt of the molecules. This is justified by the experimental results.

2. *The covering film:* this is the rest of the film (Fig. 5.1). In the absence of electric field, this part of the film has a quadrupolar ordering, with as many molecules pointing in one direction as in its opposite. The in-plane distribution is isotropic. To minimize the elastic energy of the film, the tilt of the molecules varies from nearly parallel to the substrate right above the surface layer (planar anchoring)

to perpendicular to the surface at the free surface (homeotropic anchoring). Applying an electric field induces an in-plane anisotropy. It can also modify the tilt distribution of the molecules if it overcomes the elastic energy associated with distortions of the molecular orientation [13]. This will in particular happen for thick films. We can consider two extreme cases: a) The tilt of the molecules is not modified by the field. At each level z in the film, the molecules keep the tilt they have without electric field. b) The tilt of the molecules is completely determined by the electric field; the molecules behave as in bulk.

We also take into account the fact that the orientation of the molecules might be correlated over a number N_p of molecules. This means that the surface layer is N_p molecular layers thick. The covering film can then be seen as a stack of polar layers with alternating up and down polarization, each polar layer being N_p molecular layers thick.

5.2.2 Electric-field-induced orientational order

Using the above considerations, we can calculate the orientational order of the molecules in the different regions of the films as a function of the applied field. This calculation adapts the theory of poling of bulk materials [81, 82] to the case of thin liquid crystal films.

We define the axis $\hat{\boldsymbol{\xi}}$ of a given molecule by its azimuthal angle ϕ and tilt angle θ (Fig. 5.2): $\hat{\boldsymbol{\xi}} = (-\sin\theta\cos\phi, -\sin\theta\sin\phi, \cos\theta)$. The probability of finding a molecule in an elementary solid angle $\sin\theta d\theta d\phi$ is given by $f(\theta,\phi)\sin(\theta)d\theta d\phi$ where $f(\theta,\phi)$ is the orientational distribution of the molecules. f is given by $f(\theta,\phi) = C\exp(-U(\theta,\phi)/kT)$ [83] where $U(\theta,\phi)$ is the free energy of a molecules with spherical coordinates (θ,ϕ). U has two contributions:

$$U(\theta,\phi) = U_{\text{struc}}(\theta,\phi) + U_{\text{elec}}(\theta,\phi). \tag{5.1}$$

U_{elec} is the energy of the molecular dipole $\boldsymbol{\mu}$ in the applied electric field $\boldsymbol{E}$: $U_{\text{elec}}(\theta,\phi) = -\boldsymbol{\mu}\cdot\boldsymbol{E}$. As mentioned in the previous section, the dipole moment of our molecules is directed along their molecular axis[1]: $\boldsymbol{\mu} = \mu\hat{\boldsymbol{\xi}}$. We introduce the ratio $p = \frac{\mu E}{kT}$ of the

[1] We take as convention the dipole oriented from the electro-positive to the electro-negative parts the molecules, i.e. $\boldsymbol{\mu}$ pointing towards the cyanohead of a cyanobiphenyl molecule. In the case when the

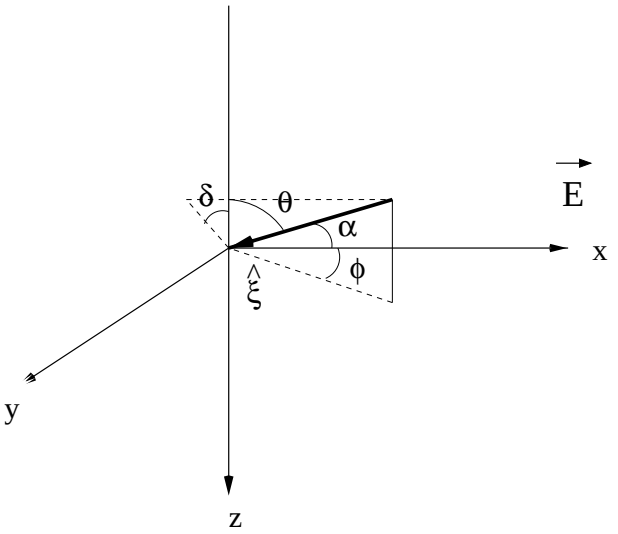

FIGURE 5.2 *Definition of the spherical coordinates* (θ, ϕ) *and* (α, δ) *of the molecular axis* $\hat{\boldsymbol{\xi}}$.

dipolar energy over the thermal energy. U_{elec} can then be written as:

$$\frac{U_{\text{elec}}(\theta, \phi)}{kT} = -p \sin\theta \cos\phi \tag{5.2}$$

U_{struc} is the free energy in the absence of the electric field and is determined by the intrinsic properties of the system. In our case, it contains the anchoring energy at the surfaces and the elastic energy associated to distortions of the molecular orientation. U_{struc} depends on the position of the molecules in the film.

5.2.2.1 *The surface layer* The substrate induces no preferred azimuthal orientation of the molecules; U_{struc} has therefore no dependence on ϕ. Assuming that the tilt of the molecules remains constant and equal to θ_0 (see section 5.2.1), U_{struc} takes the following form:

$$U_{\text{struc}}(\theta_0, \phi) = U_0 \qquad \text{if } \theta = \theta_0 \tag{5.3a}$$

$$U_{\text{struc}}(\theta, \phi) = +\infty \qquad \text{if } \theta \neq \theta_0 \tag{5.3b}$$

reorienting units contain a number $n_c = N_p^3$ of molecules with a polar ordering, $\boldsymbol{\mu}$ should be replaced by $n_c \boldsymbol{\mu}$.

The orientational distribution of the molecules in the surface layer is thus:

$$f_s(\theta_0,\phi) = C_s \exp\left[-\frac{U_0}{kT} + p\sin\theta_0\cos\phi\right] \qquad \text{if } \theta=\theta_0 \tag{5.4a}$$

$$f_s(\theta,\phi) = 0 \qquad \text{if } \theta\neq\theta_0 \tag{5.4b}$$

with

$$\frac{1}{C_s} = \int_0^{\pi}\int_0^{2\pi} f_s(\theta,\phi)\sin\theta d\theta d\phi \tag{5.5}$$

$$= \int_0^{2\pi} \exp\left(-\frac{U_0}{kT}\right)\exp(p\sin\theta_0\cos\phi)d\phi$$

$$= \exp\left(-\frac{U_0}{kT}\right)\sin\theta_0 2\pi I_0(p\sin\theta_0) \tag{5.6}$$

$I_0(X) = \frac{1}{\pi}\int_0^{\pi}\cosh(X\cos\phi)d\phi$ is the modified Bessel function of order 0 [84]. Finally we have:

$$f_s(\theta_0,\phi) = \frac{\exp(p\sin\theta_0\cos\phi)}{2\pi\sin\theta_0 I_0(p\sin\theta_0)} \tag{5.7}$$

5.2.2.2 *The covering film* Case a: Let us first consider the case in which the electric field does not modify the tilt of the molecules in the film. We call h_f the thickness of the covering film, and $\theta_f^a(z)$ the tilt of the molecules at height z in the film. Since the electric field is applied parallel to the substrate surface, there is no polarization in the film along the normal to the surface (z axis). This means that there are as many molecules with a tilt angle $\theta_f^a(z)$ as molecules with a tilt angle $\pi-\theta_f^a(z)$. The orientational distribution $f_f^a(\theta,\phi;z)$ of the molecules located at height z can be derived from $f_s(\theta,\phi)$ calculated in the former section:

$$f_f^a(\theta,\phi;z) = f_s(\theta_f^a(z),\phi) \qquad \text{if } \theta=\theta_f^a(z) \tag{5.8a}$$

$$= f_s(\pi-\theta_f^a(z),\phi) = f_s(\theta_f^a(z),\phi) \qquad \text{if } \theta=\pi-\theta_f^a(z) \tag{5.8b}$$

$$= 0 \qquad \text{if } \theta\neq\theta_f^a(z) \text{ and } \theta\neq\pi-\theta_f^a(z) \tag{5.8c}$$

The expression of $\theta_f^a(z)$ can be obtained from the minimization of the elastic energy of the film with the boundary conditions $\theta_f^a(z_1)=\frac{\pi}{2}$ on the surface layer (planar anchoring)

and $\theta_f^a(z_1 - h_f) = 0$ at the free surface[2] (homeotropic anchoring) [13]:

$$\theta_f^a(z) = \frac{\pi}{2h_f}(z - z_1 + h_f) \tag{5.9}$$

Case b: In the case where the applied electric field is strong enough to impose the tilt of the molecules, U_{struc} vanishes and the orientational distribution of the molecules is the same as in the bulk material [81, 82]. To calculate this distribution, it is convenient to introduce the spherical coordinates (α, δ) with respect to the x axis along the applied field (Fig. 5.2). The molecular axis is then $\hat{\boldsymbol{\xi}} = (-\cos\alpha, -\sin\alpha\sin\delta, \sin\alpha\cos\delta)$. The orientational distribution $f_f^b(\alpha, \delta)$, which is now independent of the height z, is given by:

$$f_f^b(\alpha, \delta) = C_f^b \exp(p\cos\alpha) \tag{5.10}$$

with

$$\begin{aligned} \frac{1}{C_f^b} &= \int_0^{\pi}\int_0^{2\pi} \exp[p\cos\alpha]\sin\alpha d\alpha d\delta \\ &= 4\pi\frac{\sinh p}{p} \\ &= 4\pi i_0(p) \end{aligned} \tag{5.11}$$

$i_0(X) = \sqrt{\frac{\pi}{2X}} I_{\frac{1}{2}}(X)$ is the spherical modified Bessel function of order 0 defined from the modified Bessel function of order $\frac{1}{2}$ [84].

5.3 Second-harmonic generation from a poled liquid crystalline film

Since the thickness of all the films we have studied is at least ten times smaller than the wavelength of light, we consider our films as being infinitely thin. We can therefore apply the theory of second-harmonic generation presented in chapter 2. The second-harmonic signal generated by our films is proportional to the square of the effective susceptibility:

$$\chi_{\text{eff}} = [\hat{\mathbf{e}}(2\omega)\cdot\bar{\mathbf{L}}(2\omega)]\bar{\boldsymbol{\chi}} : [\hat{\mathbf{e}}(\omega)\cdot\bar{\mathbf{L}}(\omega)][\hat{\mathbf{e}}(\omega)\cdot\bar{\mathbf{L}}(\omega)] \tag{5.12}$$

which depends on the nonlinear susceptibility tensor $\bar{\boldsymbol{\chi}}$, the polarization $\hat{\mathbf{e}}(\omega)$ and $\hat{\mathbf{e}}(2\omega)$ of the in-coming and out-going beams and the local field factors $\bar{\mathbf{L}}(\omega)$ and $\bar{\mathbf{L}}(2\omega)$ (see chapter 2). The main contribution to $\bar{\boldsymbol{\chi}}$ is the dipolar term arising from a polar ordering

[2] Remember that the z- axis points towards the substrate (Fig. 5.2).

in the system (section 5.3.1). We examine the other possible contributions in section 5.3.2

5.3.1 The dipolar nonlinear susceptibility tensor $\bar{\boldsymbol{\chi}}$

$\bar{\boldsymbol{\chi}}$ is the sum of a contribution $\bar{\boldsymbol{\chi}}_s$ of the surface layer and a contribution $\bar{\boldsymbol{\chi}}_f$ of the covering film.

5.3.1.1 $\bar{\boldsymbol{\chi}}_s$ *of the surface layer* In the presence of an electric field, this layer exhibits a mirror symmetry with respect to the (xz) plane containing the electric field. Its nonlinear susceptibility tensor $\bar{\boldsymbol{\chi}}_s$ had then six non-zero independent components given by (Eq. 2.2) in chapter 2 and the corresponding expression of χ_{eff} is given by (Eq. 2.5) of the same chapter.

Using the orientational distribution $f_s(\theta, \phi)$ of the molecules in the presence of an electric field (Eq. 5.4 and 5.7 in section 5.2.2.1), the non-zero components of $\bar{\boldsymbol{\chi}}_s$ become:

$$\chi_{s,xxx} = -N_s N_p \alpha^D_{\xi\xi\xi} \sin^3\theta_0 \left\langle \cos^3\phi \right\rangle \tag{5.13a}$$

$$\chi_{s,xyy} = -N_s N_p \alpha^D_{\xi\xi\xi} \sin^3\theta_0 \left\langle \cos\phi \sin^2\phi \right\rangle \tag{5.13b}$$

$$\chi_{s,xzz} = -N_s N_p \alpha^D_{\xi\xi\xi} \cos^2\theta_0 \sin\theta_0 \left\langle \cos\phi \right\rangle \tag{5.13c}$$

$$\chi_{s,zxx} = N_s N_p \alpha^D_{\xi\xi\xi} \cos\theta_0 \sin^2\theta_0 \left\langle \cos^2\phi \right\rangle \tag{5.13d}$$

$$\chi_{s,zyy} = N_s N_p \alpha^D_{\xi\xi\xi} \cos\theta_0 \sin^2\theta_0 \left\langle \sin^2\phi \right\rangle \tag{5.13e}$$

$$\chi_{s,zzz} = N_s N_p \alpha^D_{\xi\xi\xi} \cos^3\theta_0 \tag{5.13f}$$

where we define N_s as the surface density of a molecular monolayer. The moments of the ϕ-distribution appearing in the above equations can be calculated from the identity:

$$\begin{aligned} \left\langle \cos^n\phi \right\rangle &= \int_0^{2\pi} \frac{\exp(p\sin\theta_0\cos\phi)}{2\pi I_0(p\sin\theta_0)} \cos^n\phi d\phi \\ &= \frac{I_n(p\sin\theta_0)}{I_0(p\sin\theta_0)} \end{aligned} \tag{5.14}$$

$I_n(X) = \frac{1}{\pi}\int_0^\pi \exp(X\cos\phi)\cos^n\phi d\phi$ is the modified Bessel function of order n [84]. Developing the Bessel functions for small values of p yields:

$$\chi_{s,xxx} = -N_s N_p \alpha^D_{\xi\xi\xi} \sin^4\theta_0 \frac{3p}{8} + \mathcal{O}(p^3) \quad (5.15a)$$

$$\chi_{s,xyy} = -N_s N_p \alpha^D_{\xi\xi\xi} \sin^4\theta_0 \frac{p}{8} + \mathcal{O}(p^3) \quad (5.15b)$$

$$\chi_{s,xzz} = -N_s N_p \alpha^D_{\xi\xi\xi} \cos^2\theta_0 \sin^2\theta_0 \frac{p}{2} + \mathcal{O}(p^3) \quad (5.15c)$$

$$\chi_{s,zxx} = N_s N_p \alpha^D_{\xi\xi\xi} \cos\theta_0 \sin^2\theta_0 (\frac{1}{2} + \frac{p^2\sin^2\theta_0}{16}) + \mathcal{O}(p^4) \quad (5.15d)$$

$$\chi_{s,zyy} = N_s N_p \alpha^D_{\xi\xi\xi} \cos\theta_0 \sin^2\theta_0 (\frac{1}{2} - \frac{p^2\sin^2\theta_0}{16}) + \mathcal{O}(p^4) \quad (5.15e)$$

$$\chi_{s,zzz} = N_s N_p \alpha^D_{\xi\xi\xi} \cos^3\theta_0 \quad (5.15f)$$

For $p = 0$ (no field applied), $\bar{\boldsymbol{\chi}}_s$ reduces to the susceptibility of a layer on an isotropic substrate (Eq. 2.4 in chapter 2).

5.3.1.2 $\bar{\boldsymbol{\chi}}_f$ *of the covering film* Since the covering film has an up-down symmetry, it is also symmetric with respect to a reflection in the (xy) plane. This implies that:

$$\chi_{xxz} = 0; \quad \chi_{yyz} = 0; \quad \chi_{zzz} = 0$$

The expression of the remaining components depend on the model considered. Because of the up-down symmetry, it is convenient to consider the covering film as made of bilayers (which have this symmetry) so that the up-down symmetry is valid at each height z in the film. For cyanobiphenyl molecules, these bilayers are known to be interdigitated [85]. We call N_b the number of bilayers in the film formed by two interdigitated molecular monolayers. If the orientation of the molecules is correlated over N_p molecules, the number of entities with a quadrupolar ordering is N_b/N_p.

Case a: In the case when the tilt of the molecules is not modified by the electric field, the nonlinear susceptibility of a layer located at height z is the average of the susceptibility of a layer with tilt angle $\theta^a_f(z)$ and the susceptibility of a layer with tilt angle $\pi - \theta^a_f(z)$:

$$\bar{\boldsymbol{\chi}}^a_f(z) = \frac{1}{2}\left[\bar{\boldsymbol{\chi}}_s(\theta_0 = \theta^a_f(z)) + \bar{\boldsymbol{\chi}}_s(\theta_0 = \pi - \theta^a_f(z))\right]. \quad (5.16)$$

This leads to[3]:

$$\chi^a_{f,xxx}(z) = -N_s N_p \alpha^D_{\xi\xi\xi} \sin^4\theta^a_f(z) \frac{3p}{8} + \mathcal{O}(p^3) \quad (5.17a)$$

$$\chi^a_{f,xyy}(z) = -N_s N_p \alpha^D_{\xi\xi\xi} \sin^4\theta^a_f(z) \frac{p}{8} + \mathcal{O}(p^3) \quad (5.17b)$$

$$\chi^a_{f,xzz}(z) = -N_s N_p \alpha^D_{\xi\xi\xi} \cos^2\theta^a_f(z) \sin^2\theta^a_f(z) \frac{p}{2} + \mathcal{O}(p^3) \quad (5.17c)$$

To get the susceptibility of the whole covering film, we need to integrate $\bar{\boldsymbol{\chi}}^a_f(z)$ over the film using the expression of $\theta^a_f(z)$ (Eq. 5.9):

$$\chi^a_{f,xxx}(z) = -N_s N_b \alpha^D_{\xi\xi\xi} \frac{9}{64} p + \mathcal{O}(p^3) \quad (5.18a)$$

$$\chi^a_{f,xyy}(z) = -N_s N_b \alpha^D_{\xi\xi\xi} \frac{3}{64} p + \mathcal{O}(p^3) \quad (5.18b)$$

$$\chi^a_{f,xzz}(z) = -N_s N_b \alpha^D_{\xi\xi\xi} \frac{1}{16} p + \mathcal{O}(p^3) \quad (5.18c)$$

Case b: If the tilt of the molecules is completely determined by the field, the components of $\bar{\boldsymbol{\chi}}^b_f$ can be written as a function of the spherical coordinates (α, δ) Fig. 5.2 :

$$\chi^b_{f,xxx} = -N_s N_b \alpha^D_{\xi\xi\xi} \left\langle \cos^3\alpha \right\rangle \quad (5.19a)$$

$$\chi^b_{f,xyy} = -N_s N_b \alpha^D_{\xi\xi\xi} \left\langle \cos\alpha \sin^2\alpha \sin^2\delta \right\rangle \quad (5.19b)$$

$$\chi^b_{f,xzz} = -N_s N_b \alpha^D_{\xi\xi\xi} \left\langle \cos\alpha \sin^2\alpha \cos^2\delta \right\rangle \quad (5.19c)$$

The orientational distribution function $f^b_f(\alpha, \delta)$ (Eq. 5.10 in section 5.2.2.2) can be written as a development of Legendre polynomials P_n [82, 84]:

$$f^b_f(\alpha, \delta) = \sum_{n=0}^{\infty} \frac{2n+1}{4\pi} \frac{i_n(p)}{i_0(p)} P_n(\cos\alpha)$$

where $i_n(X) = \sqrt{\frac{\pi}{2X}} I_{n+1/2}(X)$ is the spherical modified Bessel function of order n defined from the modified Bessel function of order $n + 1/2$ [84].

Using the orthogonality of the Legendre polynomials one gets: $\langle P_n(\cos\theta)\rangle = i_n(p)/i_0(p)$ from which one can calculate the different moments of the α-distribution appearing in

[3]Because of the interdigitation of the molecules in the bilayers [85] we assume that the density of molecules per unit area is the same in the surface layer and in the molecular bilayers forming the covering film.

$\bar{\boldsymbol{\chi}}_f^b$:

$$\chi^b_{f,xxx}(z) = -N_s N_b \alpha^D_{\xi\xi\xi} L_3(p) \tag{5.20a}$$

$$\chi^b_{f,xyy}(z) = -N_s N_b \alpha^D_{\xi\xi\xi} \frac{1}{2}(L_1(p) - L_3(p)) \tag{5.20b}$$

$$\chi^b_{f,xzz}(z) = -N_s N_b \alpha^D_{\xi\xi\xi} \frac{1}{2}(L_1(p) - L_3(p)) \tag{5.20c}$$

$L_1(p)$ and $L_3(p)$ are so-called Langevin functions [81]:

$$L_1(p) = \coth p - \frac{1}{p} \tag{5.21a}$$

$$L_3(p) = \left(1 + \frac{6}{p^2}\right) L_1(p) - \frac{2}{p} \tag{5.21b}$$

Developing these functions for small values of p yields:

$$\chi^b_{f,xxx}(z) = -N_s N_b \alpha^D_{\xi\xi\xi} \frac{p}{5} + \mathcal{O}(p^3) \tag{5.22a}$$

$$\chi^b_{f,xyy}(z) = -N_s N_b \alpha^D_{\xi\xi\xi} \frac{p}{15} + \mathcal{O}(p^3) \tag{5.22b}$$

$$\chi^b_{f,xzz}(z) = -N_s N_b \alpha^D_{\xi\xi\xi} \frac{p}{15} + \mathcal{O}(p^3) \tag{5.22c}$$

In both cases a and b, we have $\chi_{f,xxx} = 3\chi_{f,xyy}$. In case b $\chi^b_{f,xzz} = \chi^b_{f,xyy}$, while in case a $\chi^a_{f,xzz} = \frac{4}{3}\chi^a_{f,xyy}$.

5.3.1.3 $\bar{\boldsymbol{\chi}}$ *of the whole film* Summarizing, the components of the nonlinear susceptibility of the whole film vary as follows with the factor $p = \mu E/kT$:

- χ_{xxx}, χ_{xyy} and χ_{xzz} vary linearly with p (to first order in p). They contain contributions from both the surface layer and the covering film with a ratio $\chi_{f,ijk}/\chi_{s,ijk}$ proportional to the number N_b of bilayers in the covering film. This means that $\chi_{f,ijk}$ dominates if the covering film is thick.
- χ_{zxx} and χ_{zyy} have only contributions from the surface layer and are independent of p (to first order in p).
- χ_{zzz} has only a contribution from the surface layer and is rigorously independent of p.

5.3.2 Other contributions to the second-harmonic signal

We examine now different possible contributions to the second-harmonic signal generated by a poled film and show that most of them are negligible with respect to the dipolar contribution considered above.

5.3.2.1 *Quadrupolar contribution* As explained in chapter 2 (sections 2.1.1 and 2.1.5) the covering film in the absence of applied field can generate a second-harmonic because of its quadrupolar ordering. This adds a contribution χ^Q_{ijk} to the components χ_{zxx}, χ_{zyy} and χ_{zzz} of the nonlinear susceptibility of the film given by Eq. 2.13 and 2.14. Using the orientational distribution of the molecules in the film described in section 5.2.2.2 (case a) for $p = \mu E/kT = 0$ (no field applied), one gets:

$$\chi^Q_{zxx} = \chi^Q_{zyy} = -\frac{\xi_0 N_p k}{\epsilon(2\omega)} N_b N_s \frac{\alpha^D_{\xi\xi\xi}}{16} \tag{5.23a}$$

$$\chi^Q_{zzz} = -\frac{\xi_0 k}{\epsilon(2\omega)\epsilon^2(\omega)} N_b N_s \frac{9\alpha^D_{\xi\xi\xi}}{64} \tag{5.23b}$$

where $k = \epsilon^2(\omega)2\pi/532\text{nm}^{-1}$. $\xi_0 \approx 15\text{Å}$ is the distance between two opposed molecules along their axis $\hat{\boldsymbol{\xi}}$ and $N_p\xi_0$ the distance between two opposing dipoles in the case of correlated orientations. The dielectric constants of the liquid crystal $\epsilon(\Omega) = \sqrt{n(\Omega)}$ can be deduced from the refractive index of the liquid crystal (see table 2.1 in chapter 2). For thick covering films, this quadrupolar contribution χ^Q_{ijk} should be subtracted from the measured values of χ_{ijk}.

When an electric field is applied, χ^Q_{ijk} increases by terms of order p^2 and therefore much smaller than the dipolar contribution of the covering film.

5.3.2.2 *Electric field induced second-harmonic generation (EFISH)* If a strong DC electric field is applied onto a non-polar medium, it can mix by a third-order nonlinear process with two waves at frequency ω to give a polarization at frequency 2ω [81]:

$$\mathbf{P}^{\text{EFISH}} = \bar{\boldsymbol{\chi}}^{(3)}(2\omega = \omega + \omega + 0) : \mathbf{E}(\omega)\mathbf{E}(\omega)\mathbf{E}(0) \tag{5.24}$$

where $\bar{\boldsymbol{\chi}}^{(3)}$ is the third-order nonlinear susceptibility of the medium. The effective second-order susceptibility arising from this process is:

$$\chi^{\text{EFISH}}_{ijkl} = \chi^{(3)}_{ijkl} E_l(0) \tag{5.25}$$

To compare the intensity of the EFISH signal with that of the purely second-order signal arising from the field-induced polar order, we have to compare the third-order polarizability γ of the molecules and the factor $\alpha^D_{\xi\xi\xi}\mu/kT$. For cyanobiphenyl molecules, γ is of the order of 10^{-35}esu $\approx 10^{-60}$C m^{4}J^{-3} [86], $\alpha^D_{\xi\xi\xi} \approx 10^{-29}esu\approx 0.4\times10^{-49}$C^{3}m^{3}J^{-2} [86, 87] and μ = 5D = 15×10^{-30}Cm (for one molecule). At room temperature this give: $\alpha^D_{\xi\xi\xi}\mu/kT \approx 10^{-58}$C^{4}m^{4}J^{-3} which is two orders of magnitude larger than γ. We can therefore neglect the EFISH contribution.

5.3.2.3 *Effect of electric field on $\alpha^D_{\xi\xi\xi}$* In principle, a DC electric field can modify the intra-molecular potential in which the electrons of a molecule evolve. This would lead to a change in the nonlinear polarizability $\alpha^D_{\xi\xi\xi}$ of the molecules. However this requires fields which are much larger than the ones we apply.

5.4 Experimental procedure

5.4.1 Samples

To perform our experiments, we have used substrates made of fused silica (amorphous quartz plates). The surface of these plates is isotropic (symmetry $C_{\infty v}$). On these substrates we coated two electrodes separated by a gap d of about 1mm. The electrodes were made of gold (1000Å-thick) attached to the quartz by a thin layer of chromium (100Å) (see Fig. 5.3). The electrodes were connected to an high voltage power supply producing a DC voltage V of several kV; the current was limited to 10mA.

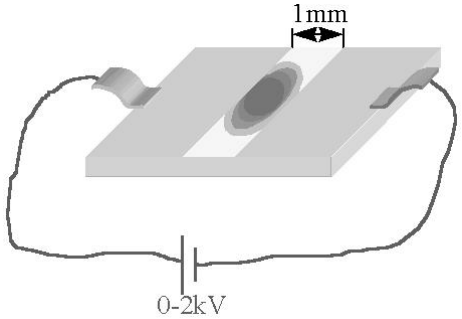

FIGURE 5.3 *Schematic representation of the sample made of a thin liquid crystal droplet deposited in between two electrodes on a fused quartz plate.*

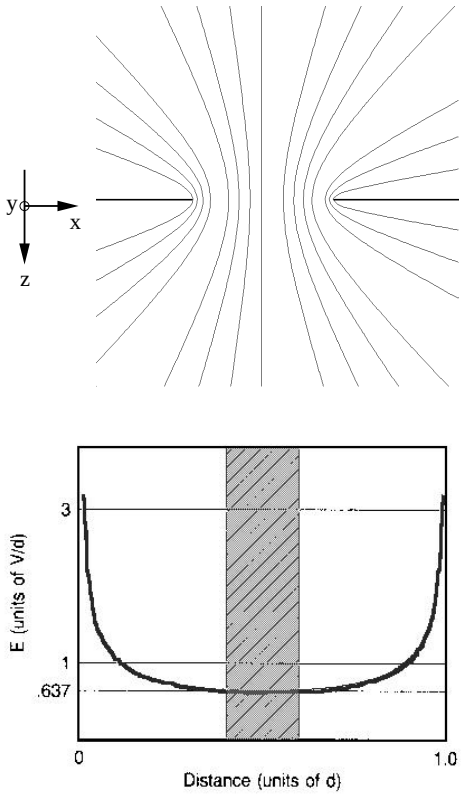

FIGURE 5.4 *Electric field produced by two flat electrodes separated by a gap. a) Equipotential lines in a plane perpendicular to the electrodes and the gap* [88]. *b) Dependence of the electric field in between the electrodes (corresponding to the field at the substrate surface) in units of the potential V over the gap d versus position in units of d* [89]. *The gray region corresponds to the center of the gap with a uniform electric field.*

The electrodes produce an electric field that is parallel to the substrate surface at the surface [89]. The intensity of this field varies across the gap. It is minimum and equal to $E = \frac{2}{\pi}\frac{V}{d}$ in the middle of the gap (see Fig. 5.4). Around this minimum the profile of the field is very flat so that there is a region of width $d/5 = 0.2$ mm in which the electric field is constant within 1%. All of our measurements were performed in this region with a laser spot of 100μm in diameter to ensure uniform field conditions. We switched the electric field with the circuit shown in Fig. 5.5 to ensure that the rise and fall time was minimum, and that current was limited in case of a short circuit. We had the probe (Fig. 5.5) connected to the oscilloscope to synchronize the accumulated data with the switching of the electric field

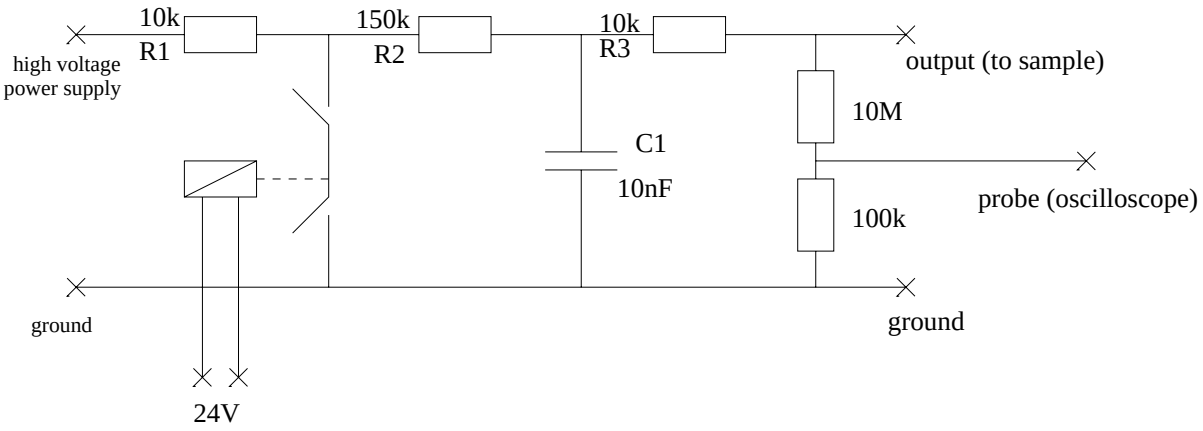

FIGURE 5.5 *Circuit to switch the high voltage on the sample.*

The maximum electric field we could apply was typically 2kV/mm. Higher fields produced arcing between the electrodes, which destroyed the sample. Since this maximum field was lowered by the presence of water vapor, we kept our samples in a cell flushed by dry nitrogen.

We deposited a multilayer of liquid crystal molecules in the gap on the substrate by evaporation from a hot source and condensation onto the substrate [80]. This deposition process makes very thin droplets of an extent of several mm in which the film thickness varies from less than a monolayer till several layers. For all results presented here, the deposition process was performed in the absence of electric field and the field was switched on afterwards. Depositing the films with the electric field on gave essentially the same results. The cell atmosphere of dry nitrogen preserved the samples from contamination. We have used two liquid crystals: 7OCB ($T_m = 55°C$, $T_{NI} = 75°C$) and 5CB ($T_m = 23°C$, $T_{NI} = 35°C$) (Fig. 5.6) [61]. Both can easily be supercooled down to room temperature. Our measurements were made in a temperature range between 16°C and 40°C. The upper limit is determined by the temperature above which the molecules evaporate from the films.

We have performed two types of experiments with these samples using second-harmonic generation measurements:

1. static measurements of the orientational order in the films for different field strengths and temperatures (presented in this chapter).

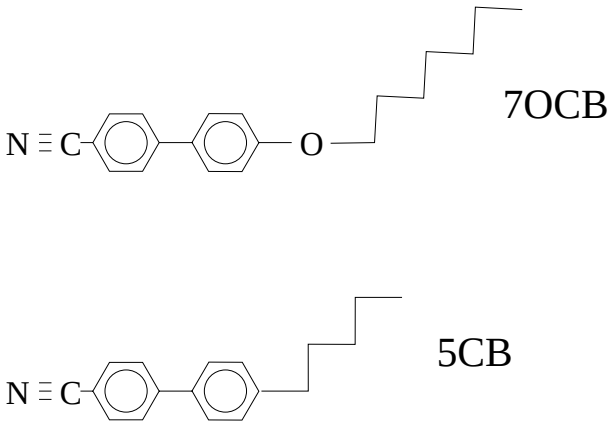

FIGURE 5.6 *The chemical structure of the liquid crystals 5CB and 7OCB used in the present work.*

2. dynamic measurements of the orientational distribution evolution as we switched on or off the electric field (presented in the next chapter).

5.4.2 Determination of the degree of polar ordering

To obtain the degree of electric-field-induced polar ordering in our films from the second-harmonic signal, we have used several methods.

5.4.2.1 *Full determination of the dipolar susceptibility* $\bar{\chi}$ From the measurements of the second-harmonic signal as a function of the in-plane orientation of the sample, we can determine all the components of $\bar{\chi}$ in arbitrary units depending on the experimental set-up (see chapter 2). To derive the absolute values of the moments of the orientational distribution, we would need to know the value of the factor $N_s\alpha^D_{\xi\xi\xi}$ in these arbitrary units. We can however use ratios of different components to eliminate this factor. For instance, using Eq. 5.15, 5.18, 5.22 and neglecting terms of $\mathcal{O}(p^2)$, one has:

$$\begin{aligned}\frac{\chi_{xxx}}{\chi_{zyy}} &= \frac{\chi_{s,xxx}+\chi_{f,xxx}}{\chi_{s,zyy}} \\ &= -\frac{\sin^2\theta_0}{\cos\theta_0}\frac{3p}{4} - \frac{2c_{xxx}}{\cos\theta_0\sin^2\theta_0}\frac{N_b}{N_p}p \end{aligned} \tag{5.26}$$

where $c_{xxx} = 9/64$ (Eq. 5.18a) in model a of the covering film and $c_{xxx} = 1/5$ in model b (Eq. 5.22a). To determine the factor $p = \mu E/kT$, which is a measure of the degree of polar ordering, we need to know two parameters.

The factor $N_b/\cos\theta_0 \sin^2\theta_0$ (where N_b is the number of bilayers in the covering film and θ_0 the tilt angle of the molecules in the surface layer) can be estimated from the ratio of the *sp* signal $S(N_b)$ (without field) at the considered point of the sample and on the signal $S(0)$ of the surface layer [37]. Both signals are proportional to the square of the corresponding value of $\chi^{\rm tot}_{zxx} = \chi^{\rm tot}_{zyy}$ (Eq. 2.7 in chapter 2) of the total nonlinear susceptibility tensor of the film. For a thick film this includes the quadrupolar contribution of the covering film (Eq. 5.23):

$$\begin{aligned}\sqrt{\frac{S(N_b)}{S(0)}} &= \frac{\chi_{s,zxx} + \chi^Q_{zxx}}{\chi_{s,zxx}} \\ &= 1 - \frac{\xi_0 k}{8\epsilon(2\omega)} \frac{N_b}{\cos\theta_0 \sin^2\theta_0} \end{aligned} \tag{5.27}$$

This leads to:

$$\frac{N_b}{\cos\theta_0 \sin^2\theta_0} = \frac{8\epsilon(2\omega)}{\xi_0 k}\left(1 - \sqrt{\frac{S(N_b)}{S(0)}}\right) \tag{5.28}$$

The value of the tilt angle θ_0 of the surface molecules can be obtained from the signal of the surface layer:

$$\frac{\chi_{s,zyy}}{\chi_{s,zzz}} = \frac{1}{2}\tan^2\theta_0. \tag{5.29}$$

With the value of θ_0, we can also determine the number of bilayers in the covering film from Eq. 5.28.

5.4.2.2 *ss signal at* $\Phi = 90°$ The expression of $\chi_{\rm eff}$ in the *s*-in-*s*-out configuration for an angle $\Phi = 90°$ between the electric field and the incidence plane of the light reduces to (see Eq. 2.5 in chapter 2):

$$\chi_{ss}(\Phi = 90°) = \chi_{xxx}\, e_{yyy} \tag{5.30}$$

Since χ_{xxx} is proportional to $\langle\cos^3\phi\rangle$ (Eq. 2.2b), $\chi_{ss}(\Phi = 90°)$ is directly proportional to the degree of in-plane polar ordering. This signal is therefore very convenient to follow the evolutions of this ordering in a film with constant number of molecules. We have used this signal for dynamics measurements (see chapter 6). As in the former method, an absolute measure of the degree of order would require to know the factor $N_s\alpha^D_{\xi\xi\xi}$. But

we can also divide $\chi_{ss}(\Phi = 90°)$ by another signal independent of p, for instance the sp signal without field for the surface layer of the same droplet[4]:

$$\frac{\chi_{ss}(\Phi = 90°)}{\chi_{sp}^{\text{surf}}(E = 0)} = \frac{\chi_{s,xxx} + \chi_{f,xxx}}{\chi_{s,zyy}} \frac{e_{yyy}}{e_{zyy}} \tag{5.31}$$

From there we can proceed as in the former method.

5.4.2.3 *Asymmetry of the sp signal in* (xz) *plane* From the expression of χ_{eff} in the s-in-p-out configuration (see Eq. 2.5 in chapter 2), one gets:

$$\frac{\chi_{sp}(\Phi = 0°) - \chi_{sp}(E = 0)}{\chi_{sp}(E = 0)} = \frac{\chi_{sp}(\Phi = 0°) - \chi_{sp}(\Phi = 180°)}{\chi_{sp}(\Phi = 0°) + \chi_{sp}(\Phi = 0°)} = \frac{\chi_{xyy}}{\chi_{zyy}} \frac{e_{xyy}}{e_{zyy}} \tag{5.32}$$

Using the expressions of χ_{ijk} (Eq. 5.15, 5.18 and 5.22) gives:

$$\frac{\chi_{xyy}}{\chi_{zyy}} = -\frac{\sin^2\theta_0}{\cos\theta_0} \frac{p}{4} - \frac{2c_{xyy}}{\cos\theta_0 \sin^2\theta_0} \frac{N_b}{N_p} p \tag{5.33}$$

where $c_{xyy} = 3/64$ (Eq. 5.18b) in model a of the covering film and $c_{xyy} = 1/15$ in model b (Eq. 5.22b). From there we can again proceed as in the first method.

5.5 Results of static experiments

Most of our measurements have been performed with 7OCB. For this material, we have measured with second-harmonic generation the degree of electric-field-induced polar ordering in thin films as a function of the applied field, film thickness and temperature. We have also done a few measurements with 5CB.

5.5.1 Effect of electric field

To determine the components of the nonlinear susceptibility tensor of the films, we have measured the dependence of the second-harmonic signal on the in-plane rotation angle Φ of the sample for four polarization combinations. In Fig. 5.7 we show the measured signal for $E = 0$ and $E = 2$ kVmm^{-1} for a film with $N_b = 5 \pm .5$ bilayers. In the absence of electric field we measure a typical signal for the expected in-plane isotropic distribution of the liquid crystal molecules: isotropic signals in the s-in-p-out and p-in-p-out configurations, a noise level which is negligible in the s-in-s-out and p-in-s-out configurations.

[4]Using the sp signal at the considered point in the droplet introduces complications because of the quadrupolar contribution.

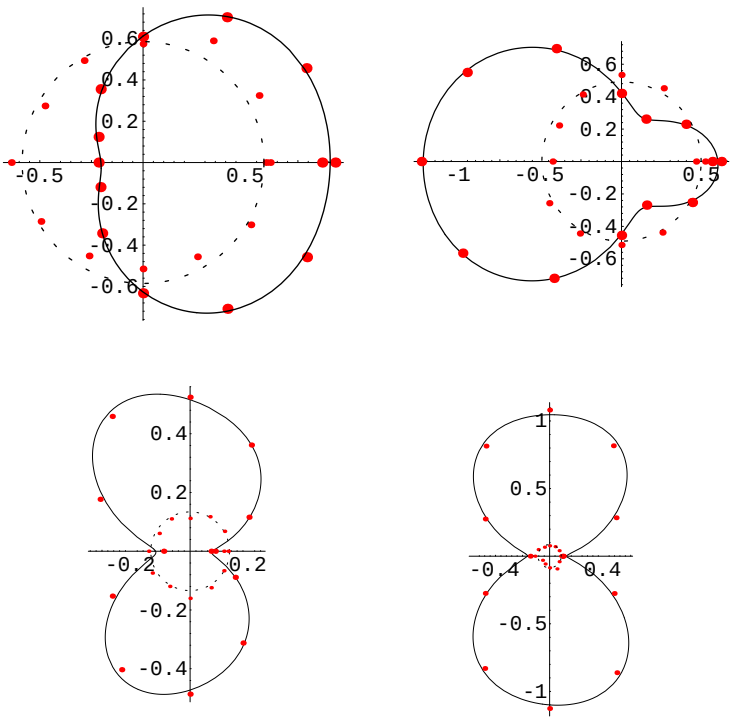

FIGURE 5.7 *Polar plots of the square root of the second-harmonic signal versus the angle Φ between the incidence plane of the laser beam and the mirror plane of the substrate surface (containing the electric field) for a 7OCB film deposited on fused quartz substrate. Clockwise we present the signals corresponding to sp (upper left), pp, ss and ps polarizations. The fit of the data is shown as solid curves (resp. dashed curves) and corresponds to $E = 2kVmm^{-1}$ (resp. $E = 0$).*

If we apply a electric field we observe that the shape of the signal changes. The symmetry of the polar plots changes from $C_{\infty v}$ (isotropic) to C_{1v} (mirror symmetry) with a mirror plane containing the electric field. The signal also increases significantly, specially the *s*-out signals. This is the signature of a polar ordering in the plane of the substrate.

The polar plots of the signal can be fitted with the theoretical expressions of the second-harmonic signal (Eq. 2.5) to obtain the components of the nonlinear susceptibility tensor of the system, and subsequently the orientational distribution function using the maximum entropy method described in section 2.1.4. In Fig. 5.8 we show the distribution

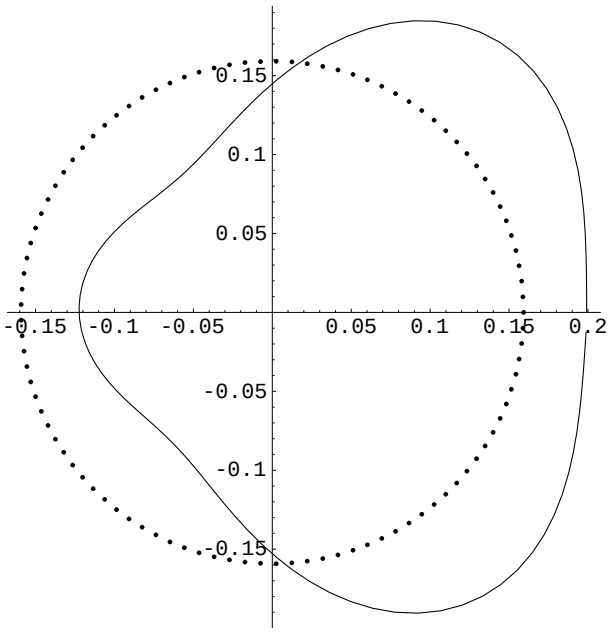

FIGURE 5.8 *The distribution function with electric field (solid) and without electric field (dotted).*

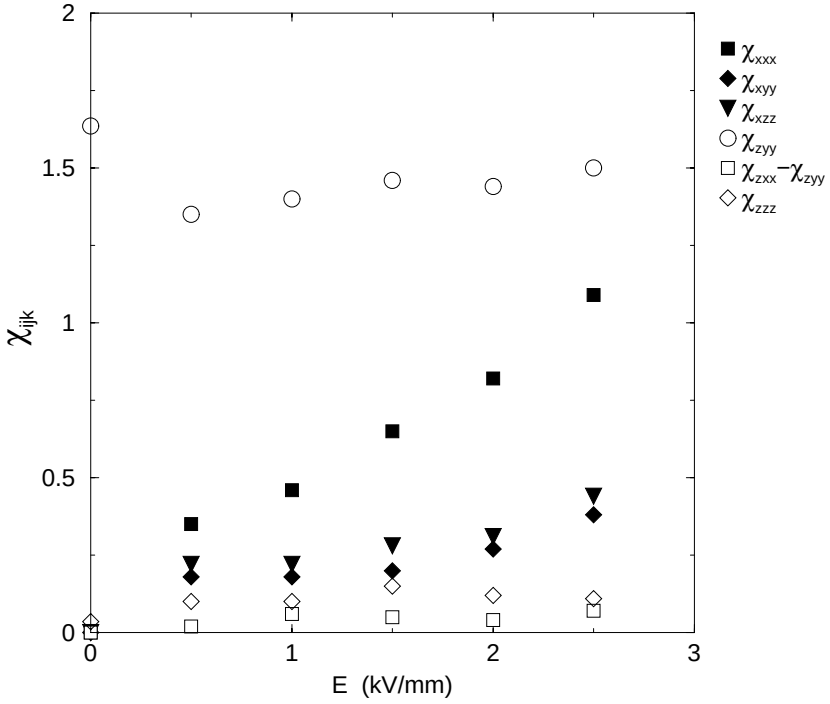

FIGURE 5.9 *The components χ_{ijk} of the nonlinear susceptibility tensor as a function of the electric field*

of the azimuthal angle[5] ϕ obtained from the data shown in Fig. 5.7. The field-induced

[5]Since we expect a strong variation of the tilt angle θ of the molecules across the film, determining the overall θ-distribution does not make sense.

distribution shows that most molecules point in the direction of the field while keeping a wide ϕ distribution.

We have performed our second-harmonic measurements for different values of the applied field and determined the field-dependence of the nonlinear susceptibility tensor $\bar{\boldsymbol{\chi}}$ of a film with $N_b = 5 \pm .5$ (Fig. 5.9) As expected from our model (section 5.3.1), χ_{zxx}, χ_{zyy} and χ_{zzz} remain essentially constant as E increases. This justifies our assumption that the applied electric field does not modify the tilt of the molecules in the surface layer. In contrast, χ_{xxx} changes significantly with electric field. It varies linearly with E and extrapolates to 0 for $E = 0$. The same is observed from χ_{xyy} and χ_{xzz} but with a smaller slope. These linear dependences show that the development of the expressions of $\bar{\boldsymbol{\chi}}$ for small values of p limited to first-order terms (section 5.3.1) is justified.

For 1.5 kVmm^{-1} $< E <$ 2.5kVmm^{-1}, we find the following ratios[6]: $\chi_{xxx} = (3.0 \pm 0.2)\chi_{xzz}$ and $\chi_{xzz} = (1.2 \pm 0.2)\chi_{xyy}$. The ratio χ_{xxx}/χ_{xzz} corresponds to what is expected from our model. For the ratio χ_{xzz}/χ_{xyy}, we expect (for $N_p = 1$, resp. $N_p = 3$):

$$\frac{\chi_{s,xzz} + \chi^a_{f,xzz}}{\chi_{s,xyy} + \chi^a_{f,xyy}} = 1.0 \text{ resp. } 1.4 \text{ (model a)} \tag{5.34}$$

$$\frac{\chi_{s,xzz} + \chi^b_{f,xzz}}{\chi_{s,xyy} + \chi^b_{f,xyy}} = 0.8 \text{ resp. } 0.6 \text{ (model b)} \tag{5.35}$$

So we can conclude that model a is the most appropriate to describe our data, i.e. that the applied field does not modify the tilt of the molecules. This is the model we will consider in the rest of our analysis.

5.5.2 Effect of film thickness

To study the effect of film thickness on the second-harmonic signal, we have scanned the signal across droplets along and in the middle of the gap created by the electrodes. In such a scan, the field strength remains constant and only the thickness of the evaporated film changes. A typical profile of the *sp* signal for $\Phi = 0°$ without field is shown in Fig. 5.10, and the corresponding profile of the *ss* signal for $\Phi = 90°$ with field (2 kVmm^{-1}) is shown in Fig. 5.11.

[6]For smaller values of E, the anisotropy of the signal is small and the relative error on the calculated values of χ_{xyy} and χ_{xzz} large (up to 50 %).

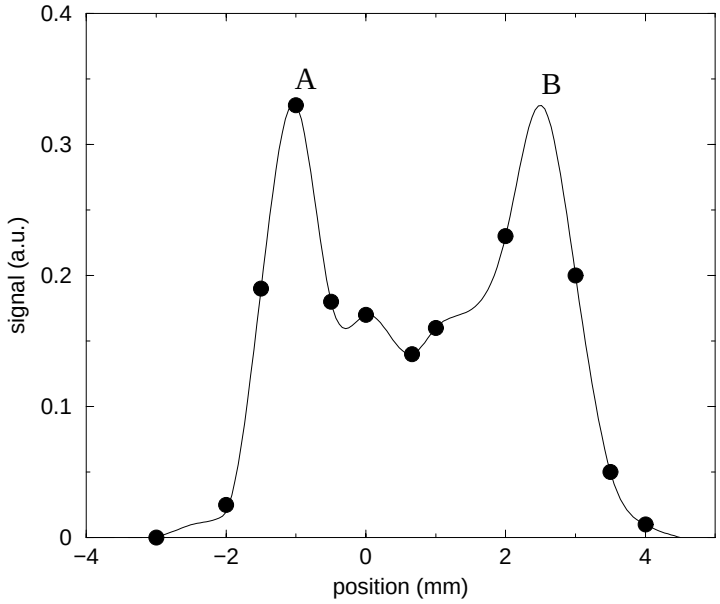

FIGURE 5.10 *Profile of the sp signal without applied field as one moves through a droplet of 7OCB along the gap .*

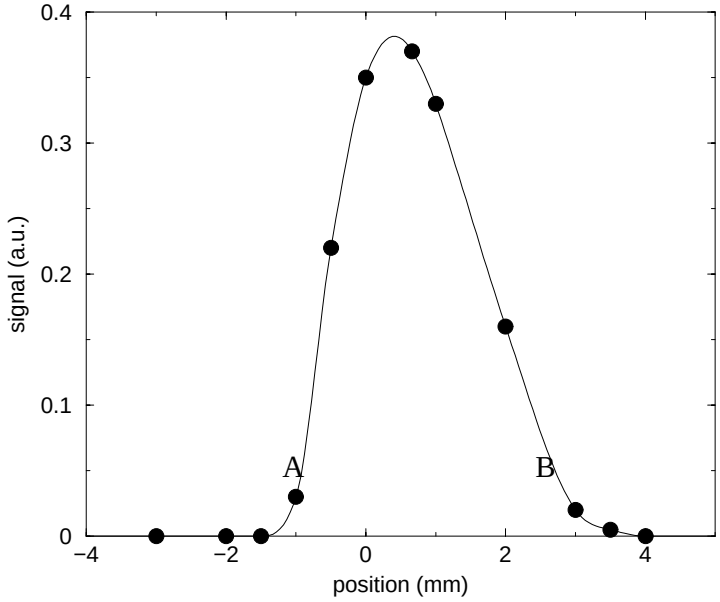

FIGURE 5.11 *Profile of the ss-signal for* $\Phi = 90°$ *as one moves through the same droplet as in Fig. 5.10.*

The *sp* profile without field shows maxima close to the edges (points A and B) corresponding to a full monolayer. Outside these two points, the signal decreases because the number of molecules in the surface layer decreases to zero. In between these two points the signal decreases because of the quadrupolar contribution of the covering film.

From the *sp*-profile without electric field, we get (see section 5.4.2) the profile of the number of layers (bilayers + surface layer) $N_b + 1$ in the film (Fig. 5.12). By comparing the profile of N_b with that of the *ss* signals with field, we see that most of the signal is generated by the covering film. However a full monolayer shows some in-plane polar ordering, to be seen at points A and B from the small *ss* signal.

The *ss* effective susceptibility χ_{ss} is proportional to the number of bilayers within the experimental error (Fig. 5.13). This means that the degree of the polar ordering induced by the electric field does not vary with film thickness nor with the position of the molecules in the film (along the z direction). From χ_{ss} and the number N_b of bilayers, we can calculate the factor $p = \frac{\mu E}{kT}$ (section 5.4.2). We find: $p = .25 \pm .05$ in the covering film and $p = .2 \pm .05$ in the surface layer. We have measured p on different samples with film thicknesses $N_b + 1$ varying from 1 to 12. We find the same values as above: $p = .25 \pm .05$.

From this value of p, we can calculate the dipole moment μ of the reorienting units in our system. The local electric field $E_{\rm loc}$ applied on the molecules is related to the applied potential $V(= 2\text{kV})$ over the gap of width $d(= 1\text{mm})$ by:

$$E_{loc} = (1 + \frac{4}{3}\pi\chi_e)\frac{2}{\pi}\frac{V}{d}. \tag{5.36}$$

This first factor relates the local field and the applied field and depends on the linear dielectric susceptibility χ_e of the material [42] and the second factor $2/\pi$ relates the field in the middle of the gap to V/d [89]. Using $\chi_e = 0.5$ [42] and $T = 293\text{K}$, we find $\mu = 78\text{D} \pm 16\text{D}$. This is much larger than the expected value of 5D for our molecules. This means that the reorienting dipoles are not single molecules but clusters containing of 17 ± 3 molecules and having a polar ordering. So p should rather be written as:

$$p = \frac{n_c \mu E}{kT} \tag{5.37}$$

where n_c is the number of molecules in a cluster.

5.5.3 Effect of temperature

To strengthen our conclusion that the reorienting dipoles of our system are formed by clusters, we have studied the temperature dependence of the field-induced polar ordering.

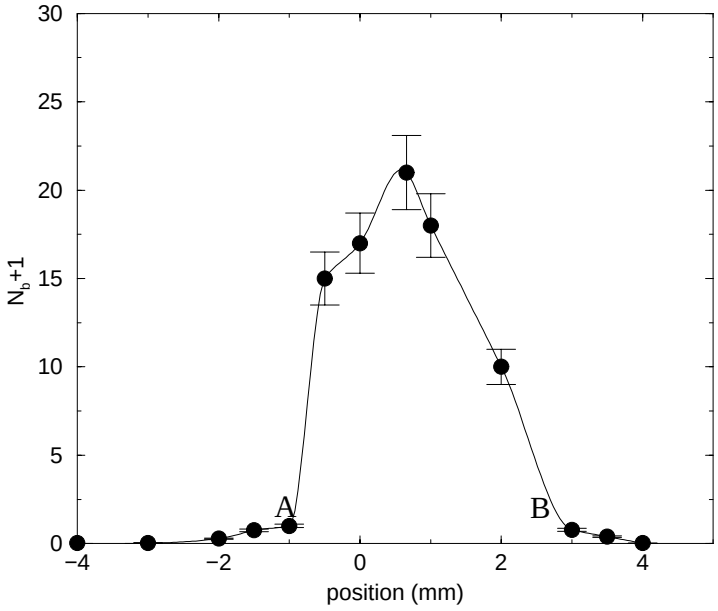

FIGURE 5.12 *The number of layers $N_b + 1$ through the droplet deduced from the data in Fig. 5.10.*

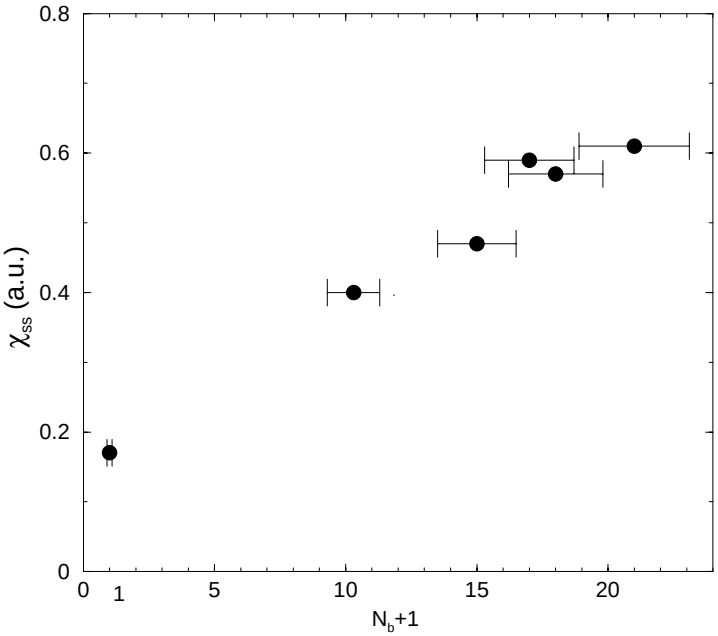

FIGURE 5.13 *The effective susceptibility χ_{ss} as a function of the number of layers $N_b + 1$ deduced from the data in Fig. 5.10 and 5.11.*

It is expected to decrease when temperature increases because of a size decrease of the clusters.

We have fully determined the nonlinear susceptibility tensor $\bar{\boldsymbol{\chi}}$ of two different samples $N_b = 12 \pm 2$ for temperatures ranging between 20° C and 40° C. This was performed both by increasing and decreasing temperature to eliminate effects due to a possible thinning of the sample. The changes of the signal we observe when changing temperature are reversible, which means that the samples are in equilibrium at each temperature.

The temperature dependence of $\bar{\boldsymbol{\chi}}$ is given in Fig. 5.14. χ_{zxx}, χ_{zyy} and χ_{zzz} stay essentially constant. This is expected since these components do not depend on $p = \frac{n_c \mu E}{kT}$ (section 5.3.1). χ_{xxx}, χ_{xyy} and χ_{xzz} decrease as temperature increases, which means that p decreases. From the variation of χ_{xxx}, we find that p decreases by a factor of 0.65 between 20° C and 40° C. However $1/kT$ decreases only by a factor 0.95. This means that the cluster size n_c has shrunk by 70% .

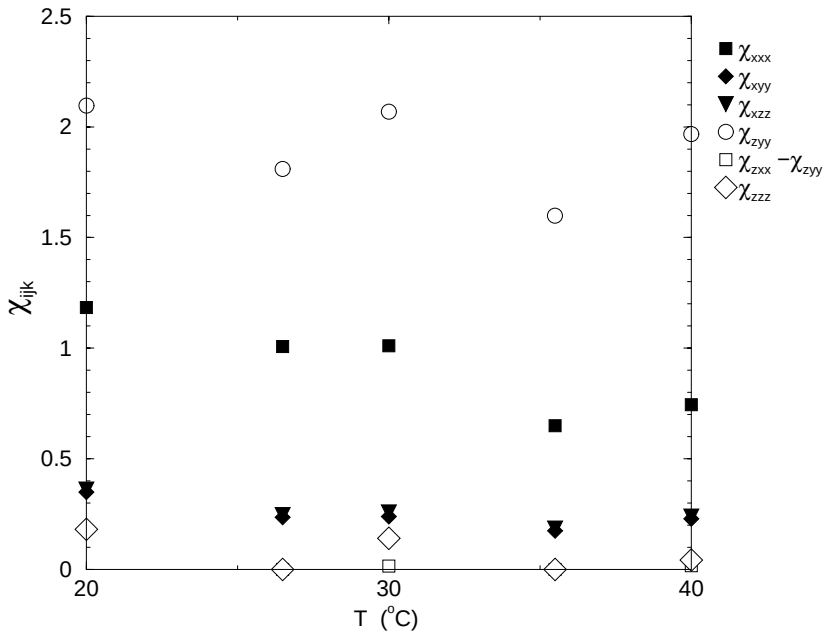

FIGURE 5.14 *The components χ_{ijk} of the nonlinear susceptibility tensor as a function of temperature. The data at 20° C, 30° C and 40° C on the one hand, and 27° C and 36° C on the other hand, correspond to different samples, which increases the scattering of the data.*

5.5.4 5CB

We have also tried to reorient molecules in films of 5CB. In Fig. 5.15 we show the profile of the *sp* signal for $\Phi = 0°$ without field, together with the *ss* signal for $\Phi = 90°$ with field (2 kVmm^{-1}). Within the background we did not see any polar ordering of the molecules

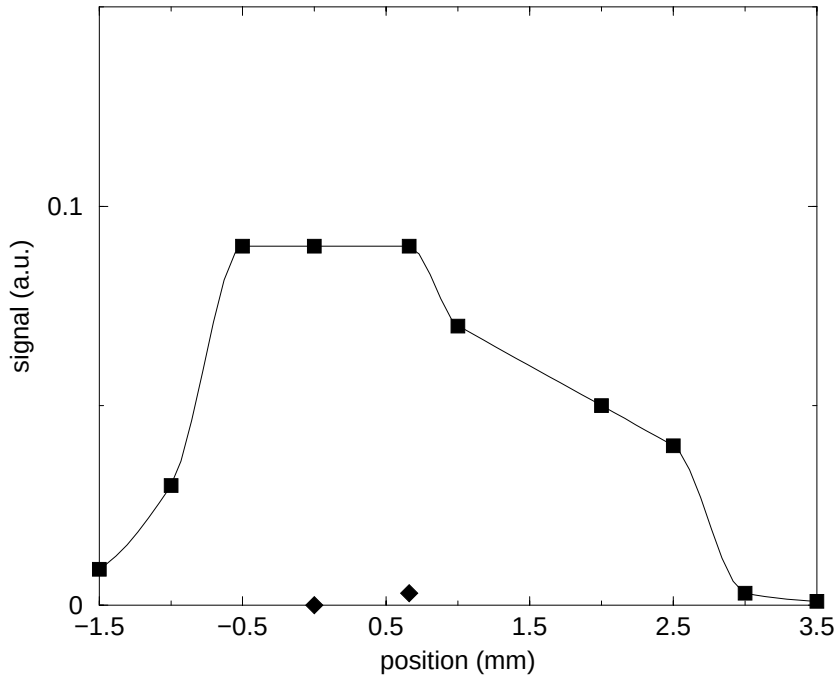

FIGURE 5.15 *Profile of the sp signal without field (■) and the ss signal for $\Phi = 90°$ with field (2kVmm^{-1}) (♦) through a droplet of 5CB.*

induced by the electric field. The orientational distribution remained isotropic. This difference of behavior with respect to 7OCB has two reasons.

- As already observed previously on different substrates, it is not possible to deposit layers of nCB molecules thicker than one monolayer using deposition by condensation [37, 80]. So the effect of the electric field on the second-harmonic signal is expected to be small as in the case of a surface layer of 7OCB molecules.
- At room temperature, 5CB is close to its melting point while 7OCB is much further below its melting point. We can then expect that, if clusters form at all in 5CB, they will be much smaller than in 7OCB. The effect of the electric field on the orientational order, which is then proportional to the factor $\mu E/kT$ in 5CB and $n_c \mu E/kT$ in 7OCB, is therefore much smaller in 5CB. So a surface layer of

5CB molecules shows no detectable reorientation, while a surface layer of 7OCB, which is in fact a layer of clusters, shows a small but detectable reorientation of the molecules (section 5.5.2).

5.6 Discussion and conclusions

From our measurements we can draw several conclusions concerning the effect of poling on thin liquid crystal films and the anchoring of liquid crystal molecules on fused quartz substrates.

5.6.1 Poling of thin liquid crystal films

Applying an electric field of a few kVmm^{-1} is able to induce a polar ordering in a thin film of alkoxy-cyanobiphenyl molecules (nOCB). This is made possible by the presence of clusters. These clusters have a dipole moment $n_c\boldsymbol{\mu}$ (with $\boldsymbol{\mu}$ being the molecular dipole moment) and reorient as a whole if an electric field is applied. If we assume that all the molecules of a cluster point exactly in the same direction, n_c is the number of molecules in the cluster. Otherwise the number of molecules is $n_c/\langle\cos\alpha\rangle$ where α is the angle between the dipole moment of a molecule and the mean dipole moment of the cluster. If the clusters are significantly disordered (small $\langle\cos\alpha\rangle$), the actual number of molecules in a cluster could be much larger than n_c. At this point we have no means to estimate $\langle\cos\alpha\rangle$. These clusters seem to exist only below the melting point of the material: they decrease in size as temperature increases towards the melting point, and they are not detectable at temperatures close to this point.

The existence of clusters is in contradiction with the well-established result that cyanobiphenyl molecules (both nCB and nOCB) form so-called dimers. These are made of two molecules with their dipole moments side-by-side in opposite directions [90–93]. These are found in all phases including the nematic and isotropic phases. In these two phases, the fraction of molecules forming dimers is found to increase as temperature decreases, reaching approximately 60 % in the nematic phase [93]. For molecules with long enough aliphatic chains to exhibit a smectic phase ($n \geq 8$), this fraction further increases as temperature decreases below the nematic/smectic transition. For other polar compounds showing a reentrant nematic phase below the smectic phase [85], it

has been speculated that the fraction of molecules forming dimers saturated in the reentrant nematic phase at approximately 85 % [94].

If a significant proportion of molecules forms dimers, they cannot participate in the formation of polar clusters. The latter would then have to be formed by the rest of the molecules, which is quite unlikely to happen. It is however not obvious that the above trends would also be found in supercooled cyanobiphenyl compounds showing no smectic phase (such as 7OCB), since the corresponding measurements have not been performed to our knowledge. In any case, the fact that we find no clusters in 5CB at room temperature is consistent with the observed dimer formation in the nematic phase of this compound [93].

There have been some theoretical [95–97] and computational [98–101] studies about the formation of polar nematic liquid crystals. They all show that a moderate molecular dipole of a few Debyes is enough to induce the formation of a nematic liquid crystal with a macroscopic polarization. Such a phase has however never been found experimentally. It would require a polar order with a macroscopic correlation length. The formation of a cluster of 20 polarly ordered molecules requires a correlation length for the polar ordering of less than three molecules in each direction. Such a local polar ordering has been observed both in density functional theory [95] and computer simulation [99] of a dipolar fluid (with a molecular dipole moment of 2.7 D) in the isotropic phase. The radial pair distribution function associated with a polar ordering shows one pronounced peak at the nearest neighbor position and becomes zero for distances larger than three molecular diameters, very much like the radial pair distribution function associated with the quadrupolar ordering. This shows that polar clusters with a lateral extent of a few molecules are likely to form in liquid crystals made of polar molecules.

Our measurements show that the tilt of the molecules in the surface layer is not modified by the application of an electric field. This can be expected because of the anchoring of these molecules on the substrate (see next section). For the same reason, we can also expect that the tilt of the molecules at the free surface is also not modified by the applied field. We have found that the same holds for the rest of the molecules in the covering film. This can be understood if we compare the energy $n_c \mu E$ of a cluster in the applied field and the elastic energy of the same cluster associated with distortions of

the molecular orientation. The latter is of the order $Kn_c a^3/h_c^2$, where $K \approx 10^{-11}$N is the elastic constant for splay and bend deformation, $a^3 \approx 625$Å^3 is the molecular volume and h_c is the thickness of the covering film [13]. The tilt of the molecules remains unchanged if the elastic energy dominates, i.e. $h_c \ll \sqrt{Ka^3/\mu E} \approx 980$Å for $E = 2$kVmm^{-2}. This thickness corresponds to 32 bilayers oriented perpendicular to the surface. All the films we have studied were significantly thinner.

The degree of polar ordering in the covering film, as measured by the factor $p = n_c \mu E/kT$, is found to be independent of the thickness of the considered film and of the position of the molecules along the normal. Within our experimental errors this polar ordering is the same as the one in the surface layer. As the tilt of the molecules is not modified by the field, the induced polar ordering arises from a change in the distribution of azimuthal angles of the molecules. The fact that p is independent on the position of the molecules in the film shows that they are essentially free to rotate in the plane of the substrate.

Finally we emphasize that in the case when clusters are present, the surface layer is a monolayer of clusters. In our experiments, the thickness of the films is determined by second-harmonic generation measurements (section 5.4.2.3). A thickness corresponding to one surface layer is determined as the point in a droplet where the *sp* signal is maximum. Likewise, during a deposition process, the deposition of a full surface layer corresponds to the point when the *sp* signal saturates before it starts decreasing [80]. This means that a monolayer corresponds to the thickness of the thickest film exhibiting a polar ordering in the absence of electric field, i.e. a layer of clusters. This fact is confirmed by the observation that the signal generated by a surface layer of 5CB molecules (which do not form clusters) on quartz is generally three to four times smaller that generated by a surface layer of 7OCB molecules (which do form clusters).

This leads us to a word of caution. It has often been claimed that the second-harmonic signal measured from the interface between a cyanobiphenyl liquid crystal and a substrate is only generated by the first monolayer of molecules in contact with the substrate. The above shows that this statement is only true for measurements performed at temperatures around and above the melting point of the material. This holds for alkyl-cyanobiphenyl molecules (nCB) which are liquid crystalline at room temperature.

This has indeed been checked, both with second-harmonic generation measurements [36] and measurements of thicknesses of Langmuir films [102] and wetting layers [103]. It is however not true for measurements on alkoxy-cyanobiphenyls (nOCB) performed below their melting point (generally located around 50-55°C). The results of these measurements on the orientational order at the surface should nevertheless remain valid. Considering the small size of the clusters it can be expected that all the molecules in a given cluster have essentially the same orientation. If this cluster has grown onto a substrate, this orientation is the one imposed by the substrate on the molecules located at its surface.

5.6.2 Microscopic anchoring on fused quartz

Since the applied electric field only induces small variations in the second-harmonic signal generated by the surface layer, it is difficult to perform measurements that are relevant for the anchoring properties of molecules. We can however draw some conclusions on these properties.

As we have seen in the former section, the molecules appear free to rotate in the plane of the substrate, even in the surface layer. This is expected since the substrate is isotropic. The only possible contribution to the azimuthal anchoring energy of the molecules associated with reorientations in the plane of the substrate is due to their adsorption onto the substrate. Because of this adsorption, each molecules is in a potential well of depth $E_{\rm ad}$; however the position of this well is not fixed and it can move if a field is applied. The effect of adsorption is therefore only felt in the dynamic behavior of the surface molecules and will be discussed in the next chapter. It would only appear in the orientational order at the surface if the adsorption energy would be such that the reorientation dynamics is much longer than the duration of the experiments (~ 10 hours). Since the adsorption energy associated with a cluster of n_c molecules is $n_c^{1/3} E_{\rm ad}$ and the dipolar energy of the same cluster is $n_c \mu E$, this would mean that:

$$\tau_f \exp\left[\frac{n_c^{1/3}}{kT} - \frac{n_c \mu E}{kT}\right] \gg 10 \text{ hours} \tag{5.38}$$

where $\tau_f \sim 10$s is the typical relaxation of clusters outside the surface layer (see chapter 6). This leads to $E_{\rm ad} \gg 3.3kT$.

From our measurements, we can also deduce that the polar anchoring energy E_θ of the molecules associated with changes in their tilt angle is much larger than the energy of the molecules in the electric field. So for a cluster of n_c molecules: $n_c^{1/3} E_\theta \gg n_c \mu E$, which means that E_θ is much larger than 10^{-1}kT per molecule. Our set-up is however not very sensitive to this polar anchoring energy, as the molecules lay already rather flat onto the substrate without the application of an electric field.

5.7 Outlook

By studying the orientational order of liquid crystal molecules on an isotropic substrate when a DC field is applied, we have investigated the effect of poling on thin liquid crystal film. The obtained information can now be used to analyze future measurements performed with anisotropic substrates to study their anchoring properties. From the present study, we can deduce the potential and limitations of our technique.

This technique is particularly suited to measure azimuthal anchoring energies of surface molecules associated with their reorientations in the plane of the substrate. With the applied fields used in the present studies (2kVmm^{-1}), we can probe energies per molecules up to approximately 10^{-1}kT. The maximum applied field is limited by the occurrence of arcing across the gap between the electrode. Improving by purity of the cell atmosphere could raise this limit.

We can in principle also measure polar anchoring energies associated with reorietations perpendicular to the substrate. However for molecules laying rather flat onto the substrate (which is the case for all measured polar liquid crystal molecules), applying a field parallel to the substrate surface cannot affect much the tilt of the molecules. The sensitivity of the technique is then very low.

6 Reorientation Dynamics in Thin Films

In this chapter we describe the reorientation dynamics of liquid crystal molecules in thin films. We show that this dynamics involves different relaxation regimes characterized by timescales ranging from less than 1ms to several hours. We characterize these different regimes and discuss their origin.

6.1 Introduction

We have seen in the former chapter that we can induce a polar ordering in thin films of 7OCB on fused quartz plates by applying a DC electric field of a few kVmm^{-1}. This polar ordering does not arise from the reorientation of the individual molecules under the effect of the applied field, but from the reorientation of clusters containing a number n_c of molecules having a polar order. $n_c = 17 \pm 4$ at 20° C and decreases to $n_c = 12 \pm 3$ at 40° C. This field-induced polar order of the clusters is different from the order induced by the substrate, which is isotropic in the plane. If the electric field is switched off, the orientational order of the molecules will relax towards an in-plane isotropic distribution. The question arises: how does this relaxation take place?

Studying this relaxation process gives information on how mobile the molecules are at the substrate surface and in the vicinity of the substrate. This mobility depends in particular on whether or not the molecules are adsorbed on the substrate once they have taken a certain orientation. There have been several dynamic studies of liquid crystals close to surfaces showing that surface molecules are less mobile than bulk molecules [75–77, 104–110]. These measurements were however probing averaged dynamic properties over a whole interface or in strongly confined systems. Understanding the results of these measurements and completely characterizing the dynamic behavior of liquid crystals at

interfaces requires understanding the dynamics of the molecules themselves. With our experimental technique, we can measure this dynamics by following the evolution of the orientational order of the molecules in thin films when an electric field is switched on or off.

After describing our experimental procedure (section 6.2), we present our measurements of the relaxation dynamics from the electric-field induced polar ordering to the substrate-induced isotropic order (section 6.3). We find that this relaxation involves four different relaxation regimes with characteristic times ranging from less than 1ms to several hours. The reverse relaxation process observed when the field is switched on shows the same relaxation processes but less distinctly. We finally discuss the possible mechanisms leading to these different regimes (section 6.4).

6.2 Samples and experimental procedure

The samples and the experimental set-up are the same as for the measurements presented in chapter 5 (section 5.4). The measurements consisted in applying an electric field onto the sample until the molecules reached their new equilibrium order. Then the electric field was switched off at a time $t = 0$ and the evolution of the second-harmonic signal was followed in time. This was done using the s-in-s-out signal for an azimuthal orientation of the sample $\Phi = 90°$. As shown in chapter 5 (section 5.4.2.2), this signal is directly proportional to the degree of polar ordering in a sample of constant thickness. The time dependence of the potential applied onto the sample was also recorded to precisely determine the position of $t = 0$. This potential was down to 0 in less than 2ms. Using a similar procedure, we have also performed measurements of the ss signal as the field was switched on. The field raised up and reached its constant level in 20ms.

Depending on the time resolution we wanted to achieve, we measured the time dependence of the signal using two different ways of accumulating data:

- accumulation of laser pulses: the number of counted photons per laser pulse were averaged over a certain number of subsequent pulses. The time-resolution is then determined by the number of accumulated pulses and can be as low as a few seconds. These measurements are not limited in time.

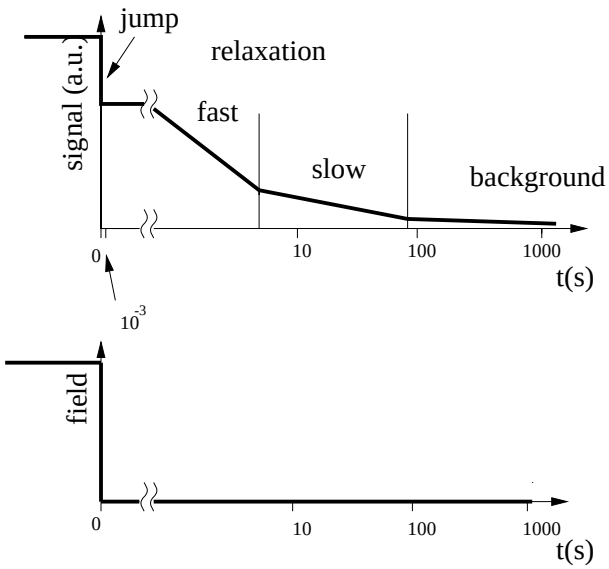

FIGURE 6.1 *Schematic representation of the relaxation of the square-root of the signal at room temperature when the electric field is switched off.*

- accumulation of time scans: the evolution of the signal after time $t = 0$ was measured by the time dependence of the number of counted photons in each laser pulse. To obtain enough statistics, the same relaxation process was repeated around 100 times and the corresponding time scans were averaged. The time-resolution is then determined by the time interval between two laser pulses, which varies between 1.25ms for the maximum repetition rate of 800 Hz of the laser (section 2.2) and 0.1s for a repetition rate of 10Hz. The measurements are then limited in time to 340 laser pulses because of the limited memory of the oscilloscope receiving the signal.

6.3 Experimental results

The overall decay of the second-harmonic signal in the *s*-in-*s*-out polarization configuration when the electric field is switched off is schematically represented in Fig. 6.1. The indicated time scales correspond to a measurement at room temperature (T=20°C). We can distinguish four different relaxation processes. There is first a jump occurring at t=0 in less than the ms time-resolution of our experiments. Then we see two relaxation processes, one that we call fast with a decay time of approximately 10s and another

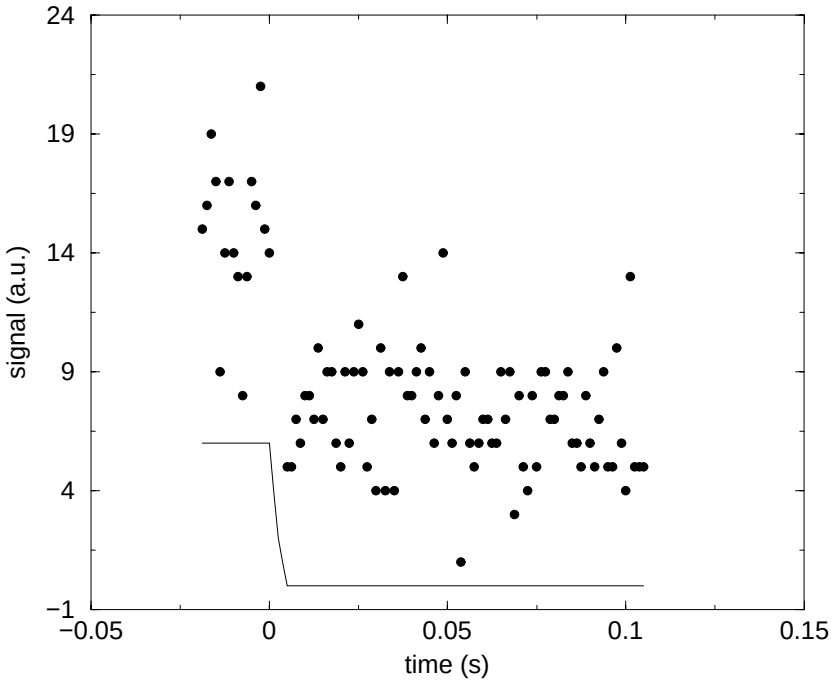

FIGURE 6.2 *Jump of the second-harmonic signal after the electric field is switched off (at t=0). The points correspond to the signal, the solid line to the electric field (a.u.).*

that we call slow, which takes a few hundred seconds. At this point, we are left with a small background signal which decays over approximately 10 hours. In the following, we examine each of these regimes in more detail. At the end of this section, we also discuss the evolution of the second-harmonic signal when the electric field is switched on (section 6.3.4)

6.3.1 Jump

Even with our smallest time resolution, obtained by accumulating time scans measured for a repetition frequency of the laser of 800Hz, we cannot resolve the decay of the second-harmonic signal observed between times t=0 and t=1ms (Fig. 6.2). We have studied the dependence of the jump on the in-plane orientation Φ of the sample by measuring the second-harmonic signal right before and after the jump as a function of Φ (Fig. 6.3). These measurements show that the jump in second-harmonic signal decreases the anisotropy of the signal but keeps its overall shape.

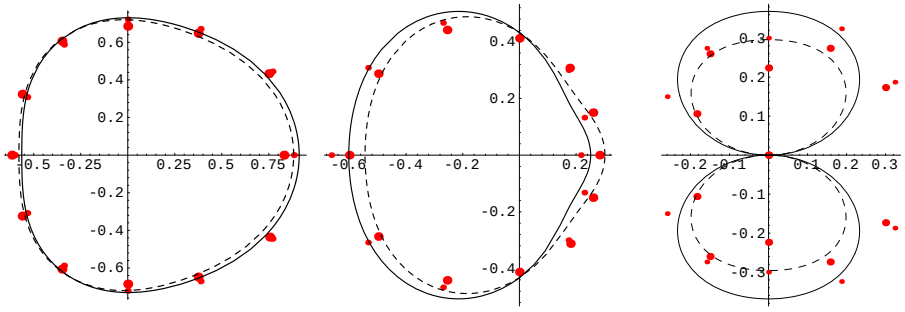

FIGURE 6.3 *From left to right, polar plots of the square root of the signal for the polarization configurations sp, pp, and ss for a film with* $N_b = 5.6 \pm 1$ *bilayers. The solid line is the fit to the signal with field on (small dots), the dashed line is the fit to the signal right after the jump (large dots).*

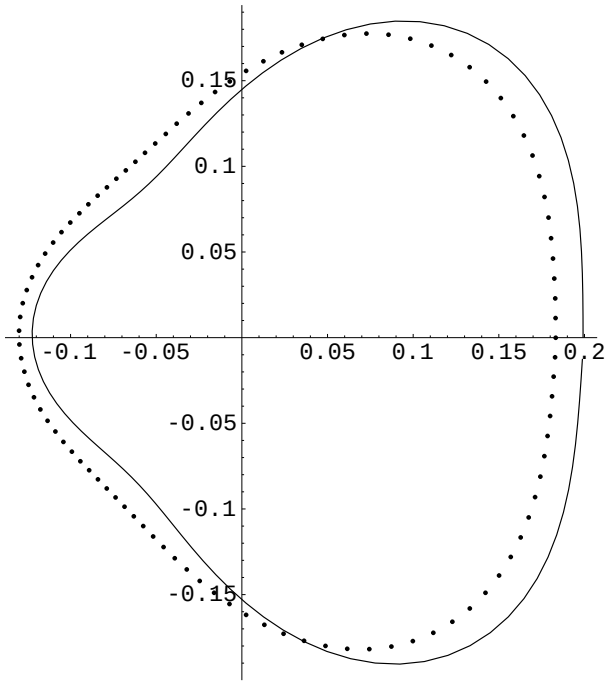

FIGURE 6.4 *The ϕ-distribution function derived from the polar plots of figure (6.3), before the jump (solid line) and after the jump (dotted line).*

One could think that this jump is not due to the reorientation of the molecules in the film but to the disappearance of a contribution to the second-harmonic signal due to the application of an electric field. In section 5.3.2 however, we have ruled out the two possible mechanisms leading to such a contribution. So we can conclude that the jump in second-harmonic signal observed at short time scales is not an artifact due to

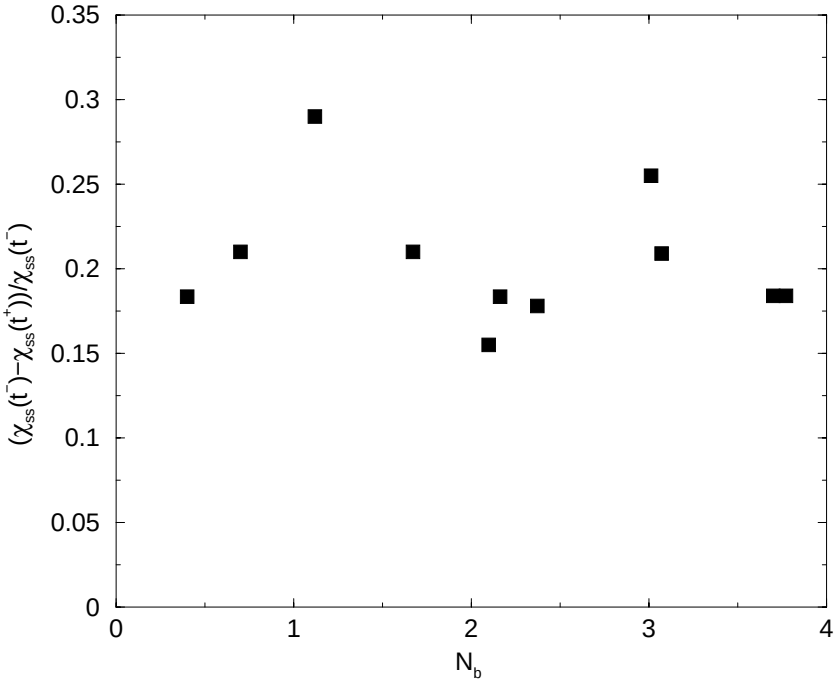

FIGURE 6.5 *Relative reduction of the anisotropy in the orientational distribution* $[\chi_{ss}(t = 0^-) - \chi_{ss}(t = 0^+)]/\chi_{ss}(t = 0^-)$ *as a function of the number of bilayers* N_b *in the film.*

the application of a field, but corresponds to a reorientation of the molecules towards an isotropic in-plane distribution.

To visualize the change of orientational order occurring during the jump, we have fitted the polar plots of Fig. 6.3 and calculated the distribution function of the azimuthal angle ϕ before and after the jump (Fig. 6.4). The distribution function right after the jump is an intermediate distribution function between the electric-field-induced and the isotropic substrate-induced distribution functions.

We have also examined the dependence of the relative reduction of anisotropy taking place during the jump (defined by $[\chi_{ss}(t = 0^-) - \chi_{ss}(t = 0^+)]/\chi_{ss}(t = 0^-)$) on the number of bilayers N_b in the film (Fig. 6.5). This reduction is found to be independent of the film thickness. This means that the relaxation process corresponding to the jump takes place essentially in the same way in the whole film.

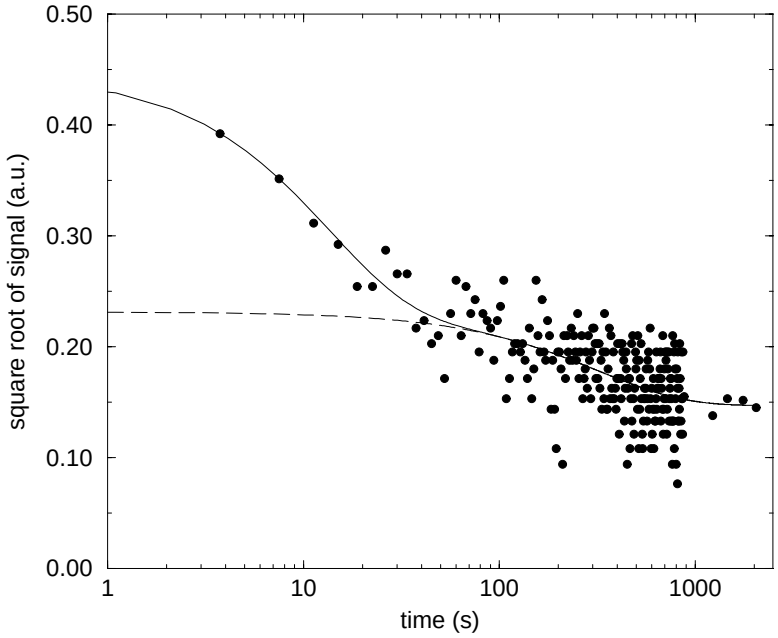

FIGURE 6.6 *Typical decay of the square root of the ss-signal at* $\Phi = 90°$ *after the poling field is switched off at time t=0. The measured film had* $N_b = 21 \pm 2$. *The solid line is a fit with Eq. 6.1 and the dashed line the slow component in this fit (characteristic decay* τ_s*).*

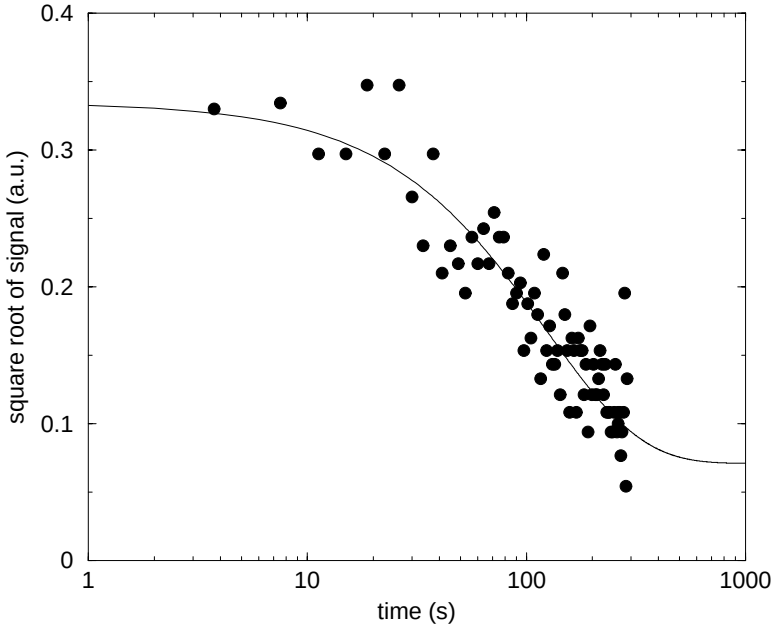

FIGURE 6.7 *The same as figure 6.6 for a film made only of a surface layer. The solid line is a fit with Eq. 6.1 with* $\exp l_f = 0$.

6.3.2 The fast and slow relaxations

A typical decay of the square root of the second-harmonic signal as a function of time (for $t > 1$ s) is shown in Fig. 6.6. Displaying this signal against a logarithmic time scale clearly reveals two distinct relaxation regimes with two distinct relaxation times. To characterize these two regimes, we have fitted the square root of the signal with a sum of two exponential functions:

$$\sqrt{S(t)} = \sqrt{S_0} + \exp(t/\tau_f + l_f) + \exp(t/\tau_s + l_s) \tag{6.1}$$

where S_0 is the background level of the signal, τ_f characterizes the fast relaxation and τ_s the slow relaxation. $\exp l_f$ and $\exp l_s$ are prefactors giving the signal intensity corresponding to each component at $t = 0$.

For all samples, $[\exp l_s]^2$ is equal (within the experimental errors) to the signal of the surface layer in the presence of the electric field. This suggests that the slow relaxation corresponds to the relaxation of the surface layer. This is confirmed by the decay of the signal generated by a film made only of a surface layer (Fig. 6.7) This decay only shows one slow relaxation regime. We also find that $\exp l_f$ decreases when N_b decreases (Fig. 6.8), showing that the fast relaxation corresponds to the relaxation of the covering film.

The relaxation of times τ_f and τ_s do not appear to vary with film thickness within the statistical scatter of our data (see Fig. 6.9). This scatter is particularly large on the measurements of τ_s. This is due to the weakness of the signal of the surface layer under the application of the field, and to the uncertainty on the level of the background for $t \to \infty$ (see section 6.3.3). We have also examined the temperature-dependence of the relaxation times τ_f and τ_s and plotted it in the form of an Arrhenius plot: $\ln \tau$ *versus* 1/kT (see Fig. 6.10). Over the studied temperature range (16°C-40°C), we find that both $\ln \tau_f$ and $\ln \tau_s$ vary linearly with 1/kT with a slope $8 \pm 2 \times 10^{-20}$J and $10 \pm 3 \times 10^{-20}$J respectively. This would correspond to activation energies of 19 ± 5kT and 24 ± 7kT (at room temperature).

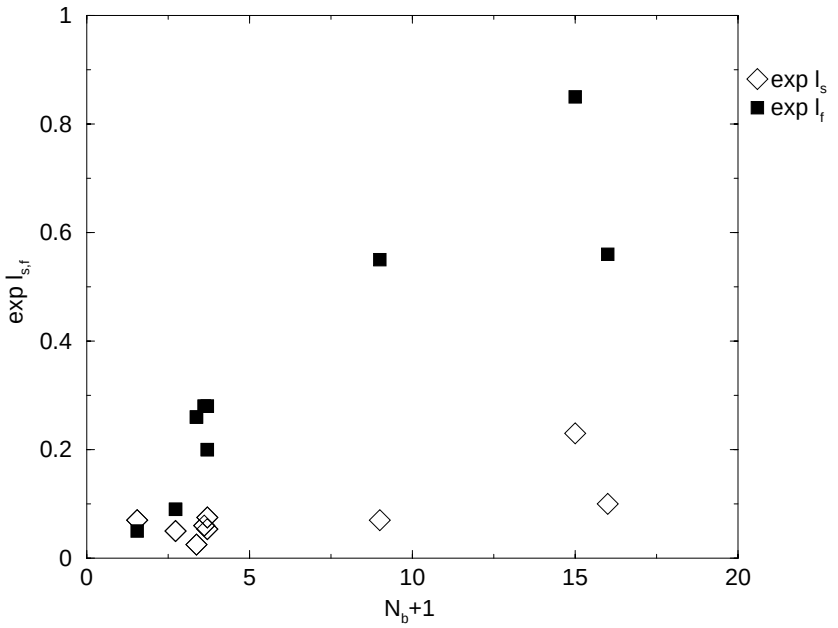

FIGURE 6.8 *The prefactors* $\exp l_f$ (■)*and the* $\exp l_s$ (◇) *as a function of the number of layers* $N_b + 1$ *in a given droplet.*

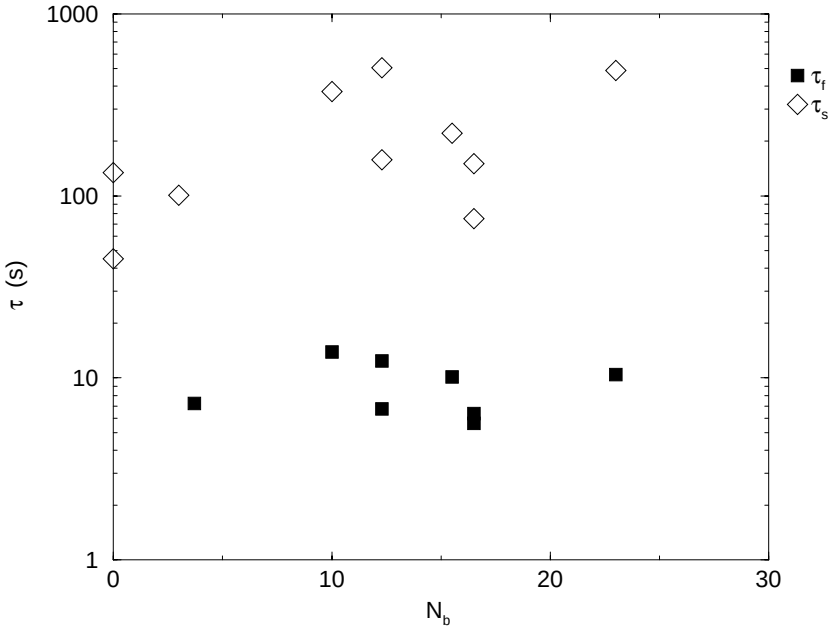

FIGURE 6.9 *The fast* (■) *and slow* (◇) *relaxation times* τ_f *and* τ_s *as a function of the number of bilayers* N_b *in the covering film at T=20° C.*

6.3.3 Background

At the end of the slow relaxation, the signal is not yet back at its noise level, although it is very small (less than 10 % of the signal with field on). At this point of the relaxation

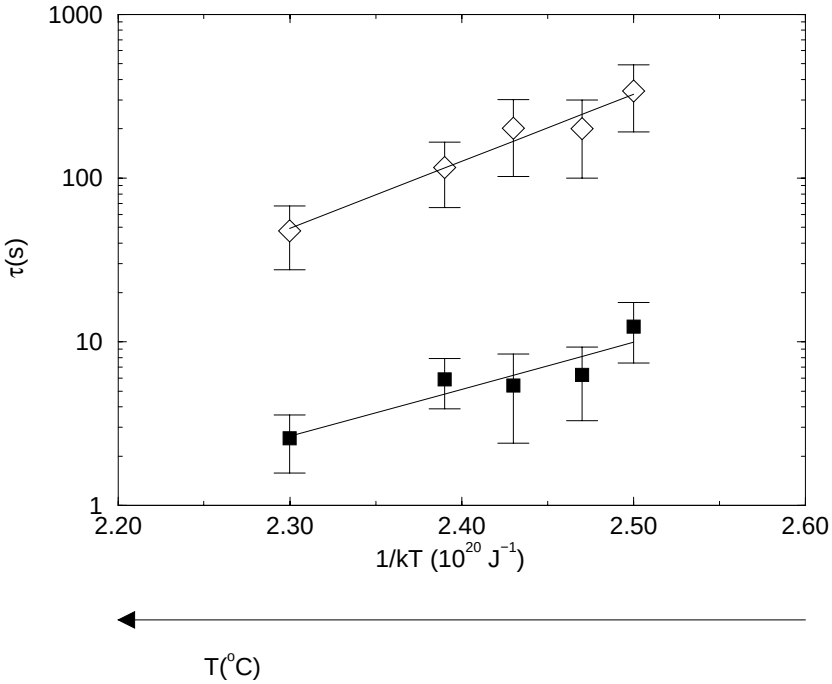

FIGURE 6.10 *Arrhenius plot of the relaxation times τ_f (■) and τ_s (◇) versus the inverse temperature.*

process, we have measured the dependence of the *ss*-signal on the azimuthal orientation Φ of the substrate. It indeed showed an anisotropy. At room temperature, this anisotropy becomes undetectable in approximately ten hours. This decay time reduces to less than an hour at $T = 40°\mathrm{C}$. However this does not mean that the anisotropy has totally disappeared in the surface layer, but only that we cannot measure it. It has already been shown that an isotropic surface can induce a preferred orientation of a liquid crystal although the anisotropy of the orientational distribution at the surface is undetectable with second-harmonic generation [70].

The level of this background signal at the end of the slow relaxation depends on the history of the sample. In particular, it increases if the duration of the poling under electric field increases. Also, for a given duration of the poling, the level of the background increases for successive poling/relaxation cycles if the electric field is switched on again shortly after the slow relaxation ended.

Because of this history-dependence and the weakness of this background, it is difficult to study this relaxation regime quantitatively and we have not attempted it.

6.3.4 Reorientation dynamics under field

When the electric field is applied on a film with an isotropic distribution of azimuthal angles, the molecules reorient towards the anisotropic distribution shown in Fig. 5.8. with a certain dynamics. This dynamics is in principle different from the dynamics of reorientation from the anisotropic to the isotropic states when the electric field is switched off. In the latter case, switching off the electric field leaves the system at $t = 0$ with a distribution of azimuthal angles ϕ out of equilibrium. The system subsequently relaxes under the effect of thermal excitations towards an isotropic distribution. When the field is switched on, the system evolution is driven by the application of an energy potential with one minimum. All dynamic regimes are then expected to be faster than in the case of a relaxation in the absence of field. The expected reduction in relaxation time is given by a factor $\exp \Delta E/kT$, where ΔE is the depth of the potential well induced by the field. From the measurements presented in chapter 5 (section 5.5.2), we have at room temperature and for a field of $2\mathrm{kVmm}^{-1}$:

$$\begin{aligned} \frac{\Delta E}{kT} = \frac{n_c \mu E}{kT} &\approx 0.25 \\ \exp \frac{-\Delta E}{kT} &\approx 0.8 \end{aligned} \tag{6.2}$$

So the effect of the applied field on the dynamics is not very large and falls within the error bars in the determination of the relaxation times τ_f and τ_s.

A typical time dependence of the *ss* signal for an azimuthal orientation $\Phi = 90°$ after a field of $2\mathrm{kVmm}^{-1}$ has been switched on is plotted in Fig. 6.11 against a logarithmic time scale. The evolution in the first milliseconds is shown in Fig. 6.12. The different regimes observed when the field is switched on are now hardly distinguishable from each other. This is due to several reasons. First switching the field on takes twenty times longer that switching it off. This makes it impossible to detect the presence of a jump of the signal at $t = 0$ as the signal follows the increase of the field during the first 20ms (Fig. 6.12). Second it is difficult to distinguish the small contributions of the slow relaxation at the background with respect to the large contribution of the fast relaxation. In the case of the relaxation in zero field, these contributions appeared clearly with respect to the essentially zero noise signal

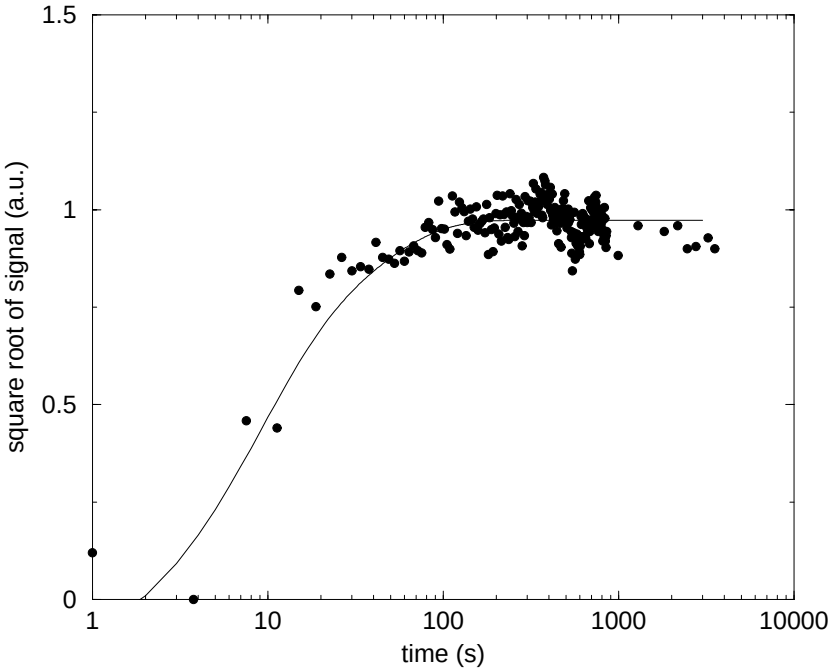

FIGURE 6.11 *Increase of the square-root of the ss signal at* $\Phi = 90°$ *after an electric field of* $2kVmm^{-1}$ *has been switched on at time* $t = 0$. *The measurements were performed on* $N_b = 12 \pm 1$ *bilayers. The solid line is a fit with two exponentials (Eq. 6.1).*

In Fig. 6.11, we can still distinguish a slow relaxation but not a possible increase of the signal at long timescales (the equivalent of the background when the field is switched off). From a fit by the sum of two exponentials (Eq. 6.1), we find at room temperature $\tau_f = 8 \pm 1$s while τ_s can be taken any value above 50s. τ_s can better be measured on the increase of the signal of a surface layer when the field is switched on (Fig. 6.13). We find $\tau_s = 40 \pm 8$. As expected from Eq. 6.2, the value of τ_f is slightly smaller than the corresponding value for the relaxation taking place when the field is switched off (section 6.3.2). The value of τ_s is smaller than predicted. This could be due to the difficulty of differentiating between the slow relaxation and the contribution of the background.

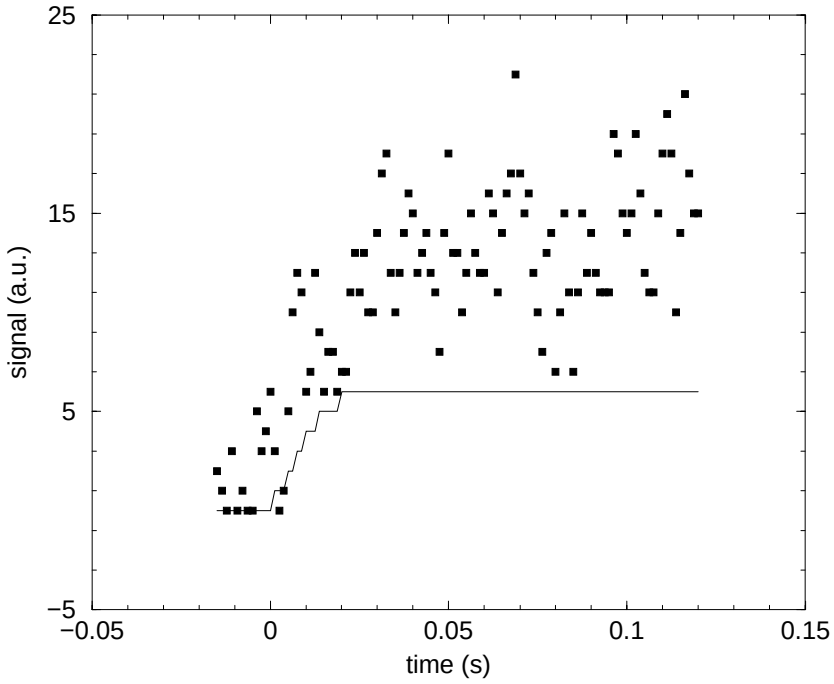

FIGURE 6.12 *Jump of the second-harmonic signal after the electric field is switched on (at t=0). The points is the signal, the solid line is the electric field (a.u).*

6.4 Discussion

Our experimental results give the following picture of the relaxation of the electric-field-induced polar ordering in thin liquid crystal films when the electric field is switched off:

1. In less than 1 ms a first relaxation process (the "jump") takes place in the whole film.
2. The remaining polar ordering of the covering film relaxes in a characteristic time τ_f varying from 10 s at 16°C to 2 s at 40°. We call this the fast relaxation.
3. The surface layer relaxes over longer time scales. Most of its order relaxes in a characteristic time τ_s (slow relaxation) varying from 300 s at 16° to 40 s at 40°
4. A residual polar ordering (background) remains in the surface layer for hours.

We need now to find which mechanisms are responsible for these different relaxation regimes.

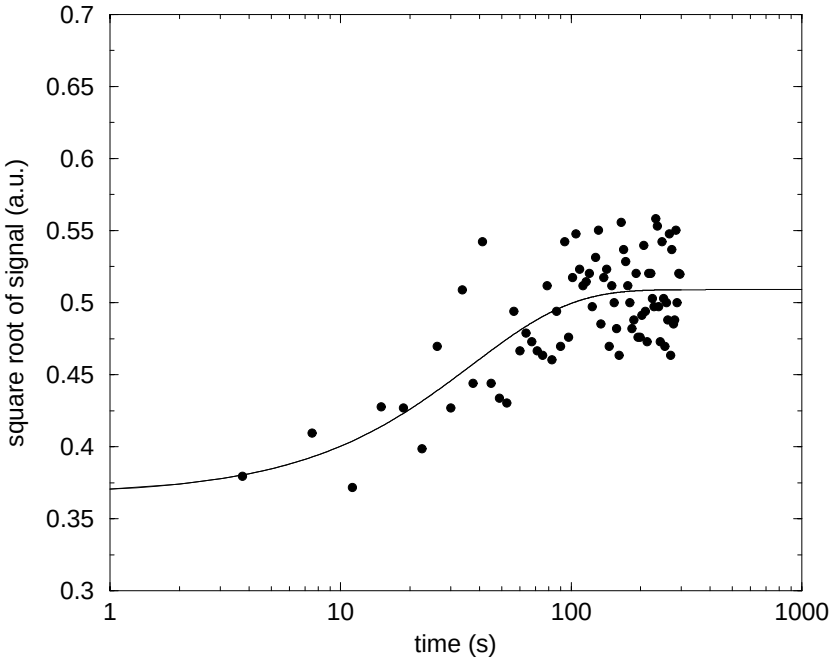

FIGURE 6.13 *The same as figure 6.11 for a film made only of a surface layer. The solid line is a fit with (Eq. 6.1) with* $\exp l_f = 0$.

The short relaxation time of the first regime (the "jump") indicates that it arises from individual reorientations of molecules or clusters. The relaxation time τ_1 of a particle of volume v in a fluid of viscosity η is given by the Debye-Stokes-Einstein law[1][112, 113]:

$$\tau_1 = \frac{6v\eta}{kT}. \tag{6.3}$$

For a nematic liquid crystal, η is the rotational viscosity $\gamma \approx 80cP = 80 \cdot 10^{-3}\mathrm{Nsm}^{-1}$ [13]. Taking for a cluster of n_c molecules, $v = n_c 625$ Å^3, we find at room temperature $\tau_1 \approx n_c 6 \cdot 10^{-8}$s. Since our liquid crystal is supercooled and in the vicinity of a substrate, the viscosity is expected to be larger than in the bulk nematic phase. This viscosity can however be three orders of magnitude higher and the proposed mechanism still be consistent with a relaxation time smaller than 1ms.

The following two regimes (fast and slow relaxations) correspond to the relaxation of most of the order of respectively the covering film and the surface layer. Within the experimental error on the determination of the relaxation times and the activation energies of these two processes, the difference between the two relaxation times

[1]We neglect the correcting factors that need to be added in the case of anisotropic particles [111].

τ_f and τ_s can be explained by the difference in activation energies of these processes: $\ln[\tau_s(20°C)/\tau_f(20°C)] = 3.3$. This energy is then the interaction energy between re-orienting clusters at the the surface and the substrate due to the adsorption of the molecules. This interaction is $n_c^{1/3}$ times the adsorption energy $E_{\rm ad}$ per molecules for a cluster of n_c molecules. Using $n_c = 17$, we find $E_{\rm ad} = 1.3$kT. This is quite small, but we should remember that it is the anisotropic part of the interaction energy associated with rotations of the molecules in the plane of the substrate. The total adsorption energy associated with a complete desorption from the surface is probably much larger.

So we can conclude that the fast and slow relaxations correspond to the same type of relaxation process, taking place in the covering film and the surface layer, with the dynamics of the latter being slowed down by the interaction of the surface molecules with the substrate. We need now to find out which type of relaxation the fast and the slow relaxations correspond to, and why they are so slow with respect to the first relaxation regime, i.e. the jump. One possibility is that it corresponds to individual reorientation of clusters in a fluid of much larger viscosity. This would imply the presence of regions in different phases with very different viscosities. However this is inconsistent with the fact that the jump is responsible for a decease of 20 % of the polar ordering independently of the thickness of the film: this means that the first relaxation process occurs rather homogeneously over the whole film.

Another possibility is that there are strong correlations between the clusters leading to a glass-type of dynamics. This type of correlations has been seen in simulations of dipolar fluids [114, 115]. This would however imply that the relaxation time of the system would strongly depend on the thickness of the sample, as this thickness determines the length scale of the dynamic correlations in the direction perpendicular to the surface [116]. We do not find such a dependence.

So we have at this point no satisfactory explanation for the large difference between the jump on the one hand and the fast and slow relaxation on the other hand. We can only say that there is a small fraction of molecules ($\sim$ 20 %) which have a liquid-like dynamics while the rest has a slow dynamics.

The last relaxation process (the background) also taking place in the surface layer, needs at least two orders of magnitude more time than the slow relaxation. This long

time scale indicates that it is due to strong interactions of molecules with the substrate, as it can happen at defects. Since these defects are not all the same, and therefore their interaction potential with the liquid crystal molecules might vary, we actually expect a relaxation of this background with a stretched exponential [117]. As in glasses this type of dynamics gives rise to significant history-dependence of the dynamics, which we have indeed observed.

Let us now compare our result with the available information on the dynamics of liquid crystal molecules at interfaces. There have been several experiments showing that in the vicinity of a surface, the dynamics of a liquid crystal slows down with respect to that of the bulk [76, 77, 105–110]. They are however based on the measurements of quantities averaged over the whole interfacial region between the surface and the bulk. Their results are therefore difficult to compare directly with ours. The reported size of the effect varies a lot. The surface dynamics was found to be 1.7 times slower than bulk dynamics by evanescent wave photon correlation spectroscopy [77], 10 times slower in anchoring breaking experiments [105], and 10^3 times slower by dielectric spectroscopy [76] and NMR [75]. NMR measurements with pyridine gave a factor 10^2 [118]. Our measurements show that several relaxation times differing by several orders of magnitude are involved close to a surface. Obviously depending on the technique and system used, different relaxation mechanisms are probed, leading to large discrepancies between the reported results.

There is also one measurement reported of the adsorption energy of liquid crystal molecules on a substrate, namely 8CB on unrubbed polymer [70]. They found a value of 82kT, which is extremely high (for instance, the hydrogen bond energy is approximately 6kT). Although the fact that this studied system is different from ours might contribute to this difference, most of it has probably another reason. The measurements performed in reference [70] consisted in aligning a bulk liquid crystal between two unrubbed polymer surfaces by putting it in a magnetic field. This alignment remains if the field is switched off because of the adsorption of the molecules at the surfaces: this is the so-called memory effect. The sample was then heated for a given time in the isotropic phase and cooled down to the nematic phase. The time necessary for the disappearance of the nematic alignment was measured as a function of temperature. An Arrhenius plot of the

decay time of the alignment gave the energy of adsorption. On the other hand, second-harmonic generation measurements were performed on the same sample and showed that the surface layer had an isotropic orientational order within the experimental sensitivity of 7% [70].

The combination of these two experiments can be interpreted in two ways. All the molecules in the surface layer can be strongly bound to the substrate with the measured energy of 82kT in an orientational distribution having an anisotropy of less than 7%. This is the conclusion that Ouchi and coworkers have drawn. This would imply a strong chemisorption of the molecules. This would in particular mean that the molecules would only desorb at high temperatures, while we already see a significant desorption at 50°C.

The other possible interpretation is that there is a small proportion of molecules which are strongly adsorbed with the measured energy of 82kT at some points onto the surface, for instance on chemical inhomogeneities or defects. The orientational order of these molecules might have a significantly higher anisotropy than 7%; however their contribution in the total anisotropy is small because of their small number. Our results are in agreement with this second interpretation. We see that most of the molecules in the surface layer are adsorbed onto the surface with a reasonable energy of a few kT and relax in a few 100s. A small fraction of the surface molecules (responsible for the background signal) relax with much longer characteristic times, meaning that their adsorption energy is much larger. These molecules are responsible for the surface memory effect observed by Ouchi and coworkers. The fact that this effect is due to the adsorption of molecules with a very slow dynamics has also been shown by the slow reorientation (over hours) of the surface director in a liquid crystal oriented by a surface memory effect when it is submitted to a field in a different direction [72].

6.5 Outlook

The measurements presented in this chapter show that our experimental technique is able to follow the dynamics of liquid crystal molecules at the interface with a substrate. With the present experimental set-up, we can probe relaxation times from a few ms to at least days. The upper limit is actually set by the life-time of the samples which

are generally very sensitive to contamination. The lower limit is given by the decay time of the electric field and the detection system. By improving both and using trigger techniques, it is possible to lower this limit down to fractions of millisecond [119]. Considering the large discrepancies between the results given by other techniques probing the interfacial dynamics in a global way, more dynamic measurements at a microscopic level are necessary to understand this dynamics.

Bibliography

[1] O. Lehmann, Z. Phys. Chem. **4**, 462 (1889).

[2] C. Mauguin, Phys. Z. **12**, 1011 (1911).

[3] C. Mauguin, C. R. Acad. Sci. **156**, 1256 (1913).

[4] C. Mauguin, Bull. Soc. Fr. Miner. **34**, 71 (1911).

[5] P. Chatelain, Bull. Soc. Fr. Miner **66**, 105 (1943).

[6] J. Cognard, Mol. Cryst. Liq. Suppl. **1**, 1 (1982).

[7] M. Schadt, Liq. Cryst. **5**, 57 (1989).

[8] M. Schadt and W. Helfrich, Appl. Phys. Lett. **18**, 127 (1970).

[9] C. Mauguin, Bull. Soc. Miner. **34**, 6 (1911).

[10] V. Freedericksz and V. Zolina, Trans. Faraday Soc. **29**, 192 (1933).

[11] G. Friedel, Ann. Phys. **18**, 273 (1922).

[12] P. Bolhuis, *Liquid-like behavior in solids, Solid-like behavior in liquids*, 1996, Utrecht.

[13] P. G. de Gennes and J. Prost, *The Physics of liquid crystals* (Clarendon Press, Oxford, 1993).

[14] G. Vertogen and W. H. de Jeu, *Thermotropic liquid crystals, Fundamentals* (Springer, Berlin, 1988).

[15] P. J. Collings and M. Hird, *Introduction to liquid crystals* (Taylor & Francis, London, 1997).

[16] G. W. Gray and J. W. Goodby, *Smectic liquid crystals* (Leonard Hill, Glazgow, 1984).

[17] B. Jérôme, Rep. Prog. Phys. **54**, 391 (1991).

[18] H. Yokoyama, Mol. Cryst. Liq. Cryst. **165**, 265 (1988).

[19] A. A. Sonin, *The surface physics of liquid crystals* (Gordon and Breach, Amsterdam, 1995).

[20] G. L. Richmond, J. M. Robinson, and V. L. Shannon, Prog. Surf. Sci **28**, 1 (1988).

[21] J. M. Chen, J. R. Bower, C. S. Wang, and C. H. Lee, Opt Comm **9**, 132 (1973).

[22] D. V. Murphy *et al.*, Surf. Sci **124**, 529 (1983).

[23] T. Rasing, Y. R. Shen, M. W. Kim, and S. G. Grubb, Phys. Rev. Lett. **55**, 2903 (1985).

[24] J. M. Hicks, K. Kemnitz, K. B. Eisenthal, and T. F. Heinz, J. Phys. Chem. **90**, 560 (1986).

[25] C. K. Chen, T. F. Heinz, D. Richard, and Y. R. Shen, Phys. Rev. Lett. **46**, 1010 (1981).

[26] G. A. Reider, A. J. Schmidt, and G. Marowsky, Opt. Comm **47**, 223 (1983).

[27] I. R. Girling *et al.*, J. Opt. Soc. Am. B **B 4**, 950 (1987).

[28] W. Chen, M. B. Feller, and Y. R. Shen, Phys. Rev. Lett. **63**, 2665 (1989).

[29] T. F. Heinz, F. J. Himpsel, E. Palange, and E. Burnstein, Phys. Rev. Lett. **63**, 644 (1989).

[30] Y. R. Shen, Nature **337**, 519 (1989).

[31] K. B. Eisenthal, Annu. Rev. Phys. Chem. **43**, 627 (1992).

[32] T. F. Heinz, in *Nonlinear Surface Electromagnetic Phenomena*, edited by H. E. Ponath and G. I. Stegeman (Elsevier Science Publishers B.V., Amsterdam, 1991), Chap. 5, p. 353.

[33] H. Hsiung and Y. R. Shen, Phys. Rev. A **34**, 4303 (1986).

[34] P. Guyot-Sionnest, W. Chen, and Y. R. Shen, Phys. Rev. B **33**, 8254 (1986).

[35] P. Guyot-Sionnest and Y. R. Shen, Phys. Rev. B **38**, 7985 (1988).

[36] P. Guyot-Sionnest, H. Hsiung, and Y. R. Shen, Phys. Rev. Lett. **57**, 2963 (1986).

[37] B. Jérôme and Y. R. Shen, Phys. Rev. E **48**, 4556 (1993).

[38] M. B. Feller, W. Chen, and Y. R. Shen, Phys. Rev. A **43**, 6778 (1991).

[39] *Micas*, Vol. 13 of *Reviews in Mineralogy*, edited by S. W. Bailey (Bookcrafters, Chelsea, 1987).

[40] E. T. Jayne, Phys. Rev. **106**, 620 (1957).

[41] O. Svelto, *Principles of Lasers*, 3rd ed. (Plenum Press, New York and London, 1998).

[42] J. D. Jackson, *Classical Electrodynamics (2nd edition)* (John Wiley & Sons, Inc., New York, 1975).

[43] W. Gibbons, P. Shanon, S. T. Sun, and B. Svetlin, Nature **351**, 49 (1991).

[44] M. Schadt, H. Seiberle, and A. Schuster, Nature **381**, 212 (1996).

[45] V. K. Gupta and N. L. Abbott, Phys. Rev. E **54**, R4540 (1996).

[46] V. K. Gupta and N. L. Abbott, Science **276**, 1533 (1997).

[47] M. Barmentlo, R. J. Hollering, and N. A. J. M. van Aerle, Phys. Rev. A **46**, R4490 (1992).

[48] D. Johannsmann *et al.*, Phys. Rev. E **48**, 1889 (1993).

[49] X. Zhuang, L. Marrucci, and Y. R. Shen, Phys. Rev. Lett. **73**, 1513 (1994).

[50] B. Jérôme, J. Phys. Condens. Matt. **6**, A269 (1994).

[51] B. Jérôme *et al.*, Phys. Rev. Lett. **71**, 758 (1993).

[52] F. Grandjean, Bull. Soc. Fr. Min. **39**, 164 (1916).

[53] N. Tikhomirova and A. V. Guinsberg, in *Advances in Liquid Research and applications*, edited by L. Bata (Pergamon Press, Oxford, 1980), p. 651.

[54] E. K. Frolova, O. G. Sarbey, and A. S. Sybashvily, Mol. Cryst. Liq. Cryst. **104**, 111 (1984).

[55] T. V. Korkishko *et al.*, Sov. Phys. Crystallogr. **32**, 263 (1987).

[56] B. Jérôme, A. Bosseboeuf, and P. Pieranski, Phys. Rev. A **42**, 6032 (1990).

[57] P. Pieranski, B. Jérôme, and M. Gabay, Mol. Cryst. Liq. Cryst. **179**, 285 (1990).

[58] P. Pieranski and B. Jérôme, Phys. Rev. A **40**, 317 (1989).

[59] B. Jérôme and P. Pieranski, Liq. Cryst. **5**, 683 (1989).

[60] G. Friedel, in *Leçons de cristallographie* (Librarie Scientifique Albert Blanchard, Paris, 1964), p. 420.

[61] Merck datasheets.

[62] J. Chakrabarti and B. Mulder, Mol. Cryst. Liq. Cryst. (1998), to appear.

[63] P. A. Lebwohl and G. Lasher, Phys. Rev. A **6**, 426 (1972).

[64] P. A. Lebwohl and G. Lasher, Phys. Rev. A **7**, 2222 (1972).

[65] P. G. de Gennes, Mol. Cryst. Liq. Cryst. **12**, 193 (1971).

[66] J. Chakrabarti and B. Mulder, Conference: Structure in Liquids, Norwich, 1996.

[67] L. M. Blinov, A. Y. Kabayenkov, and A. A. Sonin, Liq. Cryst. **5**, 645 (1989).

[68] N. Koshida and S. Kibui, Appl. Phys. Lett. **40**, 541 (1982).

[69] H. A. van Sprang, Mol. Cryst. Liq. Cryst. **97**, 255 (1983).

[70] Y. Ouchi, M. B. Feller, T. Moses, and Y. R. Shen, Phys. Rev. Lett. **68**, 3040 (1992).

[71] N. A. Clark, Phys. Rev. Lett. **55**, 292 (1985).

[72] D. Stoenescu, private communication.

[73] R. Barberi *et al.*, Eur. Phys. J. B (to appear) (unpublished).

[74] D. W. Berreman, Phys. Rev. Lett. **28**, 1683 (1972).

[75] G. P. Crawford, D. K. Yang, S. Žumer D. Finotello, and J. W. Doane, Phys. Rev. Lett. **66**, 723 (1991).

[76] F. M. Aliev and M. N. Breganov, Sov.Phys. JETP **68**, 70 (1989).

[77] C. S. Park, M. Čopič, R. Mahmood, and N. A. Clark, Liq. Cryst. **16**, 135 (1994).

[78] D. A. M. Smith and H. J. Coles, Liq. Cryst. **14**, 937 (1993).

[79] K. D. Singer, J. E. Sohn, and S. J. Lalama, Appl. Phys. Lett. **49**, 248 (1986).

[80] C. S. Mullin, P. Guyot-Sionnest, and Y. R. Shen, Phys. Rev. A **39**, 3745 (1989).

[81] P. N. Prasad and D. J. Williams, in *Introduction to nonlinear optical effects in molecules and polymers* (John Wiley & Sons, New York, 1991), Chap. 7, p. 132.

[82] J. W. Wu, J. Opt. Soc. Am. B **8**, 142 (1991).

[83] P. M. Chaikin and T. C. Lubensky, in *Principles of condensed matter physics* (Cambridge university press, Cambridge, 1995), Chap. 3, pp. 119–123.

[84] G. Arfken, *Mathematical methods for physicists* (Academic Press, San Diego, 1995).

[85] F. Hardouin, A. M. Levelut, M. F. Achard, and G. Sigaud, J .Chim.Phys **80**, 53 (1985).

[86] M. I. Barnick, L. M. Blinov, A. M. Dorozhkin, and N. M. Shtykov, Sov. Phys. JETP **54**, 935 (1981).

[87] G. Berkovic, T. Rasing, and Y. R. Shen, J. Opt. Soc. Am. B **4**, 945 (1987).

[88] M. D. Nijkerk, private communication.

[89] M. Stähelin *et al.*, J. Appl. Phys. **73**, 8471 (1993).

[90] P. Bordewijk and W. H. de Jeu, J. Chem. Phys **68**, 116 (1978).

[91] D. A. Dunmur and W. H. Miller, Mol. Cryst. Liq. Cryst **60**, 281 (1980).

[92] A. J. Leadbetter *et al.*, J. Phys. (France) **40**, 374 (1979).

[93] L. G. P. Dalmolen, S. J. Picken, A. F. de Jong, and W. H. de Jeu, J. Physique **46**, 1443 (1985).

[94] L. Longa and W. H. de Jeu, Phys. Rev. A **26**, 1632 (1982).

[95] D. Wei, G. N. Patey, and A. Perera, Phys. Rev. E **47**, 506 (1993).

[96] B. Groh and S. Dietrich, Phys. Rev. Lett. **72**, 2422 (1994).

[97] H. Zhang and M. Widom, Phys. Rev. E **49**, R3591 (1994).

[98] F. Biscarini and C. Zannoni, Mol. Cryst. 73 **73**, 439 (1991).

[99] D. Wei and G. N. Patey, Phys. Rev. Lett. **68**, 2043 (1992).

[100] D. Wei and G. N. Patey, Phys. Rev. A **46**, 7783 (1992).

[101] J. J. Weis, D. Levesque, and G. J. Zarragoicoechea, Phys. Rev. Lett. **69**, 913 (1992).

[102] J. Xue, C. S. Jung, and M. W. Kim, Phys. Rev. Lett. **69**, 474 (1986).

[103] M. P. Valignat *et al.*, Phys. Rev. Lett. **77**, 1994 (1996).

[104] Y. Marinov, N. Shonova, C. Versace, and A. G. Petrov, ILCC 1998.

[105] A. Gharbi, F. R. Fekih, and G. Durand, Liq. Cryst. **12**, 515 (1992).

[106] A. G. Petrov, A. T. Ionesco, C. Versace, and N. Scaramuzza, Liq. Cryst. **19**, 169 (1995).

[107] X. I. Wu, W. I. Goldburg, M. X. Liu, and J. Z. Xue, Phys. Rev. Lett. **69**, 470 (1992).

[108] T. Bellini, N. A. Clark, and D. W. Schaefer, Phys. Rev. Lett. **74**, 2740 (1995).

[109] A. Mertelj and M. Čopič, Phys. Rev. E **55**, 507 (1997).

[110] M. Čopič and A. Mertelj, Phys. Rev. Lett. **80**, 1449 (1998).

[111] C. M. Hu and R. Zwanzig, J. Chem. Phys. **60**, 4354 (1974).

[112] P. Debye, *Polar Molecules* (Dover, New York, 1929).

[113] G. Tarjus and D. Kivelson, J. Chem. Phys. **103**, 3071 (1995).

[114] M. E. van Leeuwen and B. Smit, Phys. Rev. Lett. **71**, 3991 (1993).

[115] G. Ayton, M. J. P. Gingras, and G. N. Patey, Phys. Rev. E **56**, 562 (1997).

[116] B. Jérôme and J. Commandeur, Nature **386**, 589 (1997).

[117] M. B. Weisman, Rev. Mod. Phys **60**, 537 (1988).

[118] J. P. Korb *et al.*, Phys. Rev. Lett. **77**, 2312 (1996).

[119] A. Dhinojwala, G. K. Wong, and J. M. Torkelson, Macromolecules **26**, 5943 (1993).

SAMENVATTING

Dit proefschrift beschrijft een studie over hoe vloeibare kristal moleculen zich gedragen in de buurt van een oppervlak. Dit betekent niet dat na deze studie alles bekend is over het gedrag van bovengenoemde moleculen in de buurt van oppervlakken. Integendeel, we hebben ons slechts op een klein deelgebiedje van dit vakgebied toegespitst en menen daar wat opheldering te hebben gebracht. Dat er nog een heleboel zaken onderzocht kunnen worden en dat er ook talloze onderzoeksgroepen werkzaam zijn in dit vakgebied, geeft aan dat deze sector, zacht gecondenseerde materie een groot fascinerend gebied is. Te bedenken dat de zacht gecondenseerde materie weer een deelgebied is van de "gehele" wetenschap geeft aan hoeveel er nog onderzocht kan worden.

Het onderzoek beschreven in dit werk naar de vloeibare kristallen in contact met oppervlakken focusseert zich enerzijds op hoe dunne films, enkele molecuullagen dik zich gedragen. Anderzijds hebben we onderzocht hoe dikke films of wel "druppels" van miljoenen lagen zich gedragen.

Vloeibare kristallen zijn stoffen die onder andere kunnen bestaan uit moleculen die er niet uitzien als bolletjes maar eerder als lange staafjes. De orde van het vloeibaar kristal zegt iets over hoe geordend de moleculen ten opzichte van elkaar gaan liggen. De geordendheid van de moleculen is te vergelijken met bijvoorbeeld die van stijve spagetti staafjes. Deze staafjes kunnen bijvoorbeeld keurig naast elkaar in het pak zitten, we zeggen dan, de staafjes zijn goed geordend. Wanneer men ze op de grond zou gooien en wijzen de staafjes alle kanten op dan zeggen we, de staafjes zijn slecht geordend. De richting van de spagetti in het pak, wordt bepaald door (open deur) de richting van het pak. De richting van een vloeibaar kristal wordt bepaald door het oppervlak. In deze studie hebben we veelal de geordendheid en de richting van vloeibare kristallen onderzocht.

De richting van een vloeibaar kristal kan, behalve door een oppervlak, ook bepaald worden door een electro-magnetisch veld. Doordat de richting kan worden opgelegd door zowel een oppervlak als door een electrisch veld, kan men met deze twee concurrerende effecten, de richting beinvloeden. Als nu de richting opgelegd door het electro-magnetische veld niet hetzelfde is als die van het oppervlak, kan de richting van het vloeibare kristal

tussen verschillende toestanden switchen. Door dit mechanisme werkt het liquid crystal display (LCD).

In hoofdstuk 2 bespreken we de technieken die we hebben gebruikt om de richting in de bulk (dit is het gedeelte van de druppel die we met het blote oog kunnen zien) van het vloeibaar kristal vast te stellen. Moleculen afzonderlijk kunnen we niet zien en dus hebben we apparatuur nodig die gevoelig genoeg is om hier uitsluitsel over te geven. Als we de richting willen bepalen van de bulk kunnen we dit doen met behulp van microscopen en polaroid glazen. Een druppel vloeibaar kristal is ook een soort polaroid glas, en door dit te verglijken met de bekende richting van een polaroid glas kan de richting van het vloeibare kristal worden bepaal. Als we de microscopische richting van de moleculen aan het oppervlak willen bepalen, in een laag die zo dik is als een molecuul, gebruiken we daarvoor een laser en een speciale techniek: tweede harmonische generatie. Deze techniek is erg geschikt om de richting van de moleculen die tegen het oppervlak aan liggen te bepalen. De moleculen die daar weer bovenop liggen zien we niet met deze techniek. De informatie die verkrijgen door deze techniek is dus van een hele dunne laag moleculen (namelijk een laag van 1 molecuul lengte dik). De orientaties van de moleculen in deze eerste laag wordt bepaald door het oppervlak. Het is hierom niet verwonderlijk dat er allerlei eigenschappen van het oppervlak terug te vinden zijn in de eerst laag vloeibaar kristal moleculen. Deze eigenschappen kunnen bijvoorbeeld zijn de symmetrieen die aanwezig zijn in het oppervlak. Door rekening te houden met deze symmetrieen is het mogelijk het probleem eenvoudiger te maken. Populair gezegd, als je weet dat bijvoorbeeld twee richtingen in het oppervlak hetzelfde zijn, hoef je slechts de vloeibare kristal moleculen langs een van deze richtingen te volgen. Hierdoor reduceereert de benodigde informatie om tot een totaler beeld te komen.

In hoofdstuk 3 beschrijven we het eerste gedeelte van de experimenten. De probleemstelling luidt: als een oppervlak een drievoudige symmetry in het vlak heeft (dit betekent, het oppervlak heeft 3 kristal assen; deze assen vallen bijvoorbeeld samen met de wijzers van een klok die plat op het oppervlak ligt. De identieke eigenschappen zijn dan op 12, op 4 en op 8 uur), langs welke richting en waarom gaat het vloeibaar kristal zich richten als de richting niet loodrecht op het vlak gaat staan? Om dit te bestuderen hebben we een oppervlak van phlogopite mica genomen. Deze soort mica bevat 3

identieke richtingen in het vlak. Het blijkt dat de richting van het vloeibaar kristal zich langs of loodrecht ten opzichte van een van de drievoudige assen orienteert. Eveneneens blijkt dat de wanneer de vochtigheid van de atmosfeer wordt gevarieerd de richting van het vloeibaar kristal overgaat van de ene toestand (loodrecht) naar de andere (parallel).

In hoofdstuk 4 geven we een mogelijke verklaring voor het experimenteel gevonden gedrag. We behandelen een mogelijke theoretische berekening die het beschreven gedrag verklaard. We vinden dat het veranderen van de richting die het vloeibaar kristal verkiest (ankerings richting) wordt veroorzaakt door een minuscule verandering in de tilt oftewel hellingshoek van de vloeibaar kristal moleculen aan het oppervlak van het phlogopite mica oppervlak. Deze verandering in de hellingshoek werd veroozaakt door het verhogen of verlagen van de aangebrachte luchtvochtigheid. Water moleculen dringen zich door de dunne film of laag vloeibaar kristal moleculen heen en gaan aan het oppervlak zitten. Daardoor verstoren ze de richting van de vloeibaar kristal moleculen.

In hoofdstuk 5 begint een nieuw onderdeel in dit proefschrift en behandeld het uitrichten van dunne films vloeibaar kristal. Vloeibaar kristal moleculen bezitten – evenals vele andere moleculen en atomen– een electromagnetische eigenschap waardoor ze gevoelig zijn voor een electro-magnetisch veld. Hierdoor reageren ze net als een kompasnaald en richten ze zich in een en dezelfde richting namelijk die van het electro-magnetisch veld. Het was al bekend dat bulk vloeibaar kristal zich liet uitrichten door een sterk genoeg electro magnetische veld (ook wel electrisch veld genoemd), maar hoe zit het met de moleculen aan het oppervlak? We weten dat er aan het oppervlak twee concurrerende effecten zijn, namelijk die van het oppervlak en die van het electrisch veld. Het is de vraag welke van de twee het sterkste is en aan de hand daarvan zal deze de richting bepalen. In hoofdstuk vijf behandelen we een stukje theorie van “poling of thin films”–dit is uitrichten van lagen moleculen– en proberen we te voorspellen hoe dit verschijnsel terug te vinden zal zijn in onze metingen. De invloed van het electische veld is vergelijkbaar met die van het oppervlak en zoals uitgelegd in hoofdstuk twee, geven moleculen aan het oppervlak een tweede harmonisch signaal. Zo ook krijgen we tweede harmonisch signaal van moleculen die onderhevig zijn aan een electrisch veld. Alleen laatstgenoemde moleculen hoeven zich niet noodzakelijk aan het oppervlak te bevinden. Als we de voorspellingen vergelijken de metingen vinden we dat we veel meer signaal

meten dan we zouden verwachten. De moleculen reageren veel sterker op het veld dan dat men in de eerste plaats zou denken. Een mogelijke verklaring hiervoor kan zijn dat de moleculen als het ware samenwerken in hun "response" op het aangebrachte electrische veld. Bij deze samenwerking van de moleculen denken we aan het vormen van klontjes of clusters. In deze clusters wijzen de moleculen dezelfde kant uit en worden niet door elkaar uit hun richting verstoord. De richting van zo'n cluster gaat langs de richting van het electro-magnetisch veld liggen. En dit verschijnsel nemen we waar. Individuele moleculen richten zich ook wel langs het electrisch veld maar door de temperatuur die de moleculen nogal doet bewegen worden deze individuele moleculen veel sneller uit hun richting gebracht dan de moleculen die zich in een cluster bevinden. Om deze bewering van het bestaan van clusters te sterken hebben we experimenten gedaan waarbij we de temperatuur verhogen. We vinden dat deze temperatuursverhoging de clusters, die te vergelijken zijn met minuscule blokjes ijs, doet smelten. Het systeem waar we aan denken is te vergelijken met een hoeveelheid smeltend ijs waarin zowel clusters (ijsblokjes) als individuele moleculen (water) aanwezig zijn.

Het laatste hoofdstuk van dit proefschrift behandeld de relaxatie dynamica van de vloeibaar kristal moleculen nadat we het electrische veld uitzetten. Bij het uitzetten van het veld vindt er een relaxatie in het materiaal plaats die gepaard gaat met het herorienteren van de vloeibaar kristal moleculen. De temperatuur die de moleculen kris kras doet bewegen maakt dat de moleculen als het ware vergeten welke kant het electrisch veld uit wees. Op zich lijkt dit experiment saai, maar dat bleek het achteraf helemaal niet te zijn. Bij het uitschakelen van het electromagnetisch veld, zagen we namelijk dat de relaxatie van de laag vloeibaar kristal moleculen verschillende relaxatie niveaus doorliep. Deze niveau's karakteriseerden zich door de verschillende tijdsduren waarmee ze gemoeid waren. Zo bleek bijvoorbeeld dat de individuele moleculen zich razendsnel (kleiner dan 0.001 seconde) herorienteerden naar een willekeurige positie. De clusters in het binnenste van de film (dit is niet de oppervlakte laag) herorienteerden zich langzamer maar op de tijdsduur van het experiment nog vrij snel (ongeveer 1-10 seconden). De moleculen in de clusters aan het oppervlak reorienteerden zich heel langzaam (van minuten tot vele uren). Het feit dat de relaxatie van de oppervlakte laag langer duurde dan de relaxatie in het binnenste van de film werd eenvoudig aangetoond

door experimenten met zeer dunne films die, laten we zeggen alleen maar clusters aan het oppervlak heeft, zich orienteerden in een veel langere periode dan dikkere films–welke clusters bevatten die niet in contact zijn met het oppervlak–.

Zoals met zoveel experimenten die worden gedaan in nieuwe gebieden van onderzoek, geeft elk gevonden antwoord weer aanleiding tot nieuw vragen. Men kan dit frustrerend ingewikkeld of fascinerend complex vinden. Ook de experimenten beschreven in dit proefschrift hebben nieuwe inzichten gebracht voor de vraag hoe vloeibare kristal moleculen zich in de buurt van oppervlakken gedragen. Ook nieuwe vragen zijn gerezen betreffende dit onderwerp die in de toekomst mogelijk hun antwoord vinden.

Bedankt!

Het schrijven van een dankwoord geeft aan dat het proefschrift “bijna” af is. Op zo’n moment kom je in een staat van euforie door het feit dat de taak er “bijna” op zit. Deze blijdschap wordt grotendeels ervaren door de schrijver van dit proefschrift maar behoort eigenlijk te worden gedeeld met alle mensen die hebben bijgedragen om dit boekje tot een geslaagd einde te brengen.

In de eerst plaats wil ik mijn promotor Daan Frenkel bedanken voor de taak die hij ogenschijnlijk moeiteloos op zich nam om mijn promotie tot een goed einde te brengen. Evenzo ben ik dankbaar voor de vele ideeën en de interessante gesprekken die wij hebben gehad over het in dit proefschrift beschreven werk.

In de tweede maar niet op de tweede plaats, wil ik Blandine Jérôme bedanken voor de bijzondere samenwerking die we de afgelopen vier jaar hebben gehad en alles wat zij voor me gedaan heeft. Je hebt me geleerd dat er altijd weer een horizon is als ik volledig was verdwaald in de wetenschap zee. Bedankt voor de steun, goeie ideeen, vrolijke humeur, enthousiasme voor de wetenschap en altijd aandacht en interesse. Het is een leerzame periode geweest waardevol voor het rest van mijn leven.

De groep orde/wanorde op het AMOLF, Wim de Jeu, Jan Commandeur, Levent Demirel, Liesbeth Mol, Andrea Fera, Arcadi Schalaginov wil ik bedanken evenals de groep complexe vloeistoffen op de UvA met Roland Meister, Peter Verschuren, Elio, Paul.

Verder heb ik ook veel hulp gehad van de technische ondersteuning Wim Barsingerhorn, Ruud Boddenberg, Jan van Elst, Jan Verhoeven, Noelle Rutte.

Tal van collega’s en ex-collega’s die ik heb zien langskomen in de tijd dat ik op AMOLF bezig ben geweest, allemaal mensen aan wie ik met plezier terug denk, Arcadi

Shalaginov, Gerard Wong, Rutger Schlatmann, Willem Jan Huisman, Jan Commandeur, Bela Mulder, Jaydep Chakrabarti, Levent Demirel, Steven de Vries, Alfons van Blaaderen, Wim Brouwer, Ben Okhuyzen, Klaas Jan van den Berg, Els, Trees, Magda, Marjan en Marileen

Mijn trouwe vrindjes, David, Simon, Peter voor het continu op de hoogte houden van de toestand in de wereld, Pieter Rein -zwoegen is een schone zaak, maar nu gaan we naar onszelf luisteren he?-.

Ten slotte bedank ik mijn ouders, Els, Aart, Jeannette, Alex en Mees die altijd grote bewondering voor mijn werk hebben gehad, en lieve Sandra, die in de periodes van drukte zo'n heerlijke rots in de branding is geweest.